NASA/TP-2007-214891

Small Aircraft RF Interference Path Loss Measurements

Truong X. Nguyen, Sandra V. Koppen, Jay J. Ely, and George N. Szatkowski
Langley Research Center, Hampton, Virginia

John J. Mielnik and Maria Theresa P. Salud
Lockheed Martin, Hampton, Virginia

August 2007

The NASA STI Program Office ... in Profile

Since its founding, NASA has been dedicated to the advancement of aeronautics and space science. The NASA Scientific and Technical Information (STI) Program Office plays a key part in helping NASA maintain this important role.

The NASA STI Program Office is operated by Langley Research Center, the lead center for NASA's scientific and technical information. The NASA STI Program Office provides access to the NASA STI Database, the largest collection of aeronautical and space science STI in the world. The Program Office is also NASA's institutional mechanism for disseminating the results of its research and development activities. These results are published by NASA in the NASA STI Report Series, which includes the following report types:

- TECHNICAL PUBLICATION. Reports of completed research or a major significant phase of research that present the results of NASA programs and include extensive data or theoretical analysis. Includes compilations of significant scientific and technical data and information deemed to be of continuing reference value. NASA counterpart of peer-reviewed formal professional papers, but having less stringent limitations on manuscript length and extent of graphic presentations.

- TECHNICAL MEMORANDUM. Scientific and technical findings that are preliminary or of specialized interest, e.g., quick release reports, working papers, and bibliographies that contain minimal annotation. Does not contain extensive analysis.

- CONTRACTOR REPORT. Scientific and technical findings by NASA-sponsored contractors and grantees.

- CONFERENCE PUBLICATION. Collected papers from scientific and technical conferences, symposia, seminars, or other meetings sponsored or co-sponsored by NASA.

- SPECIAL PUBLICATION. Scientific, technical, or historical information from NASA programs, projects, and missions, often concerned with subjects having substantial public interest.

- TECHNICAL TRANSLATION. English-language translations of foreign scientific and technical material pertinent to NASA's mission.

Specialized services that complement the STI Program Office's diverse offerings include creating custom thesauri, building customized databases, organizing and publishing research results ... even providing videos.

For more information about the NASA STI Program Office, see the following:

- Access the NASA STI Program Home Page at ***http://www.sti.nasa.gov***

- E-mail your question via the Internet to help@sti.nasa.gov

- Fax your question to the NASA STI Help Desk at (301) 621-0134

- Phone the NASA STI Help Desk at (301) 621-0390

- Write to:
  NASA STI Help Desk
  NASA Center for AeroSpace Information
  7115 Standard Drive
  Hanover, MD 21076-1320

NASA/TP-2007-214891

Small Aircraft RF Interference Path Loss Measurements

Truong X. Nguyen, Sandra V. Koppen, Jay J. Ely, and George N. Szatkowski
Langley Research Center, Hampton, Virginia

John J. Mielnik and Maria Theresa P. Salud
Lockheed Martin, Hampton, Virginia

National Aeronautics and
Space Administration

Langley Research Center
Hampton, Virginia 23681-2199

August 2007

Acknowledgments

This work was funded by the Federal Aviation Administration as part of FAA/NASA Interagency Agreement DFTA03-96-X-90001, Revision 9, as well as the NASA Aviation Safety Program (Single Aircraft Accident Prevention Project).

Available from:

NASA Center for AeroSpace Information (CASI)
7115 Standard Drive
Hanover, MD 21076-1320
(301) 621-0390

National Technical Information Service (NTIS)
5285 Port Royal Road
Springfield, VA 22161-2171
(703) 605-6000

Table of Contents

List of Tables

List of Figures

Acronyms

ATC	Air Traffic Control Transponder
CDF	Cumulative Distribution Function
CF	Correction Factor
dB	Decibel
dBd	Decibel relative to dipole antenna gain
dBm	Decibel relative to one milliwatt power
DME	Distance Measuring Equipment
GHz	Gigahertz
GPS	Global Positioning System
GS	Glideslope
IPC	Interference Path Coupling, is negative of IPL
IPL	Interference Path Loss
kHz	Kilohertz
LOC	Localizer
MHz	Megahertz
msec	milliseconds
NASA	National Aeronautics and Space Administration
PED(s)	Portable Electronic Device(s)
RF	Radio Frequency
TCAD	Traffic Collision Alert Device
TCAS	Traffic alert and Collision Avoidance System
VHF	Very High Frequency
VHF-Com	Very High Frequency Voice Communication
VOR	VHF Omnidirectional Range
VOR/LOC	VOR and LOC combined

List of Symbols

ε	Antenna's balun efficiency factor
$\lvert\Gamma_c\rvert^2$	power reflection coefficient
π	Universal constant = 3.141592654
A	Device emission power
B	Interference Path Coupling factor, negative of interference path loss in dB
C	Receiver susceptibility threshold
CF	Correction Factor
P_{in}	Input power
P_{rad}	Radiated power (linear unit)
$P_{reflected}$	Reflected power
$P^R(2)$, $P^R(3)$	Power received at points (2) and (3), respectively, in dBm
$P^T(1)$,	Power transmitted at point (1), in dBm
$\lvert S_{11}\rvert$	Antenna reflection coefficient
VSWR	Voltage Standing Wave Ratio

(This page was intentionally left blank)

Abstract

Interference to aircraft radio receivers is an increasing concern as more portable electronic devices are allowed onboard. Interference signals are attenuated as they propagate from inside the cabin to aircraft radio antennas mounted on the outside of the aircraft. The attenuation level is referred to as the interference path loss (IPL) value. Significant published IPL data exists for transport and regional category airplanes. This report fills a void by providing data for general aviation aircraft. In this effort, IPL measurements are performed on ten aircraft of different designs and manufacturers. Multiple radio systems are addressed. Along with the typical worst-case coupling values, statistical distributions are also reported that could lead to more meaningful interference risk assessment.

1 Executive Summary

Multiple studies were previously performed to address the aircraft radio system interference problem from onboard portable electronic devices (PEDs) such as laptop computers and wireless phones. In a typical problem, one would deal with characterizing device emissions in the aircraft radio bands, the interference path loss (IPL), and the aircraft radio interference thresholds. This study specifically addresses the IPL measurement. In particular, this study includes aircraft that are much smaller than in earlier efforts. Data is severely lacking for general aviation and corporate aircraft.

IPL is a measurement of propagation loss from an interference signal emanating from within the passenger cabin to a victim aircraft radio receiver. In this study, IPL measurements were conducted for ten general aviation aircraft. These aircraft carry four to 16 passengers and crew depending on models and the specific seat configurations. Included in the study was one helicopter, and a small aircraft with fiberglass composite skin that provided little shielding between external antennas and the passenger cabin.

The measurement approach was similar to the method used for larger aircraft in previous studies. A tracking spectrum analyzer was used, which had a built-in radio frequency (RF) generator that performed synchronized sweeps with the spectrum analyzer. The tracking generator produced a known output power level to the transmit antenna while the spectrum analyzer recorded the peak coupled power into the aircraft radio receiver's antenna port. A biconical antenna and a dual-ridge horn antenna were used as the transmit antennas to overcome size and bandwidth limitations of a dipole antenna.

Instead of performing spot measurements with the transmit antenna at window and door locations as in earlier efforts, each aircraft volume was first divided into zones. The transmit antenna continuously scanned each individual zone's volume. This ensured the capture of the worst case coupling in the volume, while allowing characterization and comparison of localized effects of different zones. The result was the peak coupling envelope for each zone for the frequency range. Following a standard process in RTCA/DO-294, data were normalized against the antenna's farfield gain to obtain characteristics similar to a dipole transmit antenna.

Measured data for all zones were combined and compared. In addition, the overall statistics for each aircraft were compared against other aircraft. The data comparison shows that the cumulative distribution curves for many aircraft are similar in shape, but of different magnitude. This finding may help to simplify future measurements and documentation of the results. Comparison against previously measured

large aircraft, including Boeing 737, 747, and 757, shows that peak interference coupling for these general aviation aircraft are generally much higher.

The measurements were performed for a number of aircraft radio systems, including Localizer (LOC), Very High Frequency Omnidirectional Range (VOR), Very High Frequency Voice Communication (VHF-Com), Glideslope (GS), Distance Measuring Equipment (DME), Air Traffic Control Transponder (ATC), Traffic Collision Avoidance System (TCAS) or Traffic Collision Alert Device (TCAD), and Global Positioning System (GPS).

2 Introduction

The risk of interference to aircraft radio systems caused by portable electronic devices (PEDs) is a concern during flight. Existing aviation regulations require that the aircraft operator determine the acceptable use of portable electronic devices on their aircraft. For various reasons, use of most non-transmitting PEDs such as laptop computers, is allowed during flight, while use of intentional transmitters such as wireless devices and phones is prohibited. For air carrier aircraft, the air carrier enforces PED regulations through visual inspections and passenger announcements before and during critical phases of flights. For general aviation aircraft, enforcing appropriate PED use is the responsibility of the pilot. Informal communications with general aviation pilots and passengers indicate that the deliberate or inadvertent use of transmitting devices, including wireless phones, during a flight is likely.

The interference subject is typically studied by addressing the typical *source – path loss – victim* problem. Addressing the elements of the problem include measuring and bounding the emission level of typical devices, the propagation loss, and the interference thresholds for the radio receivers. There have been many past studies addressing these three elements. Examples include emissions measurements from wireless devices in aircraft radio bands [1][2]. Aircraft radio receiver interference thresholds data may be found in [3]-[5].

The propagation loss, also referred to as interference path loss (IPL), is simply the interference signal attenuation between the source location within the cabin (where PEDs are typically located) and the aircraft radio receiver. Low IPL could result in strong interference signals at the receiver, causing an increased likelihood of interference.

A good summary of the publicly available IPL data was documented in [1][5]. These data sets included the lowest IPL values for several large aircraft, such as Boeing 747, 757 and 737. On a much more limited scale, IPL data were also available for smaller aircraft, such as Canadair Regional Jet, ATR72, and Embraer 120. These aircraft can hold 25 seats or more.

For even smaller aircraft, there is currently very little publicly available IPL data. Small aircraft may have lower IPL values (or higher interference coupling values) than large aircraft, since propagation distances between locations within the cabin and the aircraft radio antennas could be significantly shorter. Lower IPL translates into higher probability of interference.

As a part of the collaborative effort between the Federal Aviation Administration's Aviation Safety Organization and the National Aeronautics and Space Administration's Aviation Safety Program, this report documents the effort to measure IPL data on ten general aviation aircraft. They differed in sizes, designs, antenna locations, window sizes, diameters, and other parameters that can affect the IPL values. Also included was an aircraft with fiberglass composite skin that provided little shielding, and a helicopter with large window areas.

In addition to the traditional minimum IPL values, this paper also reports the data cumulative distribution function for each system. These distributions may be more useful in assessing the likelihood of interference than the typical worst case scenarios.

2.1 Objective

The primary objective of this study is to measure IPL for general aviation aircraft. These IPL measurements are essential in assessing interference risks to aircraft radio receivers.

2.2 Scope

In this effort, the IPL measurements were restricted to aircraft that can carry from four to 16 passengers and crew, depending on aircraft seat configuration. The aircraft radio systems considered included communication and navigation radio receivers.

The measurements were limited to "in-band" measurements, or measurements in the radio frequency band for the receiver. They were also limited to interference coupling through the aircraft antennas. Other coupling mechanisms, i.e. via cables and apertures in the enclosure, were excluded. Interference coupling outside of the aircraft radio receiver's bands was considered less of a concern and were not considered.

2.3 Approach

As previously discussed, assessment of aircraft radio receiver interference is typically accomplished by addressing the *source – path loss – victim* components of the equation:

$$A + B \geq C, \tag{2.3-1}$$

for all in-band frequencies, where

"*A*" is the maximum RF emission from a PED in dBm,

"*B*" is the maximum interference path coupling factor (IPC) in dB, and is usually a negative value. "*–B*" is referred to as the minimum IPL and is usually positive.

"*C*" is the receiver's minimum in-band, on-channel interference threshold in dBm.

If the minimum interference threshold, "*C*", is lower than the maximum interference signal level at the receiver's antenna port, "*(A + B)*", there is a potential for interference. This is typical of the "worst case" analysis, in which the worst cases of all components are assumed. "Worst case" analysis can be overly conservative if the worst-case data are far from the norm.

In order to avoid overly conservative analysis, one proposed approach is to perform the analysis using some statistical parameters other than the worst-case. Thus, the chosen statistical parameters of "A" are added to similar statistical parameters of "B", and the results are compared to some other statistical forms of "C". The desired statistics parameters are not yet agreed upon by the technical community for the aircraft interference problem.

In this effort, the primary focus was to capture the worst-case coupling value, "B". This was to provide data in similar form as in [1][5]. The secondary focus was to report the statistical distribution of the IPL data, from which acceptable statistical parameters may be determined. These two guidelines helped shaped the measurement process to be discussed later.

In performing the IPL measurements, the method used was similar to the method used in [1][5], but with small variations. A tracking generator delivered known transmit power level out of a small antenna simulating an interference source in the cabin. A spectrum analyzer, while performing synchronized sweeps with the tracking generator, captured the envelope of the simulated signals coupled into the aircraft antenna and cabling.

The attenuation level between the transmitted signal and the measured signal is referred to as the IPL value, the negative of which is the *IPC*, or *IPC = -IPL*. The worst case coupling factor is simply the maximum *IPC* value, or *B = Maximum (IPC).* Further details are discussed in Section 3.

For the remainder of this document, the use of IPL and IPC terms are loosely interchangeable except where noted. They refer to the same data but with one being negative of the other. IPC is often more intuitive in data plots and analysis, whereas the IPL term is more widely recognized.

2.4 Report Organization

The IPL measurements are described in Section 3. Section 3.1 shows the radio systems and aircraft considered. Section 3.2 describes the measurement process. Section 3.3 describes the equipment and settings used. Sections 3.4 and 3.5 describe the data calibration, corrections and analysis.

Section 4 reports the measurement results for different aircraft and system combinations. Section 5 provides a summary and comparison of the data reported in Section 4. Appendix A shows the development of the transmit antenna's mismatch and efficiency correction factor.

3 Aircraft Interference Path Loss Measurements

This section describes the different aircraft and systems considered, the measurement process, the equipment, the data calibration and the statistical analysis. The process chosen was suitable for the small aircraft sizes considered. It met the primary goal of capturing the aircraft worst case coupling, but provided sufficient data details for statistical analysis.

3.1 Aircraft and Systems Considered

Table 3.1-1 lists the ten aircraft on which the IPL measurements were performed. Most aircraft fuselages were of metal construction, except for the Cirrus SR-22 model which had fiberglass composite with all composite skin. Experiments show that the composite skin in the Cirrus SR-22 provides little RF shielding between the internal cabin and radio antennas mounted on the top of the aircraft. Also included was a Bell 407 helicopter with large window areas. In Table 3.1-1, each model was also assigned an integer number that could be useful in tracking data and plots in Section 5. The numbers were associated with the measurement order. Pictures of the aircraft are located in Section 4 along with the data.

This effort was intended to address the following systems to the maximum extent possible: Localizer (LOC), Very High Frequency Omnidirectional Range (VOR), Very High Frequency Voice Communication (VHF-Com), Glideslope (GS), Distance Measuring Equipment (DME), Air Traffic Control Transponder (ATC), Traffic Collision Avoidance System (TCAS) or Traffic Collision Alert Device (TCAD), and Global Positioning System (GPS). In all aircraft, the VOR and LOC systems shared the same external antenna and cable. As a result, the measurements were combined, and the VOR/LOC term was used to denote the merged measurement and results. Table 3.1-2 tabulates the systems considered in this study and the corresponding measurement frequency ranges.

The systems and their antennas varied widely among the aircraft used. They varied in receiver and antenna designs, manufacturers, and mounting locations. There were often secondary systems that did not share the same make, design and antenna with the primary system. Due to aircraft size, time restriction and system similarity, many of the secondary systems available were not measured.

Table 3.1-1: Aircraft Designations

Aircraft Designation	Aircraft Model	Types, Tail No.
1- Cirrus SR-22	Cirrus SR-22 GTS	Four seat light composite, N307A
2- Cessna 172R	Cessna 172R Skyhawk	Four seat light, N5199A
3- Bell 407	Bell 407	Seven-place utility helicopter, N415AC
4- LearJet 35A	Bombardier LearJet 35A	Ten to 12-seat light/midsize corporate jet, N604S
5- Sabreliner 65	Rockwell Sabreliner 65	Ten to 12-seat medium corporate jet, N91BZ
6- Citation II	Cessna Citation II (Model 550)	Eight to 12-seat light corporate jet, N89D
7- Baron B-58	Raytheon Beechcraft Baron B-58	Four- to six-seat business, N939P
8- Piper Saratoga	Piper PA-32R-301 Saratoga II HP	Six-seat light, N63PV
9- Gulfstream GII	Gulfstream GII	Ten to 16-seat large corporate jet, N183PA
10- King Air 200	Raytheon King Air 200	Eight to 12-seat medium corporate turboprop, N404FA

Table 3.1-2: Aircraft Bands Considered and Spectrum

Aircraft Band	Receive Spectrum (MHz)	Measurement Frequency Range (MHz)
LOC	108.1-111.95	108 - 118
VOR	108-117.95	
VHF-Com	118 - 138	118 - 138
GS	328.6 - 335.4	325 - 340
DME	962 - 1213	960 - 1220
ATC	1030	1020 - 1040
TCAS	1090	1080 - 1100
GPS	1575 ± 2	1565 - 1585

3.2 Measurement Process

Fig. 3.2-1 illustrates the representative interference coupling paths between the aircraft windows and door, and a top-mounted antenna. For metal aircraft, windows and door seams typically provide the strongest coupling paths to the external antennas [6]. Fig. 3.2-2 illustrates a typical setup that is very similar to that used in the past studies [1], but with a small change. The volume of each aircraft is first divided into zones (described in more detail in Section 4), and the measurements are performed with the transmit antenna sweeping over the volume of each zone. Zone measurement also includes sweeping over windows and door seams. Measurement data represent the peak coupling envelope for a zone. The zone scans also include changing antenna polarizations. In contrast, measurements in [1] were performed with the transmit antenna statically stationed at each window or sweeping over a door seam.

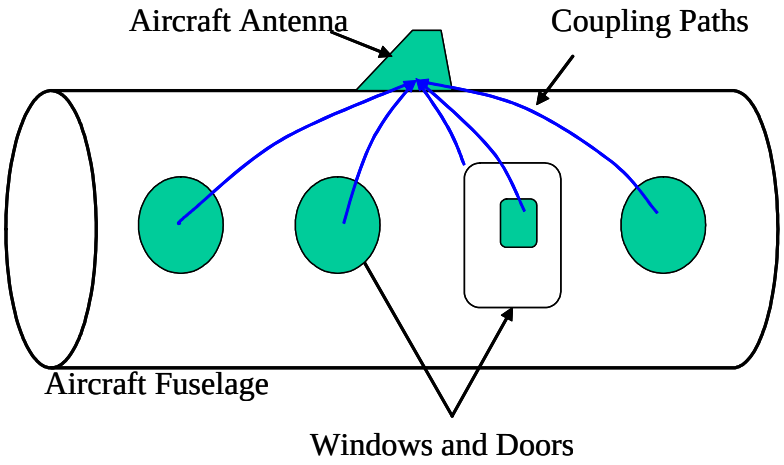

Figure 3.2-1: Representative main IPL coupling paths for a top-mounted aircraft antenna (metal aircraft).

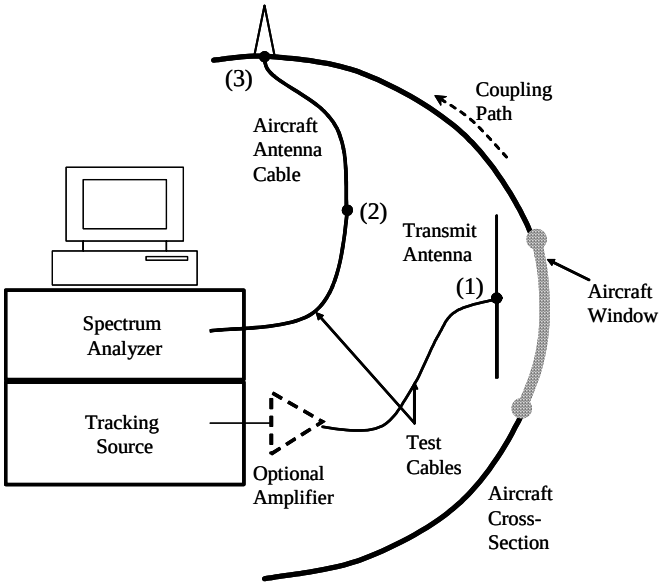

Figure 3.2-2: Typical set-up for passenger cabin excitation and a top-mounted aircraft antenna.

While performing synchronized sweeps with the tracking generator, a spectrum analyzer captures the envelope of the simulated signal that coupled into aircraft antennas. A small antenna simulates a transmitting source in the cabin. Referring to figure 3.2-2, the IPL value is the attenuation, in dB, between transmitted power at point (1) and the measured power at point (2). For GPS, IPL is defined to be the difference in power between locations (1) and (3). These measurement locations are specified in the IPL measurement process outlined in [5]. Or,

$$IPL = P^{T}_{(1)} - P^{R}_{(2)} \quad \text{for most systems, and} \tag{3.2-1}$$

$$IPL = P^{T}_{(1)} - P^{R}_{(3)} \quad \text{for GPS,} \tag{3.2-2}$$

where $P^T_{(1)}$ is power transmitted at point (1); $P^R_{(2)}$, and $P^R_{(3)}$ are power received at points (2) and (3), in dBm, respectively.

Measurement at point (2) is performed at the receiver, while measurement at point (3) is performed at the output of the aircraft antenna. These points correspond to the specific locations at which individual receiver interference threshold is defined [5].

For most GPS measurements in this document, lack of access to the rear of the GPS antenna made it difficult to measure at point (3) directly. As a result, measurements at point (2) were performed, and Eq. 3.2-1 was applied instead. This deviation resulted in additional uncertainties due to the unknown aircraft GPS antenna cable loss. Since GPS antennas were typically close to their receivers, the cable loss was expected to be small, possibly less than 2 dB.

The following subsections provide additional measurement details about the transmit antennas, the zone volumetric scan, and the IPL measurements.

3.2.1 Transmit Antenna Volumetric Scan

The volume of each aircraft was divided into small zones for volumetric scanning. While the tracking generator and the spectrum analyzer performed synchronized sweeps, test personnel moved the transmit antenna physically throughout volume of each zone, and the maximum envelope trace was recorded. Due to the large antenna physical sizes, the limited unoccupied space within each cell (space taken by seats and other structures) and the fast instrument response rate, a sweep of the entire zone could be achieved very quickly, typically in less than one minute for one polarization. Each zone typically included scans for vertical and horizontal polarizations. Once complete, the entire volume of the passenger cabin, the cockpit, and in many cases the cargo bay, were covered. Care was taken to avoid bumping the antenna against metal aircraft structures, as it could result in step discontinuities in the spectrum analyzer's traces.

3.2.2 Transmit Antennas

The transmit antennas used for IPL measurements are typically specified to be half-wave dipoles [5]. To overcome bandwidth limitations and size associated with dipole antennas, a biconical antenna was used for frequencies below 350 MHz, and a dual-ridge horn antenna above 960 MHz. The biconical antenna was in-band (low mismatch and efficient) from 300 MHz to 1 GHz, but was usable down to 100 MHz. The biconical antenna was omnidirectional in one plane, while the dual-ridge horn antenna was directional. A correction was applied to the data for the transmit antenna gain (relative to a dipole) to conform to the standard practice recommended in [5]. Section 3.4 discusses this correction in greater details.

3.2.3 Indoor Measurements

Most measurements were performed with the aircraft located inside three different hangars located at Norfolk International Airport. Extreme weather conditions posed potential health hazards if the measurements were performed outside. While this setup was not ideal, limited experimentation confirmed that data were not significantly affected if aircraft antennas were kept far away from building structures.

There are benefits to performing measurements inside a hangar, however. The hangars helped shield the aircraft from strong local transmitters operating in the measurement bands. As a result, fewer data

points were tainted by the ambient signals that required manual removal from the data set. The Gulfstream GII was the only aircraft measured outside the hangar.

3.3 Instruments and Settings

An Agilent E4407B spectrum analyzer with an internal tracking generator was used for all measurements. In each measurement band, continuous 401-point frequency sweeps were performed while the instrument was set at trace maximum hold. With the exceptions of the GPS band, an external amplifier was used at the output of the tracking source in the majority of the measurement to overcome the noisy ambient environment, thereby improving measurement quality. Instrument settings were pre-determined and stored in the spectrum analyzer's memory to allow quick recalls during the measurement. This approach allowed for fast switching between measurement bands and reduced operator errors. At the end of a zone sweep, the trace was downloaded to a computer for later processing.

Table 3.3-1 documents the typical spectrum analyzer settings. The instrument settings were optimized for measurement speed and sensitivity. Laboratory verifications were conducted to ensure sufficient sweep time to accommodate propagation delays. The actual reference level and attenuation settings occasionally varied from the listed values to accommodate the wide data range.

GPS antennas are designed to deal with very low level in-band signals, and can be easily overloaded with strong in-band signals. For every aircraft, tests were performed to verify that the GPS antenna was operating in its linear range, and that its sensitive front-end was not powered. This verification was accomplished by repeating the measurements at the strongest coupling locations but at a reduced power level. The GPS antenna was operating in its linear range if the new data were also reduced by a similar amount. On one occasion, data for the entire aircraft was retaken with reduced transmitted power level.

Table 3.3-1: Typical Instrument Settings

Band	Tracking Source Power (dBm)	Resolution Bandwidth	SweepTime (milliseconds)	Default Reference Level (dBm)
VOR/LOC	0 , -10 (*)	100 kHz	50	-10
VHF-Com	0, -10 (*)	100 kHz	50	-10
GS	0, -10 (*)	100 kHz	50	-10
DME	0, -10 (*)	100 kHz	100	-10
ATC	0, -10 (*)	100 kHz	50	-10
TCAS	0, -10 (*)	100 kHz	50	-10
GPS	-10	100 kHz	50	-10

(*) -10 dBm tracking source power setting if an external power amplifierwas used (27 dB nominal gain).

3.4 Data Calibration and Corrections

In addition to the raw IPL data, cable loss, system noise floor, and ambient noise environment reaching the measurement systems were also measured. Microsoft Excel was used for post calibration and processing. Data were processed according to Eq. 3.2-1 and Eq. 3.2-2. Statistical calculations were performed using custom Matlab scripts.

Other correction factors were also applied. As previously discussed, one factor accounted for the transmit antenna being other than a dipole. The other correction removed the effects of the GPS

antennas' built-in pre-amplifiers. These corrections are discussed in further details in the following subsections.

3.4.1 Correction for Transmit Antenna Gain

Due to bandwidth and size limitations associated with a standard dipole, a biconical antenna and a dual-ridge-horn antenna were used. As a result, corrections must be applied to account for the difference between the antenna used and the ideal dipole antenna. The goal is to have similar results as if a dipole antenna were used, but without the size and bandwidth limitations. For the biconical antenna, this correction factor mainly accounts for antenna mismatch and efficiency when used out-of-band. For the dual-ridge-horn antenna, the correction factor mainly accounts for the directional pattern relative to a dipole. The specific antennas used were:

- Dual-Ridge-Horn Antenna: A.H. Systems Model SAS-571
- Biconical Antenna: Schwarzbeck BBVU 9135 biconical elements with UBAA 9114 4:1balun

The negative of the *farfield* gain (relative to a dipole) was used as the correction factor in compliance with [5]. Since the antennas were not used in a farfield environment, this was not the ideal correction factor. However, this choice was considered to yield a reasonable level of uncertainty. Table 3.4-1 lists the farfield gain correction factors used, determined from the manufacturers' data sheets.

Table 3.4-1: Measurement Transmit Antenna Characteristics

Radio Systems Considered	Meas. Freq Range (MHz)	Antenna Type	Band Ave. Farfield Gain Correction Factor (dBd)
VOR/LOC	108 - 118	Biconical	+12.85
VHF-Com	118 - 138	Biconical	+10.9
GS	325 – 340	Biconical	-1.03
DME	960 – 1220	Dual-Ridge Horn	-5.32
ATC	1020 – 1040	Dual-Ridge Horn	-4.85
TCAS	1080 – 1100	Dual-Ridge Horn	-5.26
GPS	1565 – 1585	Dual-Ridge Horn	-7.5

One other correction approach which was investigated in this measurement effort is developed in Appendix A. This approach corrects only for antenna mismatch and efficiency, while assuming directivity to be similar to the reference dipole antenna. This approach might be considered as an alternative to [5], though all data presented in this report has been obtained using the standard correction given in [5]. An omnidirectional antenna must be used for this approach.

Antenna mismatch can be easily measured with a network analyzer. However, antenna efficiency is generally more difficult to estimate. A simple method to measure the biconical antenna's efficiency is proposed in Appendix A. Calculations and measurements from the Appendix A result in the correction factors of +8.66, +9.99 and +0.74 dB for the VOR/LOC, VHF-Com and GS bands, respectively.

In theory, the differences between these values and the correction factors in Table 3.4-1 are mainly due to the difference in antenna directivity between the ideal dipole and the biconical antenna. However, it is insufficient to justify the 4.19 dB difference for the VOR/LOC, as the directivity is only 2.15 dB for a dipole. It is suspected that a large part of the 4.19 dB is caused by measurement error associated with antenna gain value, which was obtained from the antenna's data sheet. Antenna parameters are difficult to measure accurately near 100 MHz and below in a typical facility.

In summary, each of the two alternatives has disadvantages. A disadvantage of the correction approached used in this paper include uncertainties due to the use of farfield gain factors in nearfield environments. The disadvantages of the alternative approach include difficulties in measuring and correcting for antenna efficiency, restricted to omnidirectional antennas, and the gain difference relative to a dipole-antenna is ignored.

Again, the results of the calculations in Appendix A are for comparison only and are not used in any of the data presented. The presented data used the farfield gain correction factor in accordance with [5].

3.4.2 Correction for Aircraft GPS Antenna Pre-Amplifier Gain

For aircraft systems other than GPS, aircraft receiver interference thresholds are specified at the receiver. IPL measurements, therefore, include aircraft cable loss for the systems as illustrated in Eq. 3.2-1 and Figure 3.2-2. On the other hand, GPS interference thresholds are specified at the output of the aircraft's *passive* GPS antenna. If the GPS antenna is active, the threshold is specified at the output of the antenna before the signal amplification stage [7]. In the case of an active antenna, the data must be corrected to remove the effects of the built-in pre-amplifier. The net result is to reduce the IPC by an amount equal to the antenna pre-amp gain value.

Table 3.4-2 lists the pre-amplifier value associated with each aircraft GPS antenna model. In the vicinity of mid-band frequency, these values often vary slightly with frequencies and receiver supply voltage. For the data processing, the nominal gain values used were chosen at mid-band frequency and at nominal supply voltage from the receiver.

Table 3.4-2: Aircraft GPS Antennas and Their Internal Pre-Amplifier Gain

Meas. Order	Aircraft Designation	Measured Antenna	Antenna Models	Antenna Pre-amp Gain (dB)
1	Cirrus SR-22	GPS2	Garmin GA-56	15.7
2	Cessna 172R	GPS	Bendix/King KA-92	26.5
3	Bell 407	GPS	Bendix/King KA-92	26.5
4	LearJet 35A	GPS	Universal 10704	26.5
5	Sabreliner 65	GPS1	Universal 10704	26.5
6	Citation II	GPS1 GPS2	Bendix/King KA-92 Garmin A-33/34*	26.5 26.5
7	Baron B-58	GPS	Garmin GA-56*	15.7
8	Piper Saratoga	GPS	Garmin GA-56*	15.7
9	Gulfstream GII	GPS1	Universal 10704	26.5
10	King Air 200	GPS	Garmin GA-56*	15.7

* Antenna pre-amplification gain data provided by the manufacturer through personal communications.

3.5 Data Statistical Analysis

The statistical cumulative distribution function (CDF) is computed for each data set. Each point on the curve associates an IPC value with a CDF value. The CDF value is the computed statistical probability of having the coupling measurement data being *equal or less than* the associated IPC value. Thus, the peak coupling value has the CDF of 1, meaning there is 100 percent probability of having measured data being equal to or less than the peak value. Except for the noise floor, all data traces and all frequency points within each trace are used in the calculation. As a result, the CDF curve accounts for variations due position, polarization and frequency changes.

Each data set's maximum and mean IPC values are also computed with the 98, 95, 90, 80, and 50 percentile values. The mean values are also provided, and were computed in linear units before converting back to the dB values. These calculations were performed using a simple custom Matlab script.

4 Measurement and Results

Table 4-1 lists the aircraft and systems for which the IPL was measured. Since there is no obvious method to group the aircraft, the aircraft are listed according to the order the measurements were performed. This order was largely determined by aircraft availability.

Each aircraft volume was divided into zones, each typically associated with the volume space near an aperture such as window or door. Within each zone, the transmit antennas perform two volumetric scans, one each for horizontal and vertical polarizations. A zone scan includes physically moving the transmitting antenna throughout the entire volume of that zone. Angular scans were also performed to ensure isotropic illumination from within the zone. Special attention was paid to the windows, door seams, and cockpit locations. Cargo bays were included if accessible. During each zone volumetric scan, the spectrum analyzer and the tracking generator continuously performed frequency sweeps, and the

maximum envelope was retained. Once all the zones were measured, the entire available aircraft volume and all transmit antenna orientations were included.

For the first five aircraft listed in Table 4-1, the aircraft volumes were divided into very small zone sizes for good statistical spatial sampling. The volume of the four-seat Cirrus SR-22 model was divided into 18 zones. The 12-seat LearJet 35A and the seven-seat Bell 407 helicopter models (with large window areas) were each divided into 37 zones. However, the fine sampling resulted in long measurement times that became a factor in larger aircraft, or aircraft with a high number of systems. As a result, the zone sizes were enlarged for the remaining five aircraft, reducing the total number of zones relative to the aircraft volume. The number of zones was roughly equal the number of aircraft windows, doors, cockpit seats, cargo bay and galley areas combined. The volumes of the 12-seat Cessna Citation, the 16-seat Gulfstream GII, and the 12-seat King Air 200 were divided into 18, 17, and 16 zones, respectively. This change allowed the measurement to be completed in the allotted time.

Experiments indicated that this approach had very good repeatability. Using the same setup and equipment, a small number of test measurements show that the peak IPC reading for each zone could be repeated within 0.5 to 1.0 dB.

All aircraft doors were closed during the measurements to simulate in-flight condition. Special attention was paid to RF or power cables that must be routed to the outside of the cabin. This was to minimize re-radiation of the signals within the cabin which could then reach the aircraft antennas. Typically, the cables were taped tightly to the aircraft metal surfaces and in the direction away from the aircraft main cabin and antennas.

The measured data were processed according to Section 3, and the results are presented in Sections 4.1 to 4.10 in the order shown in Table 4-1. For each system, an IPC chart is shown that includes the results of individual zone scans. Each trace represents the calibrated and processed IPC data from the volumetric scanning of each zone, where each zone represents a small volume space in the cabin. Due to the high number of traces, the individual traces are not identified here. Also shown are the measurement noise floor and ambient trace that were calibrated and processed as if it was real data. This trace verifies that sufficient measurement dynamic range was used, and helps to identify data points that were affected by strong ambient signals.

Ambient signals were typically represented by strong but narrowband spikes. On many occasions, the ambient signals were sufficiency strong to corrupt parts of the measured data. Those data points were easily identified and were individually removed from the traces before the plotting and the statistical calculations. As a result, data gaps in many traces can be observed. The systems most affected by strong ambient signals typically included LOC, GS, DME and VHF-Com bands.

The CDF curve is also reported for each IPC data set. Several IPC percentile values are also listed. These values are extracted from the CDF curves. Also reported are the number of frequencies per sweep, the number of location scans, and the total number of data points used in the statistical calculations. The number of points is roughly the product of 401 frequencies and the number of position scans. In the cases where there were data points eliminated from the population due to strong ambient signals, the count is reduced accordingly. Pictures of the aircraft are also shown in the figures preceding the data.

Table 4-1: Aircraft Radio Systems Measured on Different Aircraft

	VOR/LOC	VHF-Com	GS	DME	ATC	TCAS	GPS
Cirrus SR-22	VOR/LOC	VHF-Com1 VHF-Com2	GS		ATC	TCAS	GPS2
Cessna 172R	VOR/LOC	VHF-Com1	GS		ATC		GPS
Bell 407	VOR/LOC	VHF-Com1			ATC		GPS
LearJet 35A	VOR/LOC	VHF-Com2	GS	DME1	ATC		GPS
Sabreliner 65	VOR/LOC	*	GS				GPS
Citation II	VOR/LOC	VHF-Com1 VHF-Com2	GS	DME	ATC	TCAD	GPS1 GPS2
Baron B-58		VHF-Com1 VHF-Com2	GS		ATC	TCAS	GPS2
Piper Saratoga	VOR/LOC	VHF-Com1 VHF-Com2	GS	DME	ATC		GPS
Gulfstream GII	VOR/LOC	VHF-Com1 VHF-Com2	GS	DME	ATC	TCAS	GPS1
King Air 200	VOR/LOC	VHF-Com1 VHF-Com2	GS	DME1 DME2	ATC		GPS

4.1 Cirrus SR-22

Figure 4.1-1: Cirrus SR-22 GTS.

Figure 4.1-2: Sample external antennas, rear connectors of a radio receiver.

4.1.1 VOR/LOC

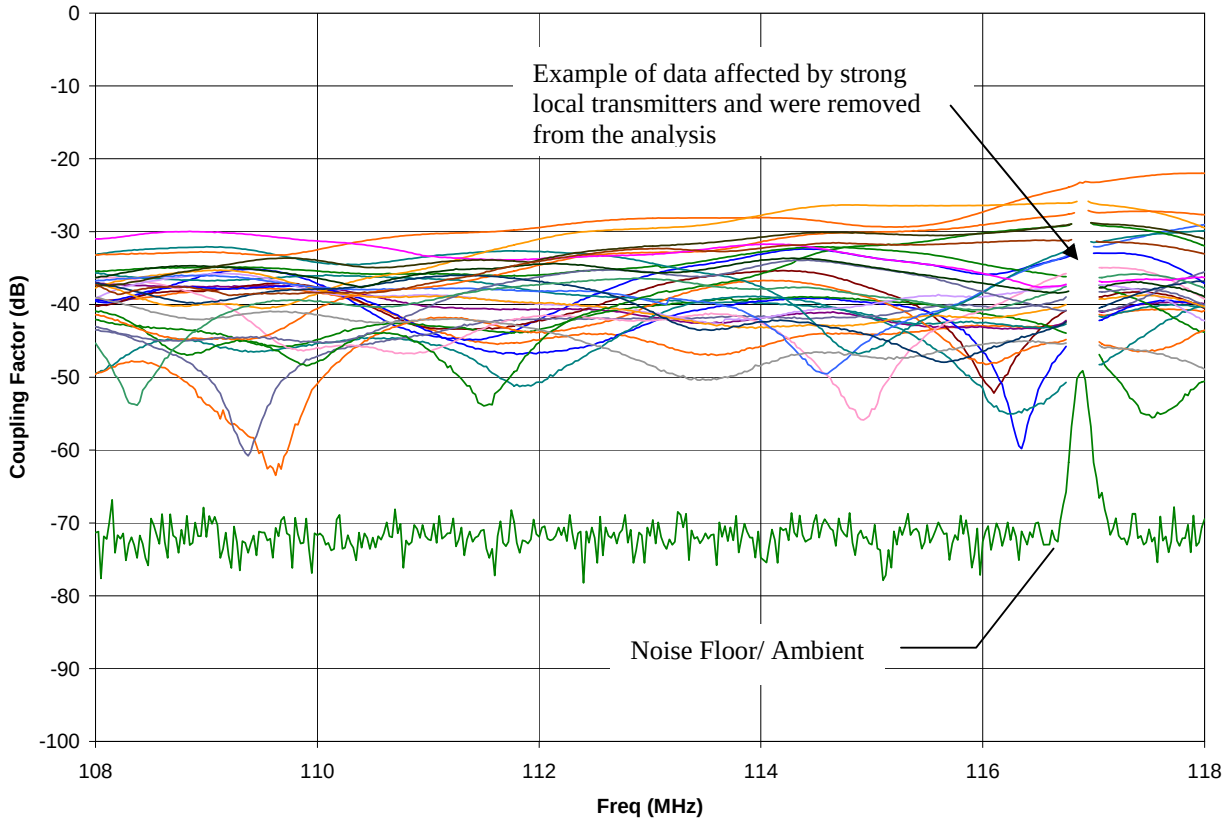

Figure 4.1-3a: Cirrus SR-22 VOR/LOC IPC scans at locations within aircraft fuselage.

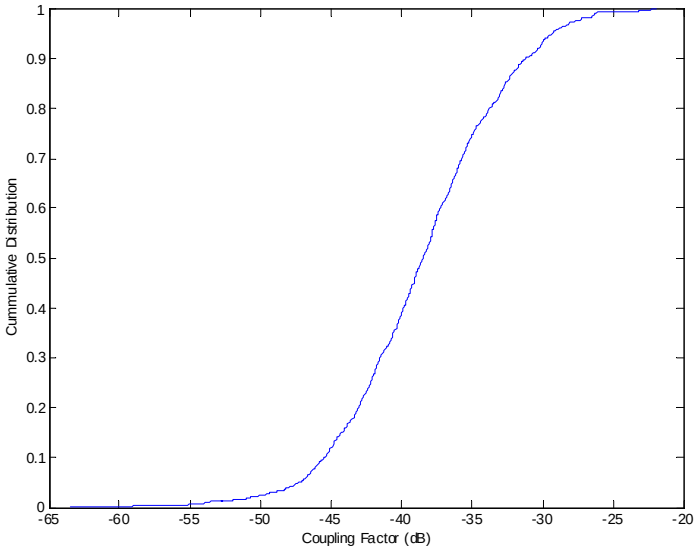

IPC Statistics		
Maximum	-22.0	dB
98 percentile	-27.2	dB
95 percentile	-29.3	dB
90 percentile	-31.2	dB
80 percentile	-33.7	dB
50 percentile	-38.5	dB
Mean	-35.0	dB
No. of Points	10974	
No. of Position Scans	28	
Freqs per Sweep	401	

Figure 4.1-3b: Cirrus SR-22 VOR/LOC IPC statistics.

4.1.2 VHF-Com1

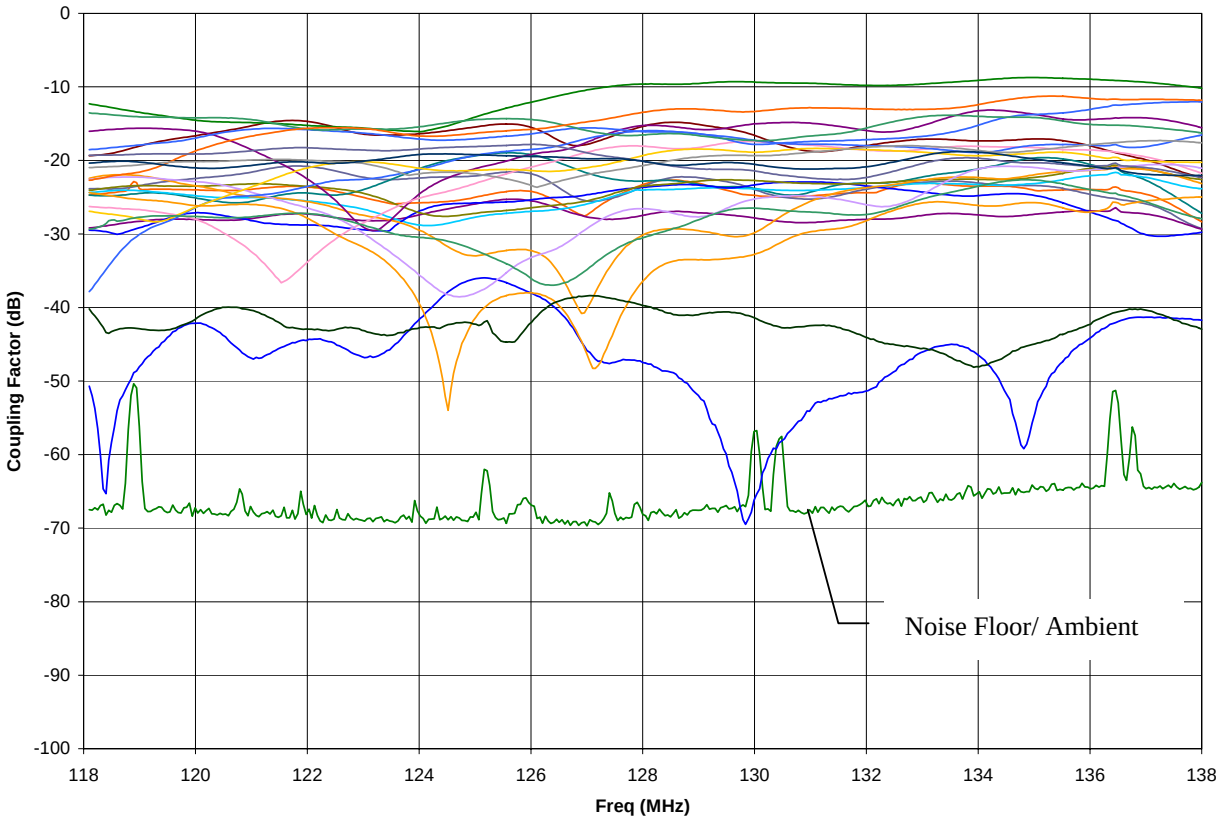

Figure 4.1-4a: Cirrus SR-22 VHF-Com1 IPC scans at locations within aircraft fuselage.

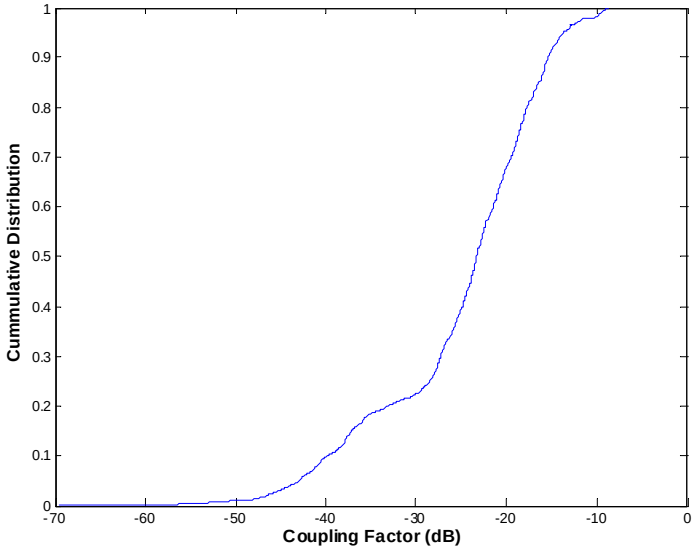

IPC Statistics		
Maximum	-8.7	dB
98 percentile	-10.6	dB
95 percentile	-13.6	dB
90 percentile	-15.4	dB
80 percentile	-17.7	dB
50 percentile	-23.3	dB
Mean	-19.3	dB
No. of Points	11228	
No. of Position Scans	28	
Freqs per Sweep	401	

Figure 4.1-4b: Cirrus SR-22 VHF-Com1 IPC statistics.

4.1.3 VHF-Com2

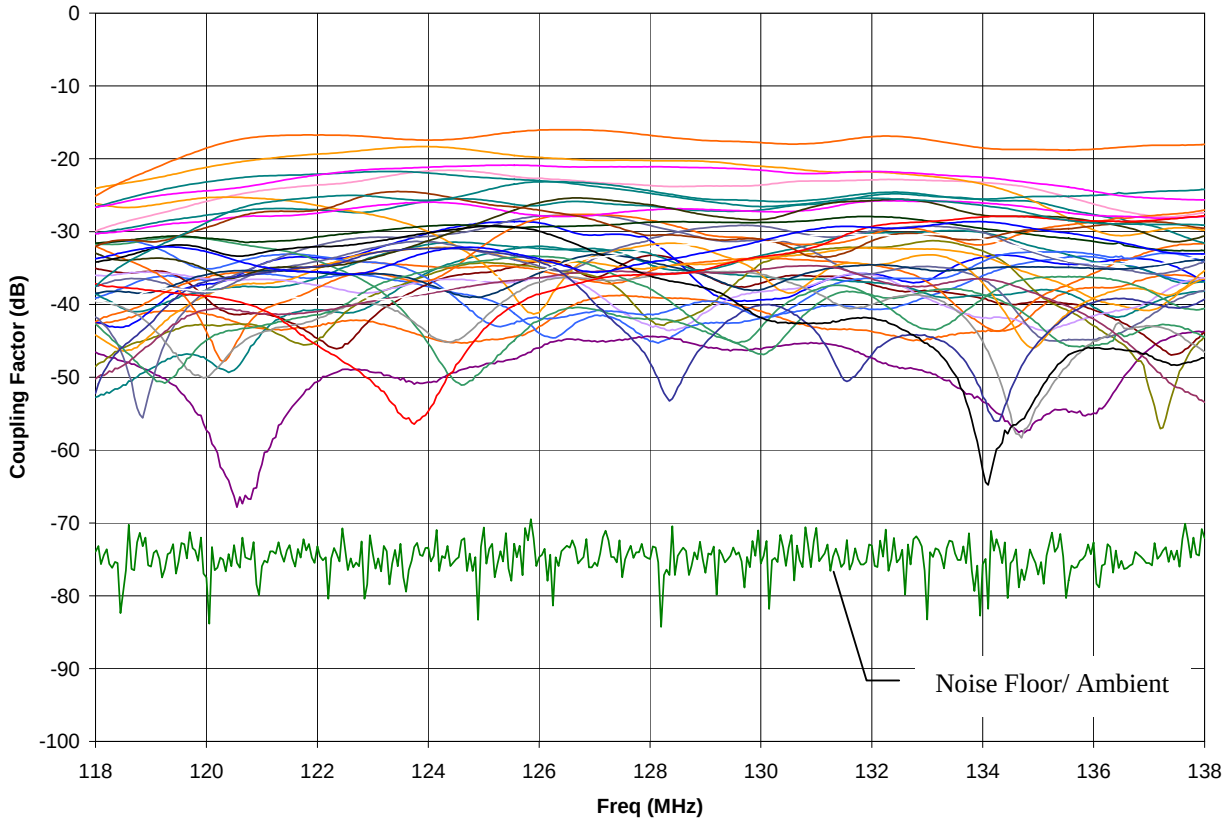

Figure 4.1-5a: Cirrus SR-22 VHF-Com2 IPC scans at locations within aircraft fuselage.

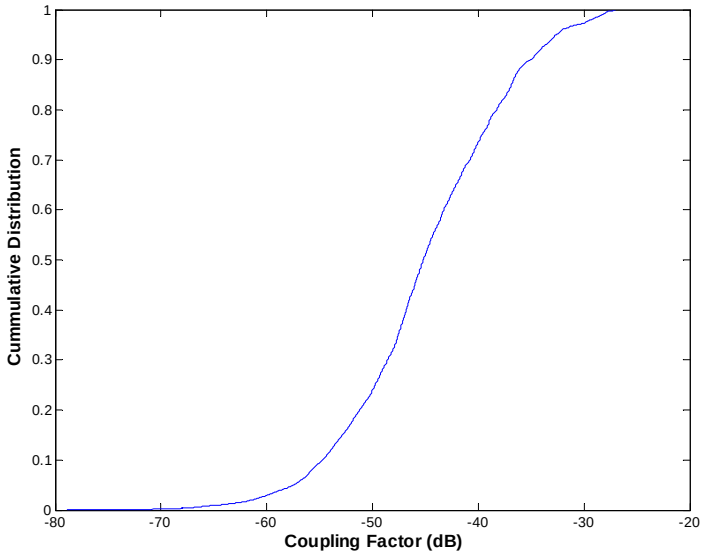

IPC Statistics		
Maximum	-27.1	dB
98 percentile	-29.3	dB
95 percentile	-32.6	dB
90 percentile	-35.0	dB
80 percentile	-38.3	dB
50 percentile	-45.2	dB
Mean	-39.1	dB
No. of Points	14837	
No. of Position Scans	37	
Freqs per Sweep	401	

Figure 4.1-5b: Cirrus SR-22 VHF-Com2 IPC statistics.

4.1.4 GS

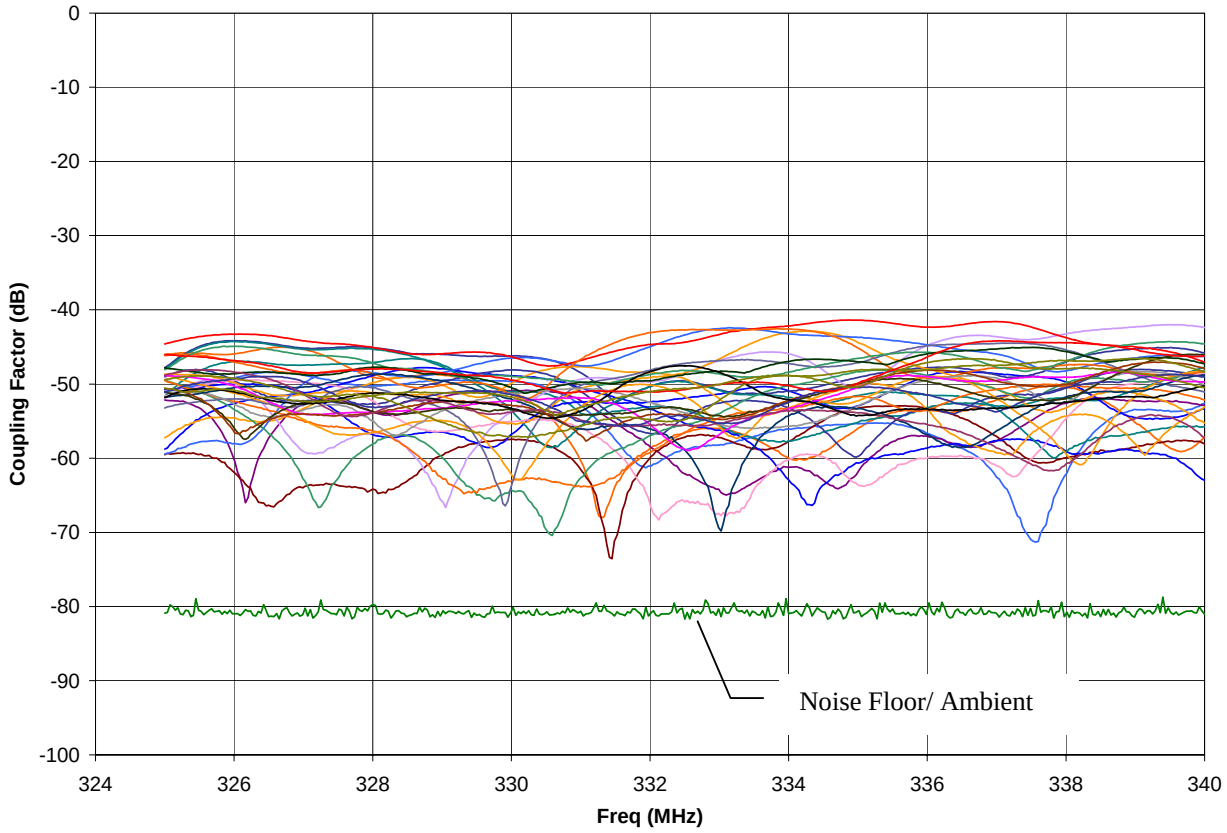

Figure 4.1-6a: Cirrus SR-22 GS IPC scans at locations within aircraft fuselage.

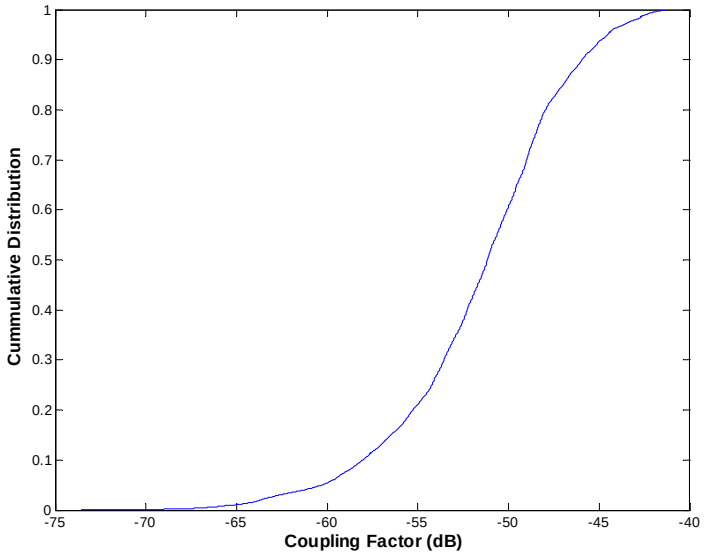

IPC Statistics		
Maximum	-41.4	dB
98 percentile	-43.0	dB
95 percentile	-44.5	dB
90 percentile	-45.9	dB
80 percentile	-48.0	dB
50 percentile	-51.2	dB
Mean	-49.5	dB
No. of Points	13634	
No. of Position Scans	34	
Freqs per Sweep	401	

Figure 4.1-6b: Cirrus SR-22 GS IPC statistics.

4.1.5 ATC

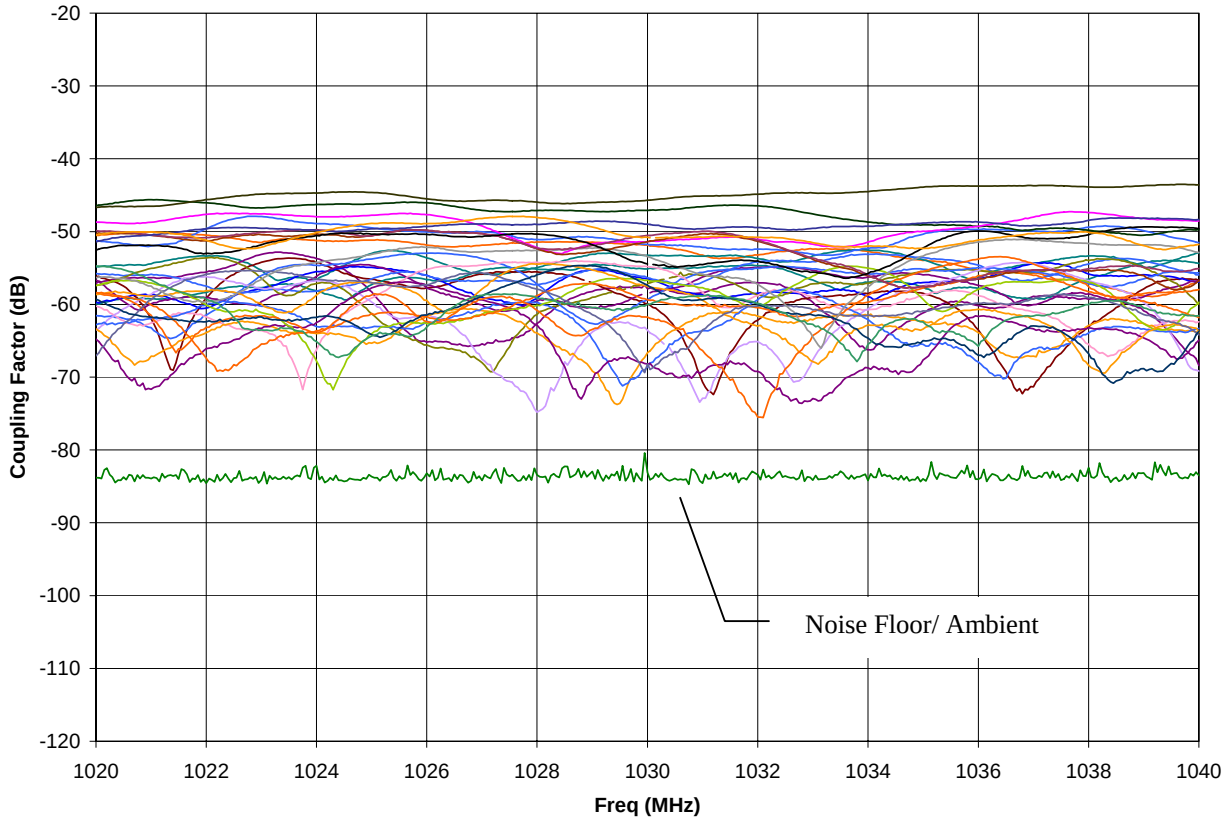

Figure 4.1-7a: Cirrus SR-22 ATC IPC scans at locations within aircraft fuselage.

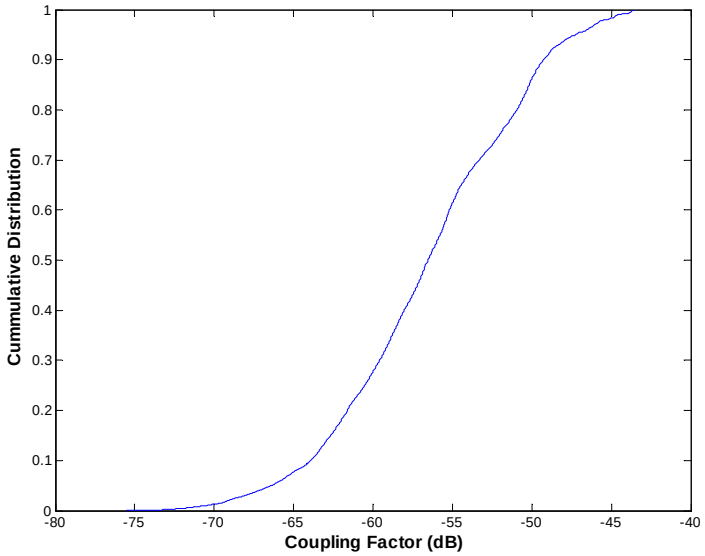

IPC Statistics		
Maximum	-43.5	dB
98 percentile	-45.3	dB
95 percentile	-47.2	dB
90 percentile	-49.2	dB
80 percentile	-50.9	dB
50 percentile	-56.6	dB
Mean	-53.1	dB
No. of Points	12821	
No. of Position Scans	32	
Freqs per Sweep	401	

Figure 4.1-7b: Cirrus SR-22 ATC IPC statistics.

4.1.6 TCAS

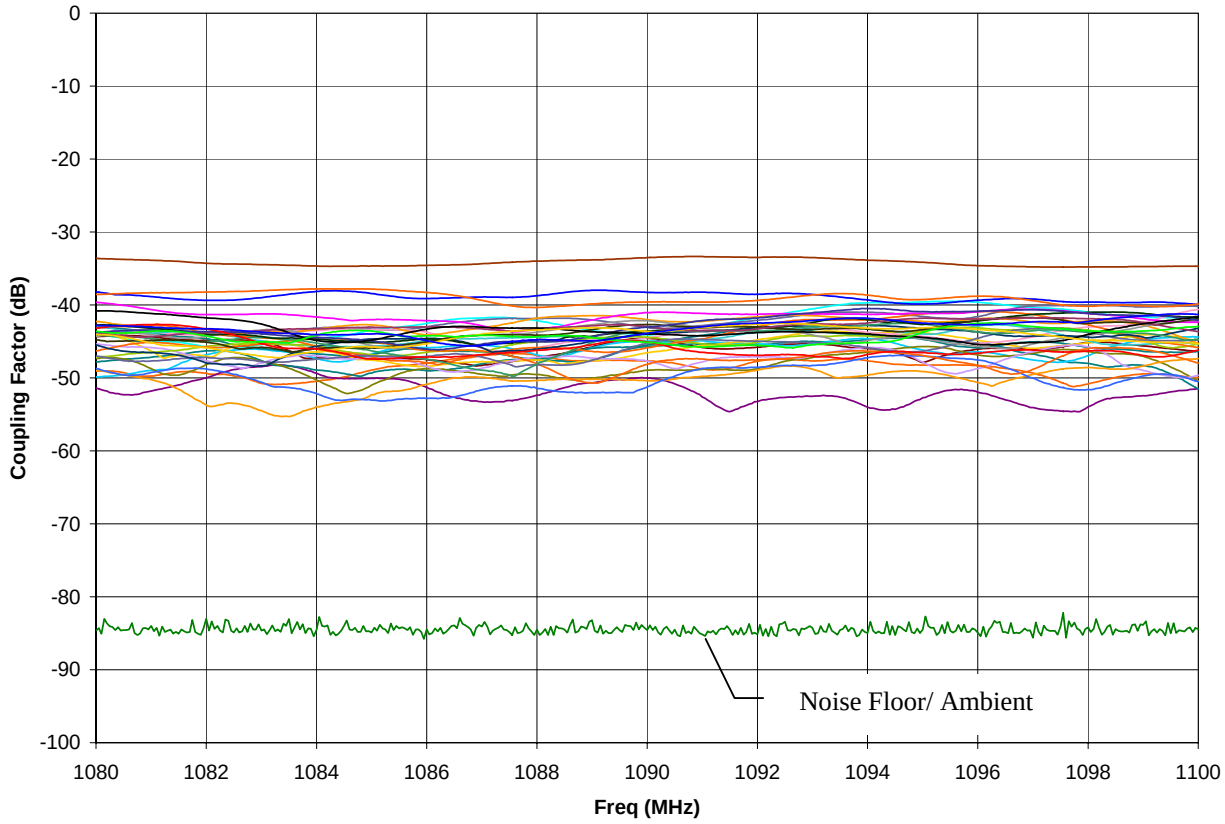

Figure 4.1-8a: Cirrus SR-22 TCAS IPC scans at locations within aircraft fuselage.

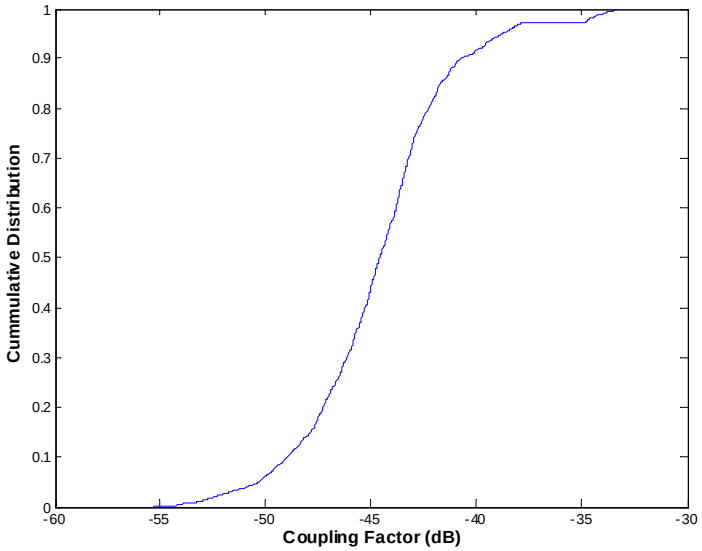

IPC Statistics		
Maximum	-33.4	dB
98 percentile	-34.6	dB
95 percentile	-38.7	dB
90 percentile	-40.7	dB
80 percentile	-42.3	dB
50 percentile	-44.6	dB
Mean	-43.0	dB
No. of Points	14436	
No. of Position Scans	36	
Freqs per Sweep	401	

Figure 4.1-8b: Cirrus SR-22 TCAS IPC statistics.

4.1.7 GPS2

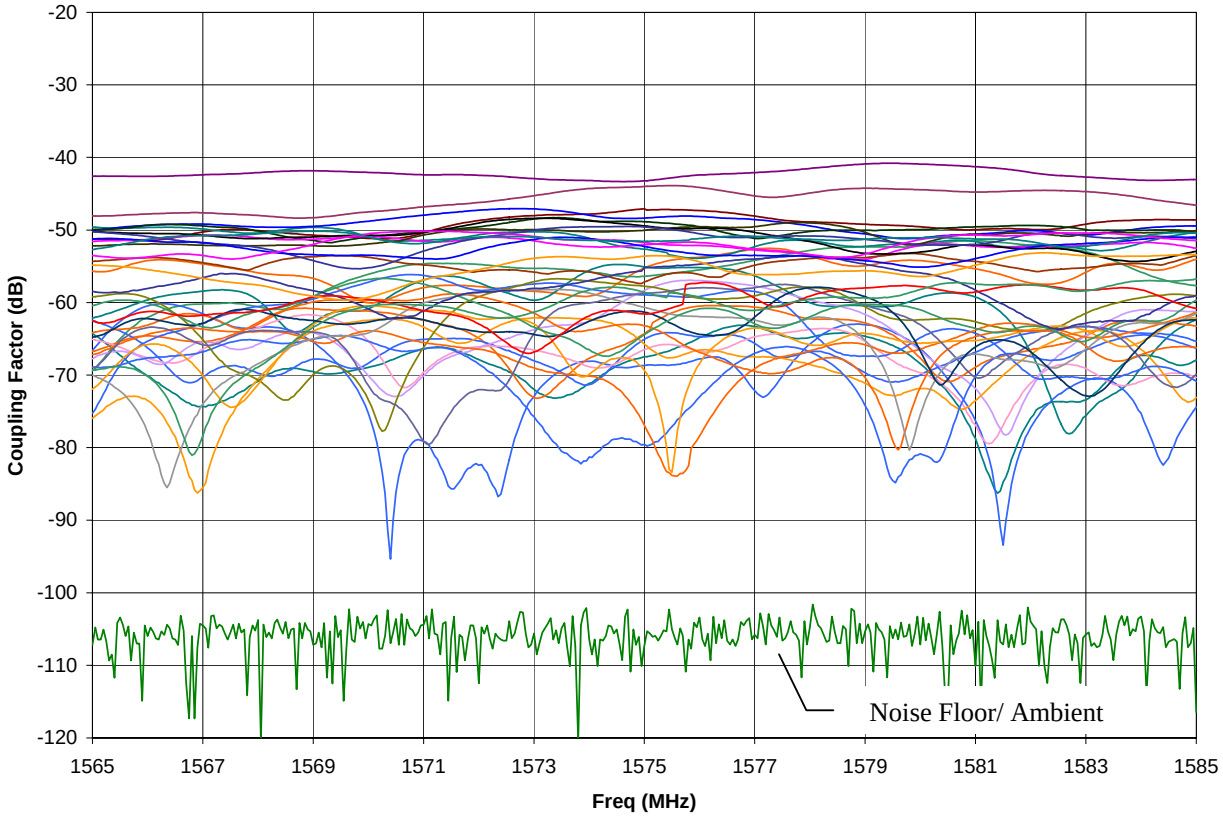

Figure 4.1-9a: Cirrus SR-22 GPS IPC scans at locations within aircraft fuselage.

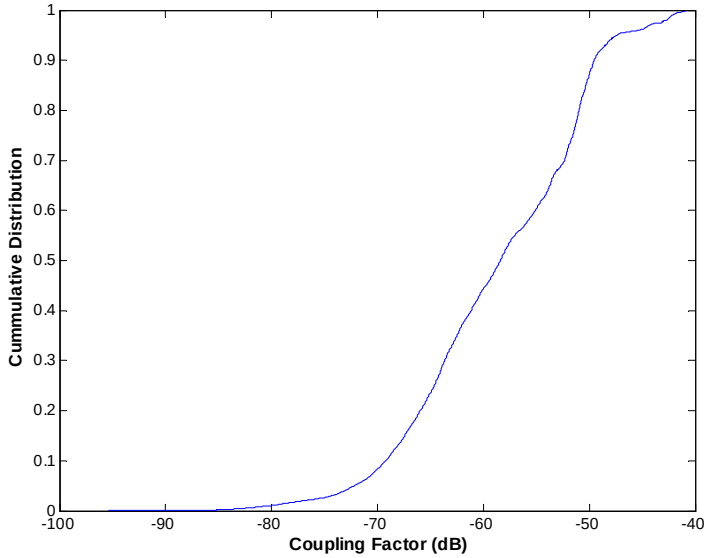

IPC Statistics		
Maximum	-40.8	dB
98 percentile	-42.7	dB
95 percentile	-47.4	dB
90 percentile	-49.6	dB
80 percentile	-51.0	dB
50 percentile	-58.4	dB
Mean	-52.6	dB
No. of Points	15238	
No. of Position Scans	38	
Freqs per Sweep	401	

Figure 4.1-9b: Cirrus SR-22 GPS IPC statistics.

4.2 Cessna 172R

Figure 4.2-1: Cessna 172R.

Figure 4.2-2: Powering the GPS antenna using a bias-Tee. External VHF antennas.

4.2.1 VOR/LOC

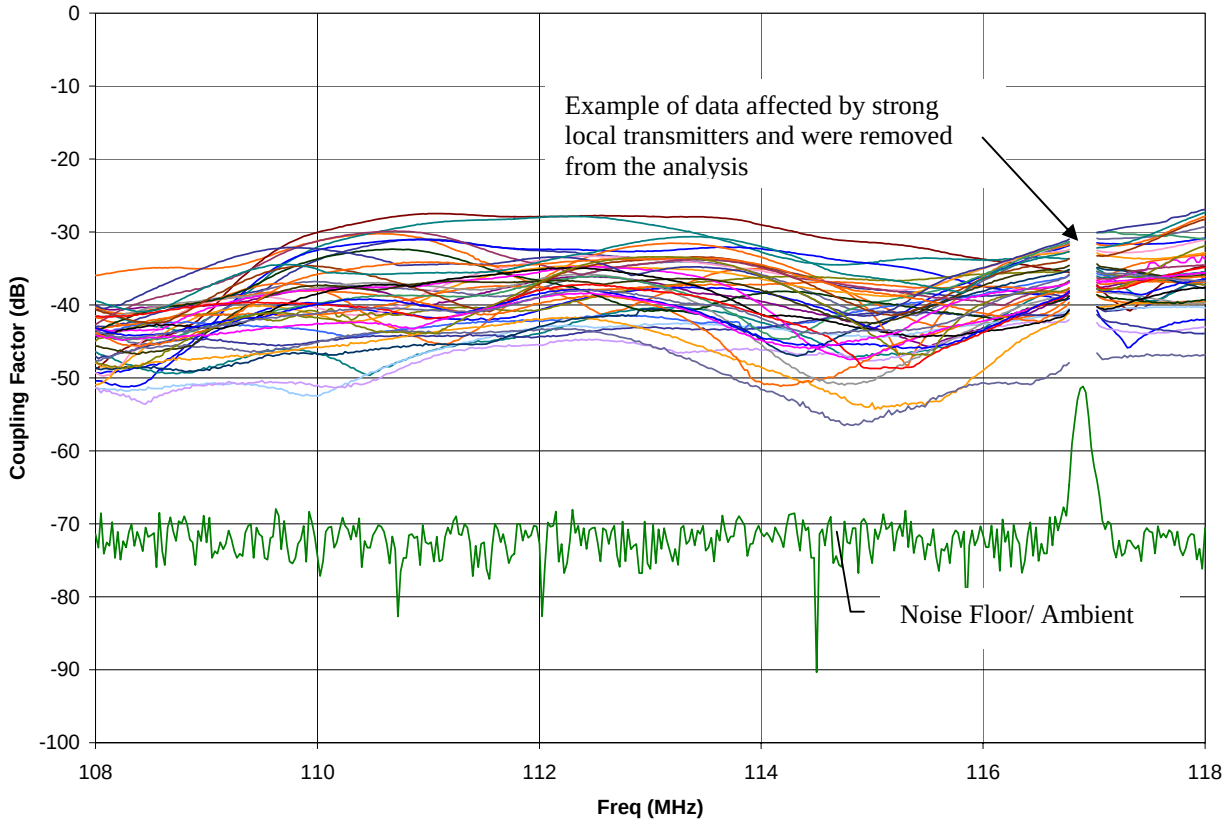

Figure 4.2-3a: Cessna 172R VOR/LOC IPC scans at locations within aircraft fuselage.

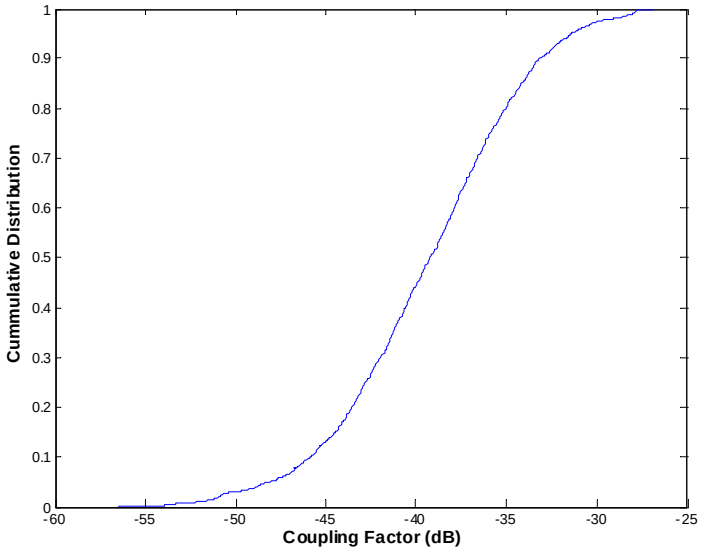

IPC Statistics		
Maximum	-26.9	dB
98 percentile	-29.2	dB
95 percentile	-31.3	dB
90 percentile	-33.1	dB
80 percentile	-35.0	dB
50 percentile	-39.2	dB
Mean	-36.7	dB
No. of Points	14896	
No. of Position Scans	38	
Freqs per Sweep	401	

Figure 4.2-3b: Cessna 172R VOR/LOC IPC statistics.

4.2.2 VHF-Com1

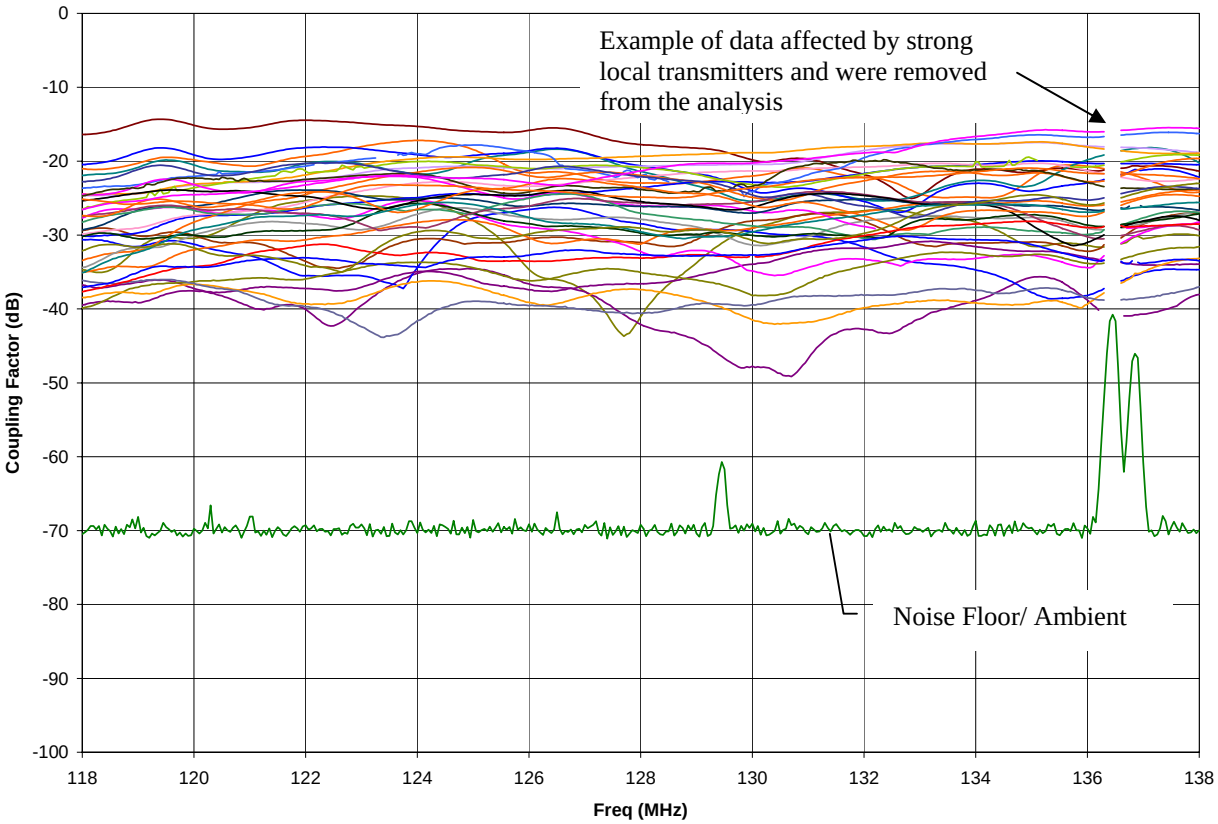

Figure 4.2-4a: Cessna 172R VHF-Com1 IPC scans at locations within aircraft fuselage.

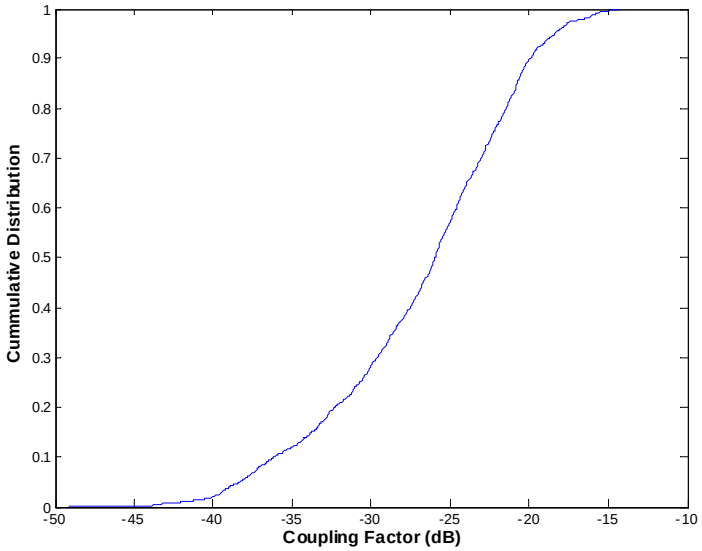

IPC Statistics		
Maximum	-14.3	dB
98 percentile	-16.5	dB
95 percentile	-18.3	dB
90 percentile	-20.0	dB
80 percentile	-21.5	dB
50 percentile	-26.1	dB
Mean	-23.7	dB
No. of Points	14520	
No. of Position Scans	37	
Freqs per Sweep	401	

Figure 4.2-4b: Cessna 172R VHF-Com1 IPC statistics.

4.2.3 GS

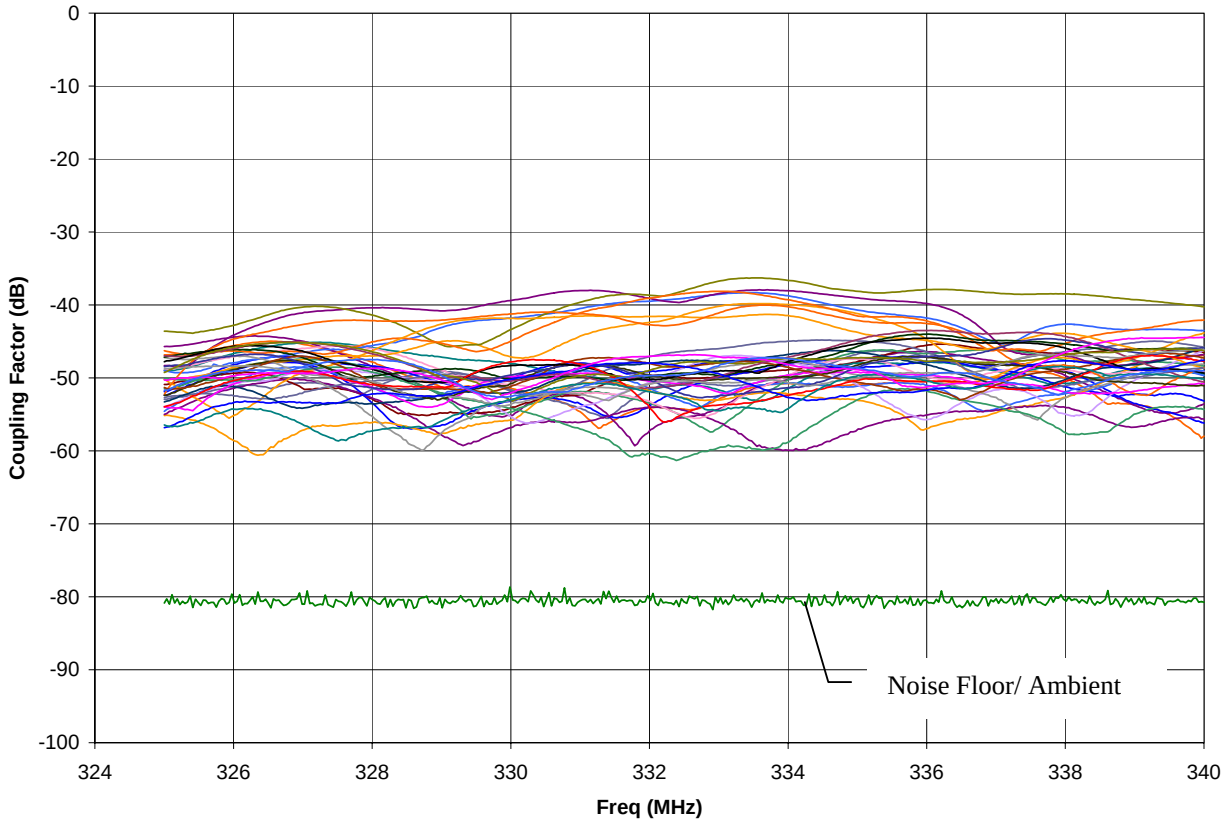

Figure 4.2-5a: Cessna 172R GS IPC scans at locations within aircraft fuselage.

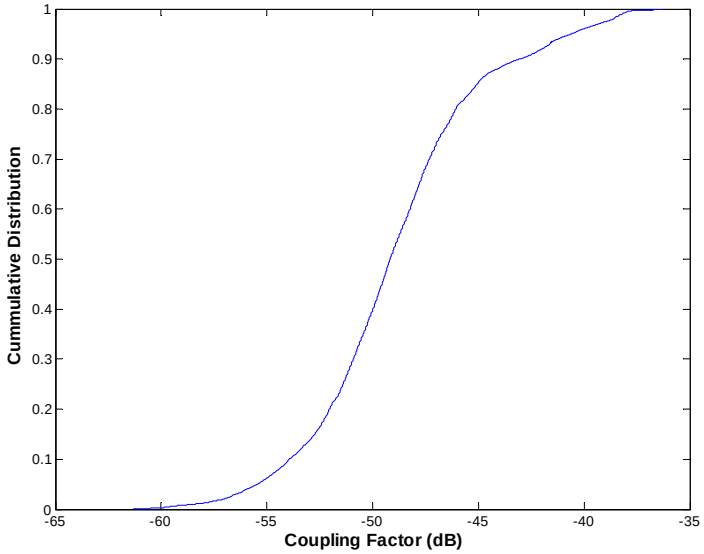

IPC Statistics		
Maximum	-36.3	dB
98 percentile	-38.6	dB
95 percentile	-40.6	dB
90 percentile	-43.0	dB
80 percentile	-46.1	dB
50 percentile	-49.2	dB
Mean	-46.6	dB
No. of Points	15238	
No. of Position Scans	38	
Freqs per Sweep	401	

Figure 4.2-5b: Cessna 172R GS IPC statistics.

4.2.4 ATC

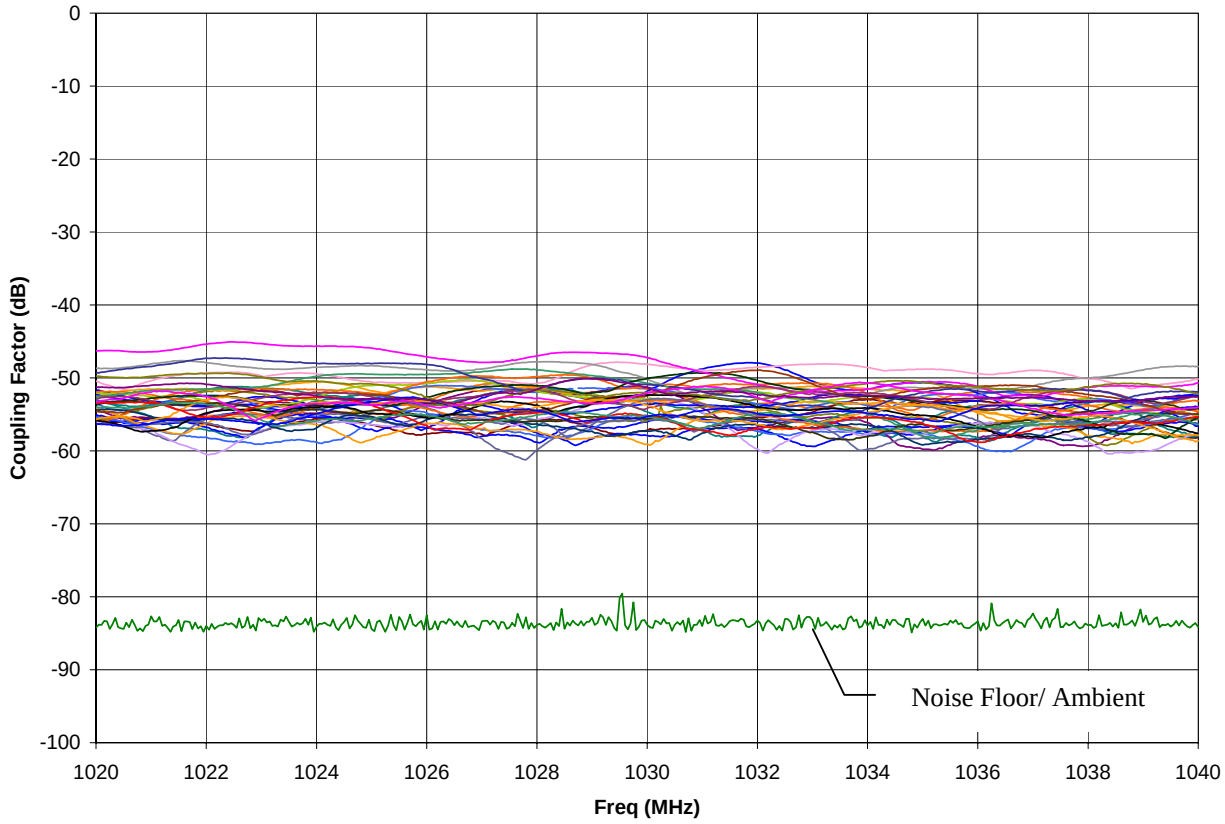

Figure 4.2-6a: Cessna 172R ATC IPC scans at locations within aircraft fuselage.

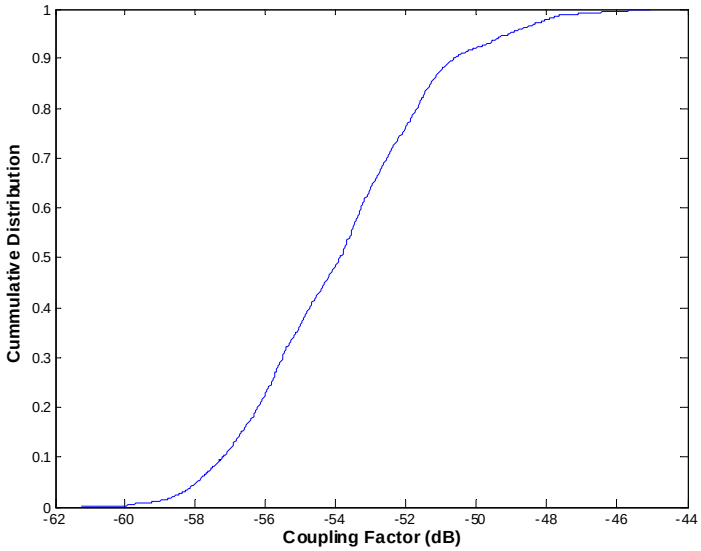

IPC Statistics		
Maximum	-45.1	dB
98 percentile	-47.9	dB
95 percentile	-49.0	dB
90 percentile	-50.6	dB
80 percentile	-51.7	dB
50 percentile	-53.9	dB
Mean	-53.02	dB
No. of Points	15226	
No. of Position Scans	38	
Freqs per Sweep	401	

Figure 4.2-6b: Cessna 172R ATC IPC statistics.

4.2.5 GPS

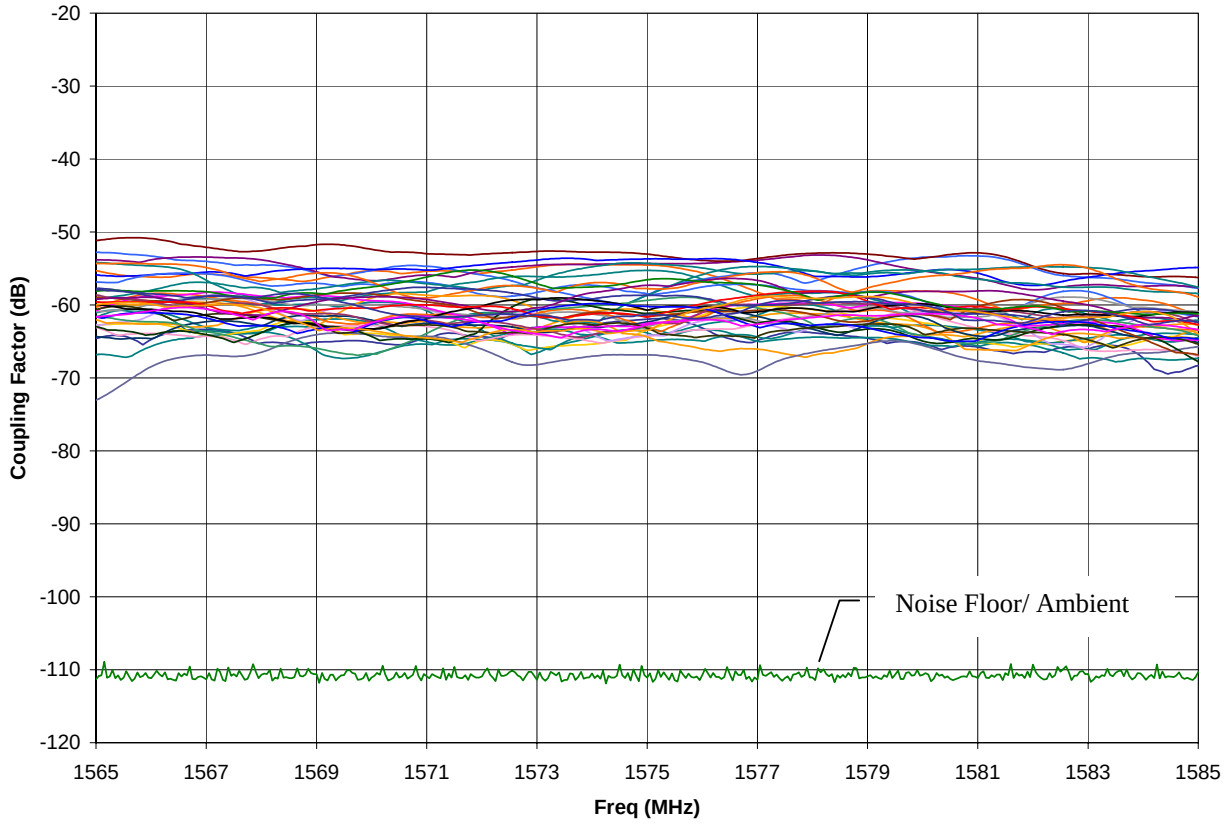

Figure 4.2-7a: Cessna 172R GPS IPC scans at locations within aircraft fuselage.

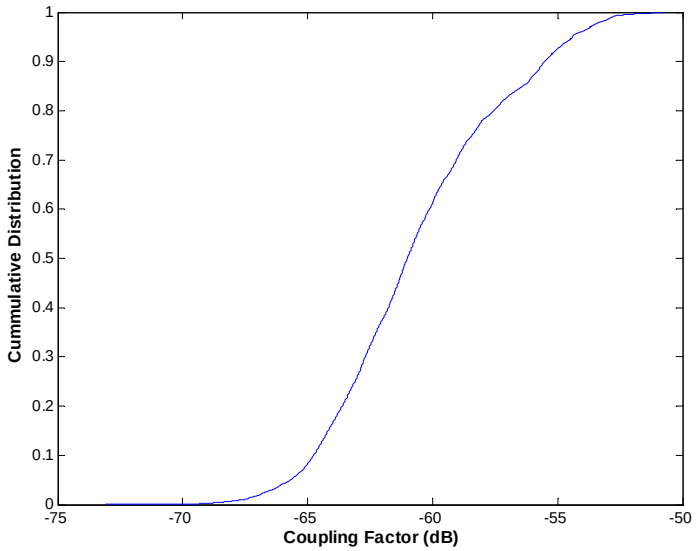

IPC Statistics		
Maximum	-50.8	dB
98 percentile	-53.3	dB
95 percentile	-54.4	dB
90 percentile	-55.5	dB
80 percentile	-57.6	dB
50 percentile	-61.0	dB
Mean	-59.2	dB
No. of Points	15238	
No. of Position Scans	38	
Freqs per Sweep	401	

Figure 4.2-7b: Cessna 172R GPS IPC statistics.

4.3 Bell 407

Figure 4.3-1: Bell 407 helicopter.

Figure 4.3-2: Spectrum analyzer and biconical antenna.

4.3.1 VOR/LOC

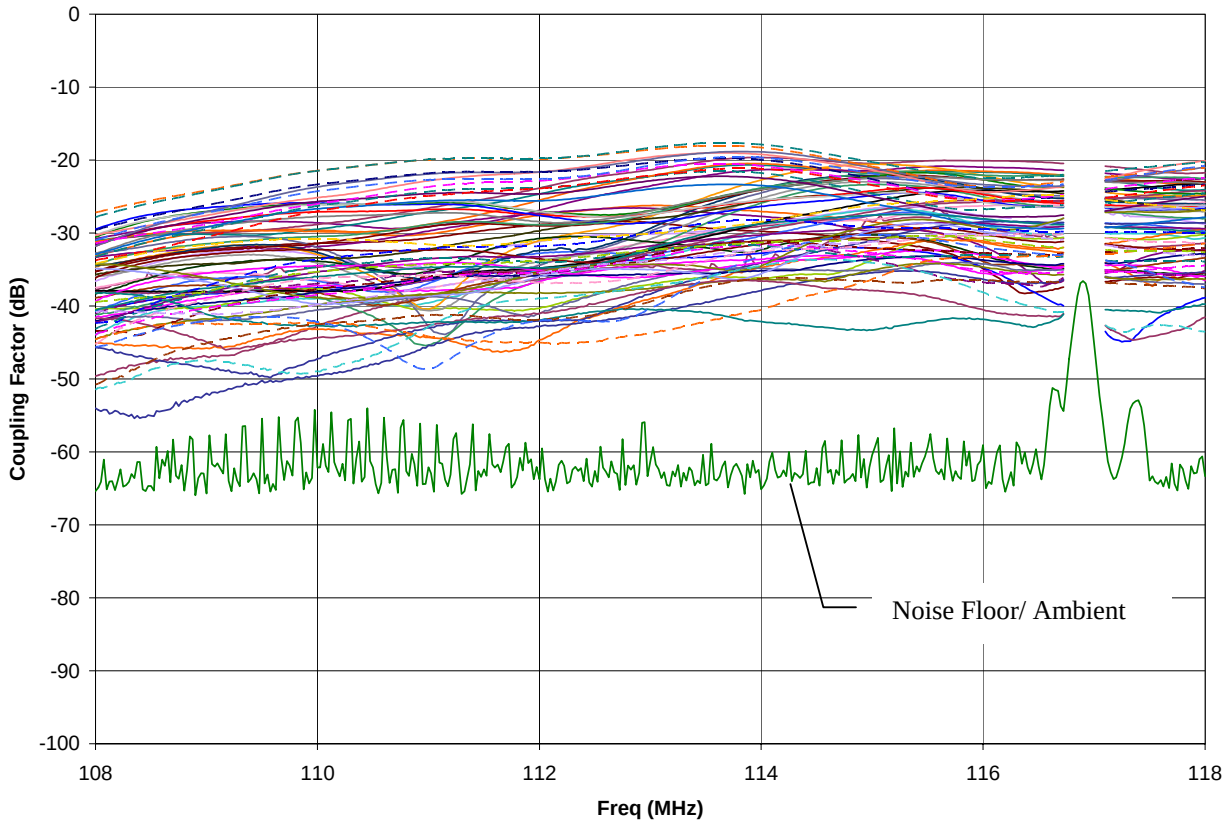

Figure 4.3-3a: Bell 407 VOR/LOC IPC scans at locations within aircraft fuselage.

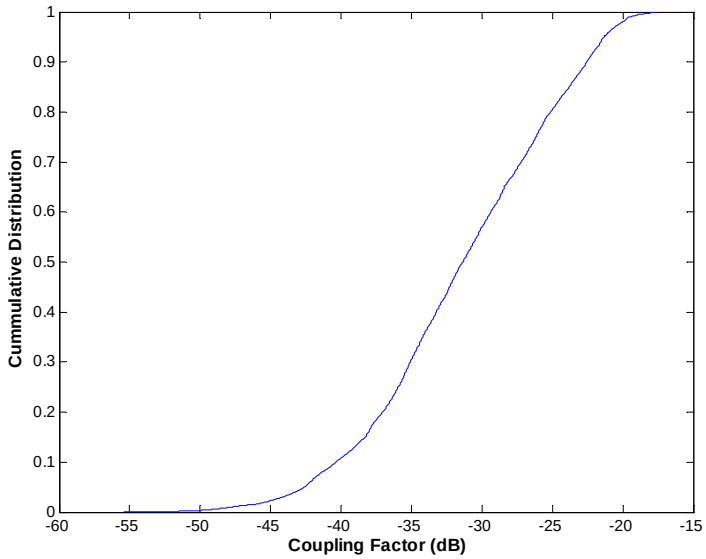

IPC Statistics		
Maximum	-17.6	dB
98 percentile	-20.0	dB
95 percentile	-21.3	dB
90 percentile	-22.6	dB
80 percentile	-25.1	dB
50 percentile	-31.4	dB
Mean	-27.3	dB
No. of Points	27453	
No. of Position Scans	71	
Freqs per Sweep	401	

Figure 4.3-3b: Bell 407 VOR/LOC IPC statistics.

4.3.2 VHF-Com1

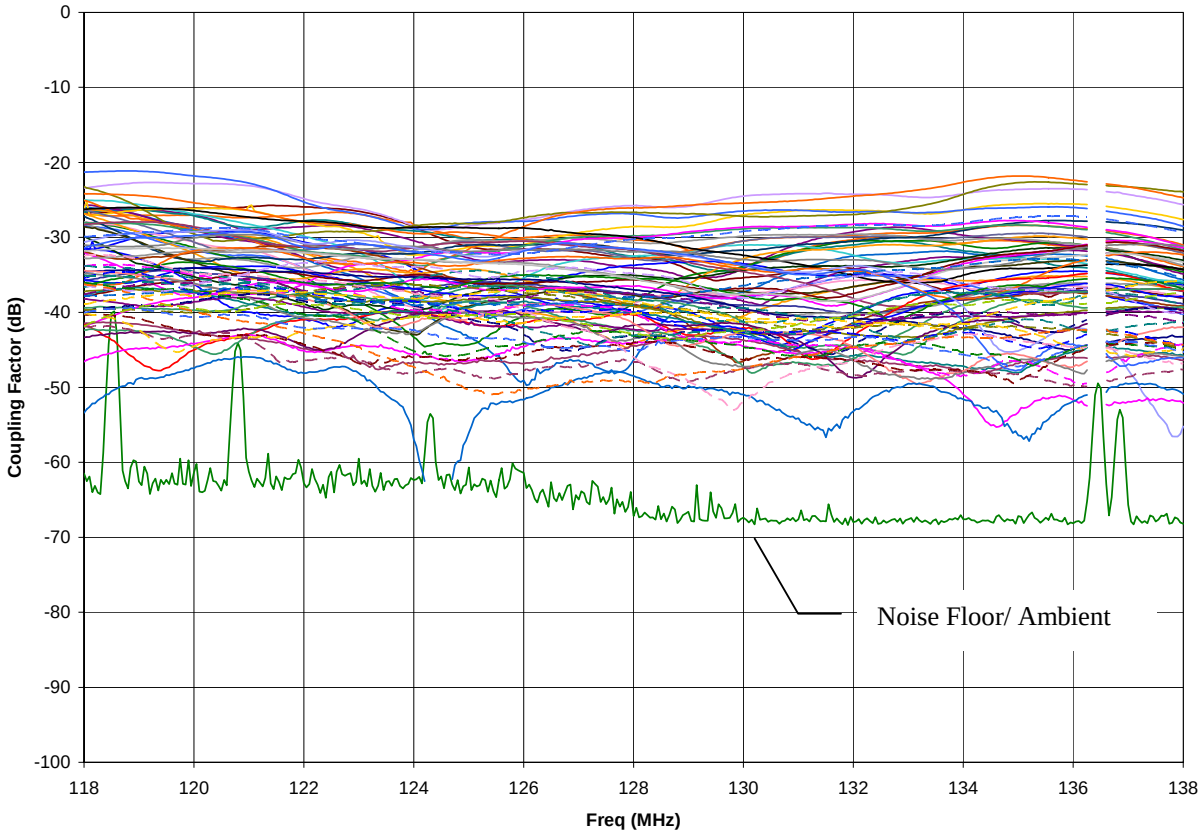

Figure 4.3-4a: Bell 407 VHF-Com1 IPC scans at locations within aircraft fuselage.

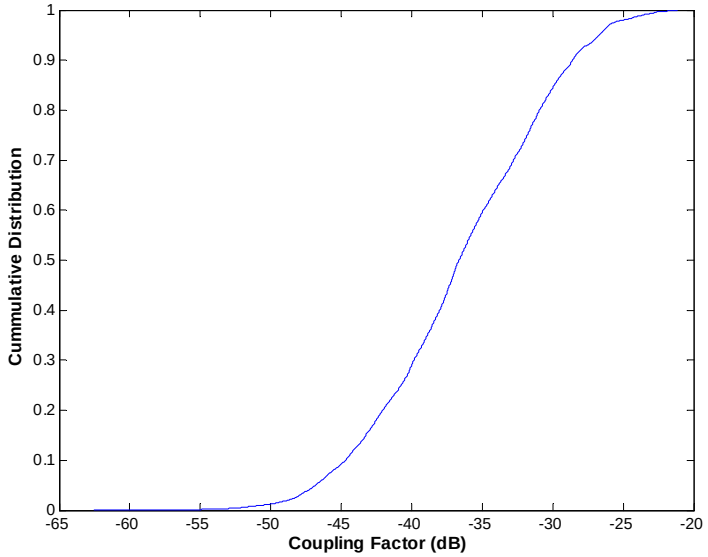

IPC Statistics		
Maximum	-21.2	dB
98 percentile	-25.1	dB
95 percentile	-26.7	dB
90 percentile	-28.6	dB
80 percentile	-30.9	dB
50 percentile	-36.6	dB
Mean	-32.7	dB
No. of Points	29221	
No. of Position Scans	74	
Freqs per Sweep	401	

Figure 4.3-4b: Bell 407 VHF-Com1 IPC statistics.

4.3.3 ATC

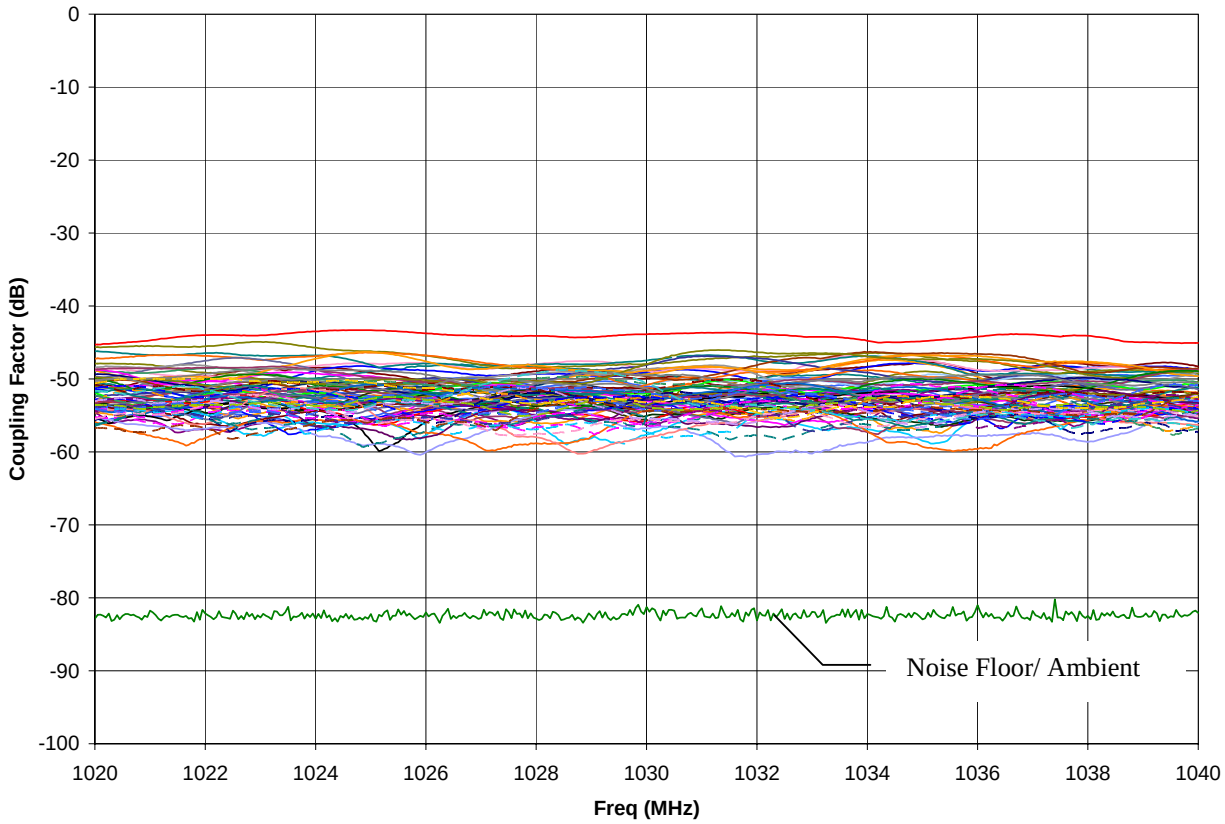

Figure 4.3-5a: Bell 407 ATC IPC scans at locations within aircraft fuselage.

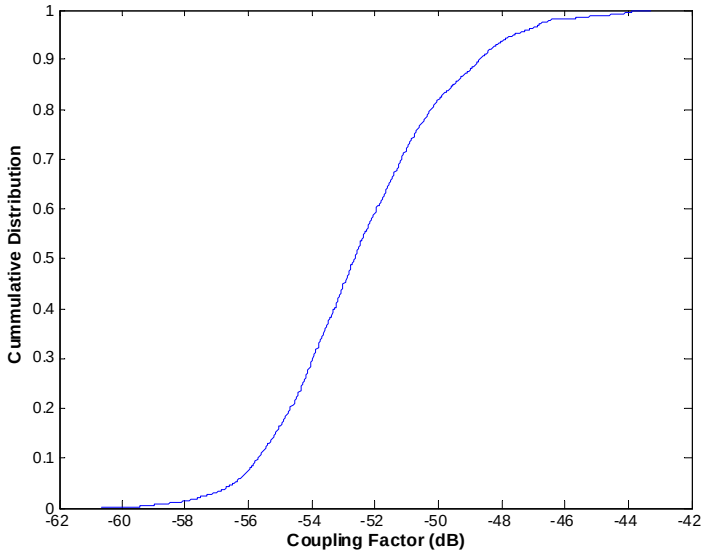

IPC Statistics		
Maximum	-43.3	dB
98 percentile	-46.4	dB
95 percentile	-47.6	dB
90 percentile	-48.7	dB
80 percentile	-50.2	dB
50 percentile	-52.7	dB
Mean	-51.5	dB
No. of Points	29592	
No. of Position Scans	74	
Freqs per Sweep	401	

Figure 4.3-5b: Bell 407 ATC IPC statistics.

4.3.4 GPS

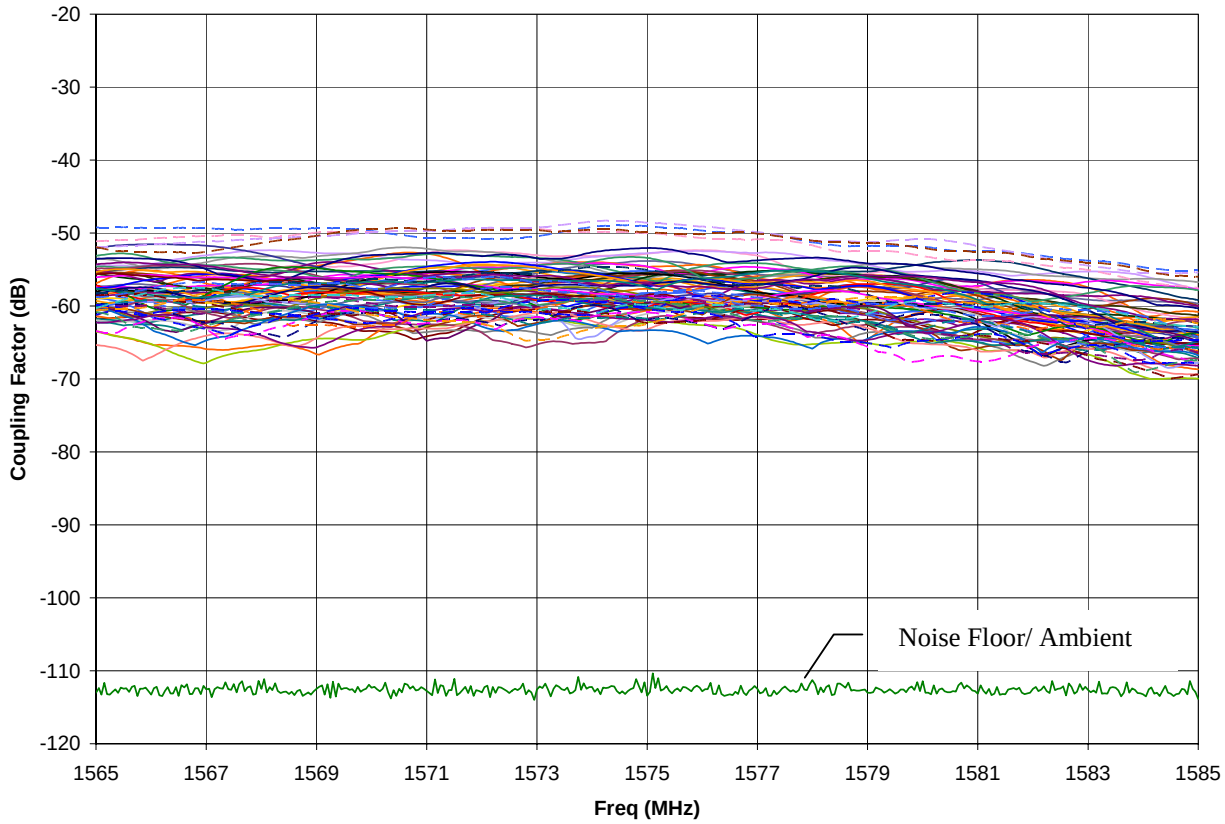

Figure 4.3-6a: Bell 407 GPS IPC scans at locations within aircraft fuselage.

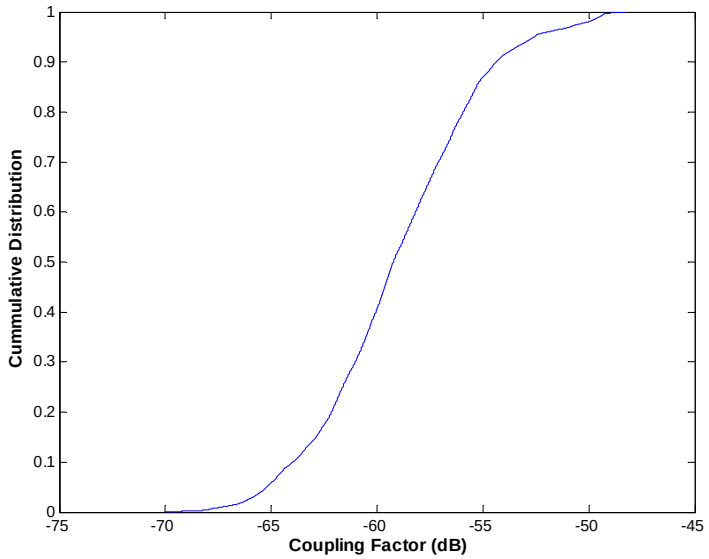

IPC Statistics		
Maximum	-48.3	dB
98 percentile	-50.0	dB
95 percentile	-52.6	dB
90 percentile	-54.4	dB
80 percentile	-55.9	dB
50 percentile	-59.2	dB
Mean	-57.3	dB
No. of Points	29273	
No. of Position Scans	73	
Freqs per Sweep	401	

Figure 4.3-6b: Bell 407 GPS IPC statistics.

4.4 LearJet 35A

Figure 4.4-1: LearJet 35A.

Figure 4.4-2: LearJet 35A avionic bay.

4.4.1 VOR/LOC

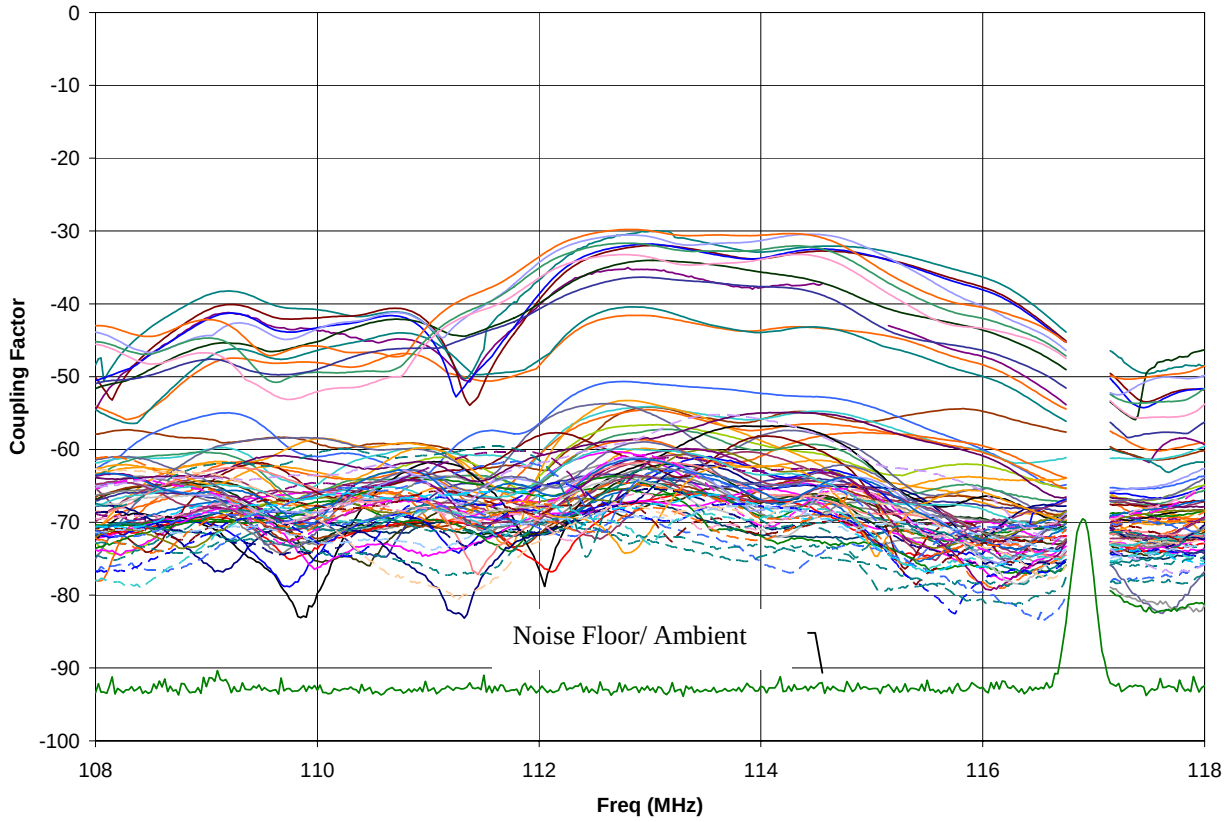

Figure 4.4-3a: LearJet 35A VOR/LOC IPC scans at locations within aircraft fuselage.

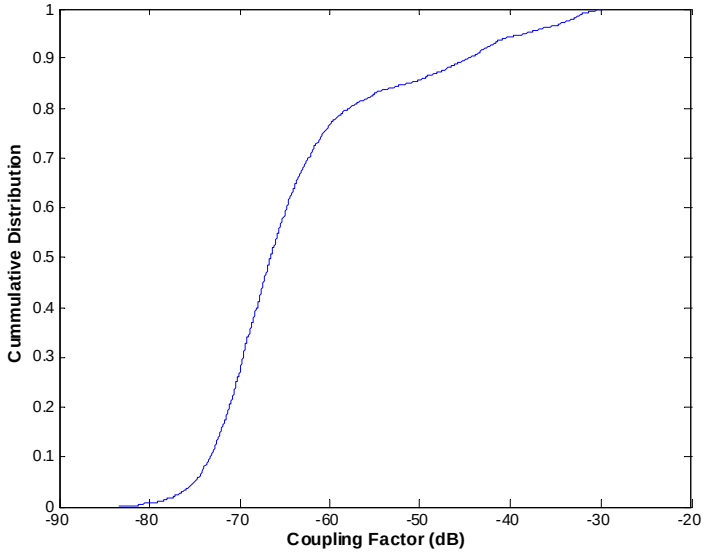

IPC Statistics		
Maximum	-29.8	dB
98 percentile	-32.9	dB
95 percentile	-38.3	dB
90 percentile	-44.7	dB
80 percentile	-57.8	dB
50 percentile	-66.6	dB
Mean	-45.6	dB
No. of Points	27769	
No. of Position Scans	72	
Freqs per Sweep	401	

Figure 4.4-3a: LearJet 35A VOR/LOC IPC statistics.

4.4.2 VHF-Com2

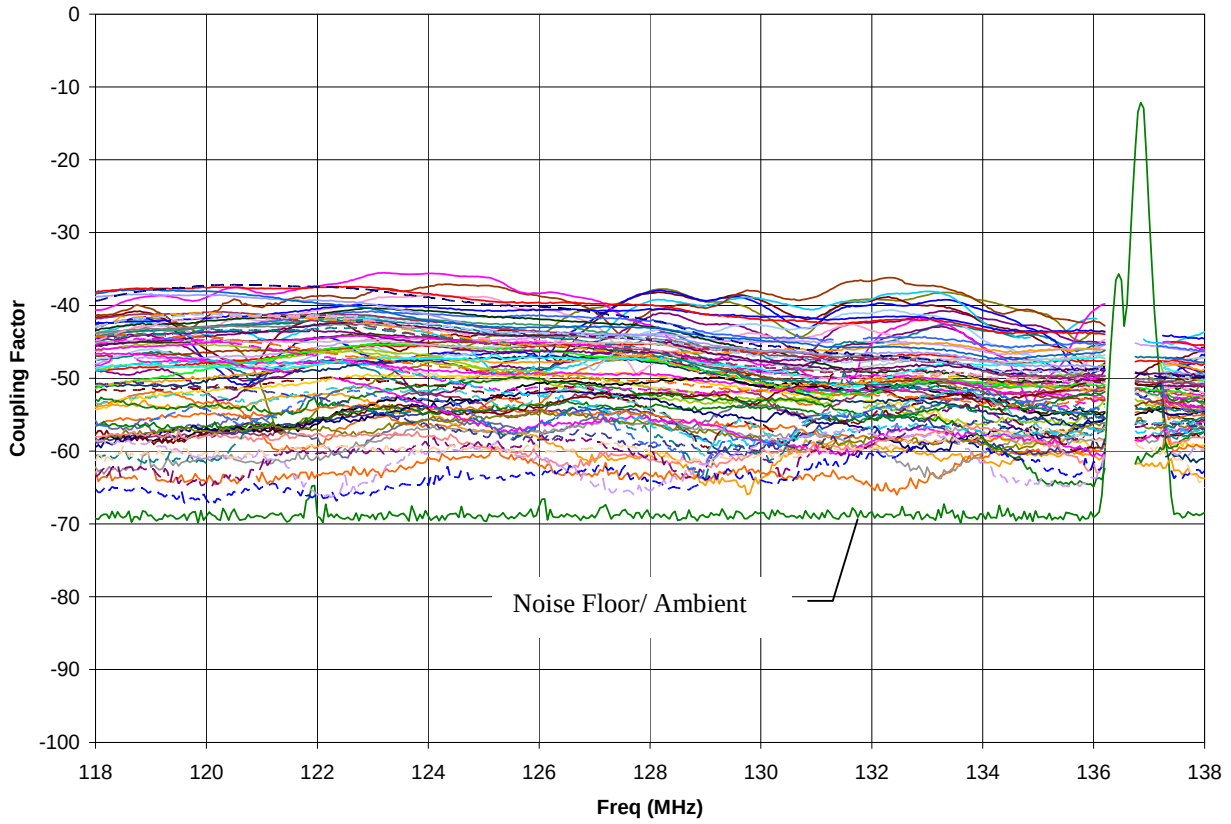

Figure 4.4-4a: LearJet 35A VHF-Com2 IPC scans at locations within aircraft fuselage.

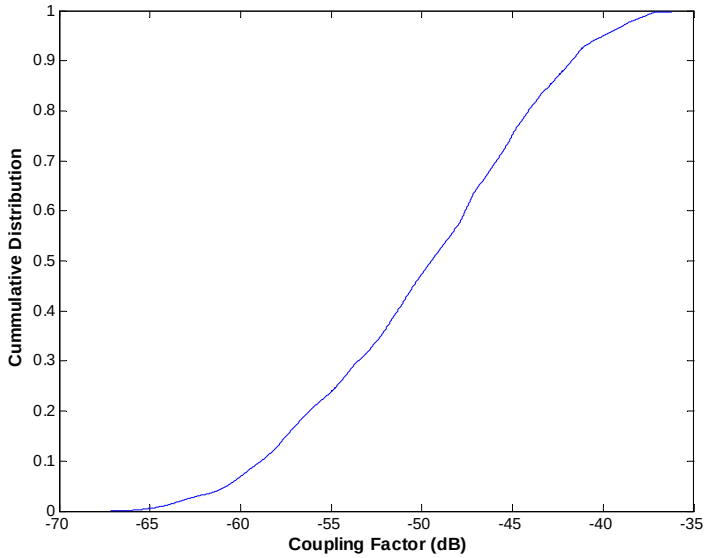

IPC Statistics		
Maximum	-35.5	dB
98 percentile	-38.3	dB
95 percentile	-40.0	dB
90 percentile	-41.7	dB
80 percentile	-44.1	dB
50 percentile	-49.5	dB
Mean	-46.0	dB
No. of Points	27549	
No. of Position Scans	72	
Freqs per Sweep	401	

Figure 4.4-4b: LearJet 35A VHF-Com2 IPC statistics.

4.4.3 GS

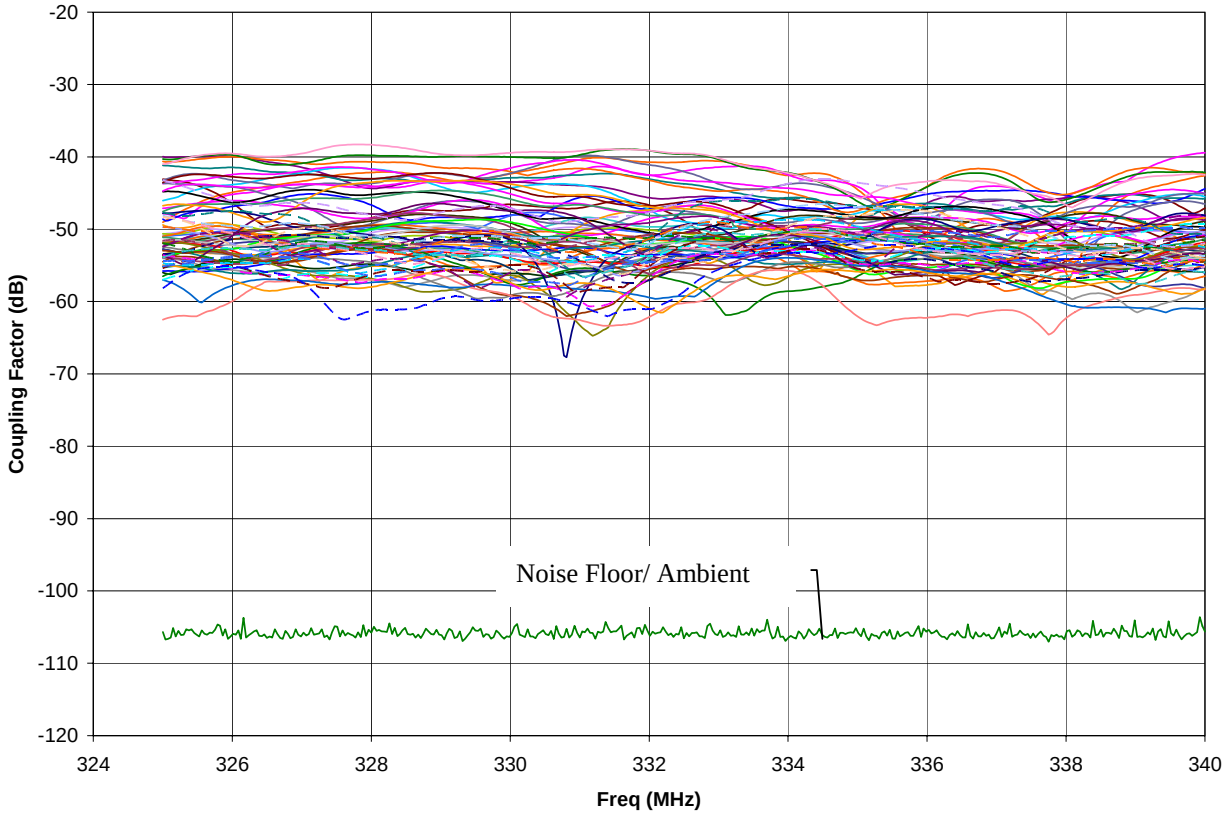

Figure 4.4-5a: LearJet 35A GS IPC scans at locations within aircraft fuselage.

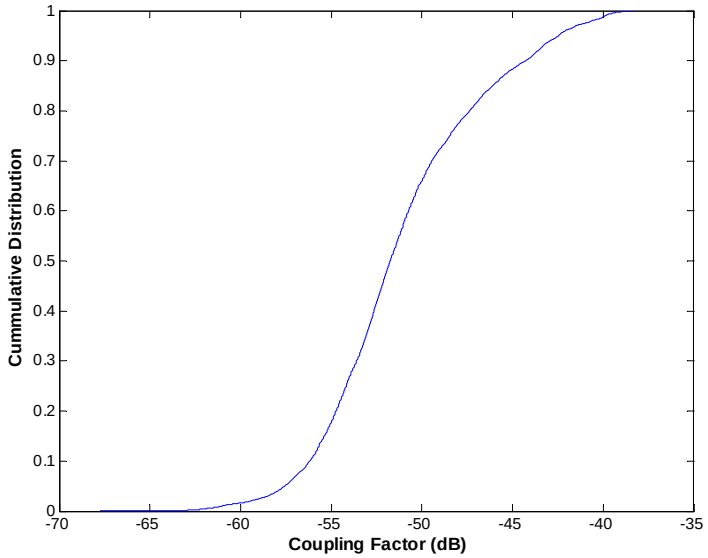

IPC Statistics		
Maximum	-38.3	dB
98 percentile	-40.6	dB
95 percentile	-42.5	dB
90 percentile	-44.2	dB
80 percentile	-47.4	dB
50 percentile	-51.7	dB
Mean	-48.5	dB
No. of Points	28872	
No. of Position Scans	72	
Freqs per Sweep	401	

Figure 4.4-5b: LearJet 35A GS IPC statistics.

4.4.4 DME1

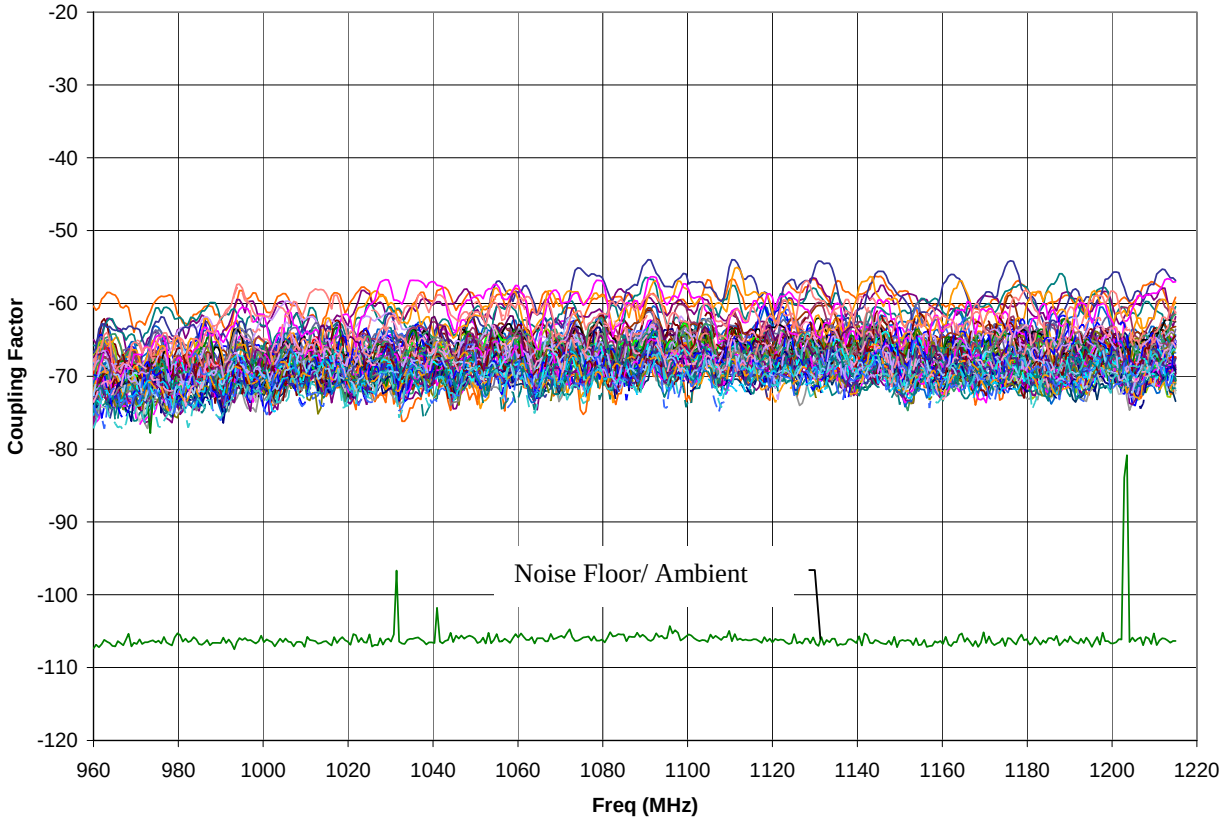

Figure 4.4-6a: LearJet 35A DME1 IPC scans at locations within aircraft fuselage.

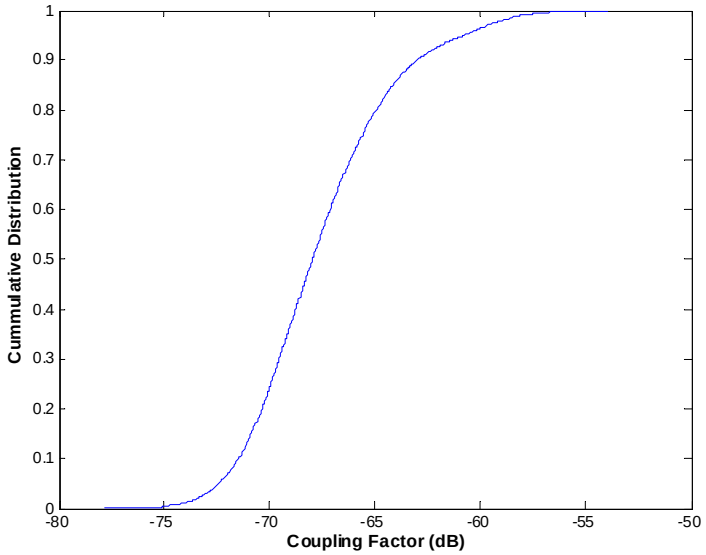

IPC Statistics		
Maximum	-54.0	dB
98 percentile	-58.9	dB
95 percentile	-60.8	dB
90 percentile	-63.0	dB
80 percentile	-64.9	dB
50 percentile	-68.0	dB
Mean	-65.9	dB
No. of Points	28872	
No. of Position Scans	72	
Freqs per Sweep	401	

Figure 4.4-6b: LearJet 35A DME1 IPC statistics.

4.4.5 ATC

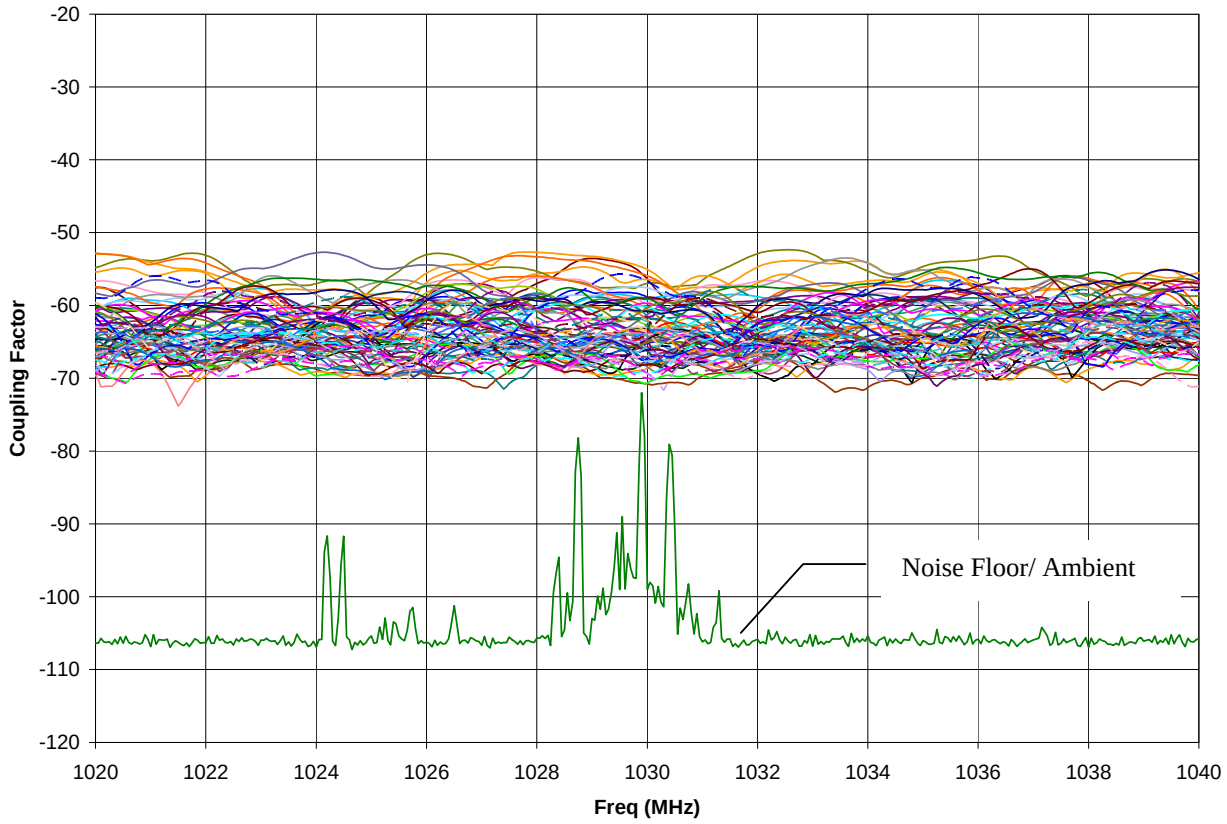

Figure 4.4-7a: LearJet 35A ATC IPC scans at locations within aircraft fuselage.

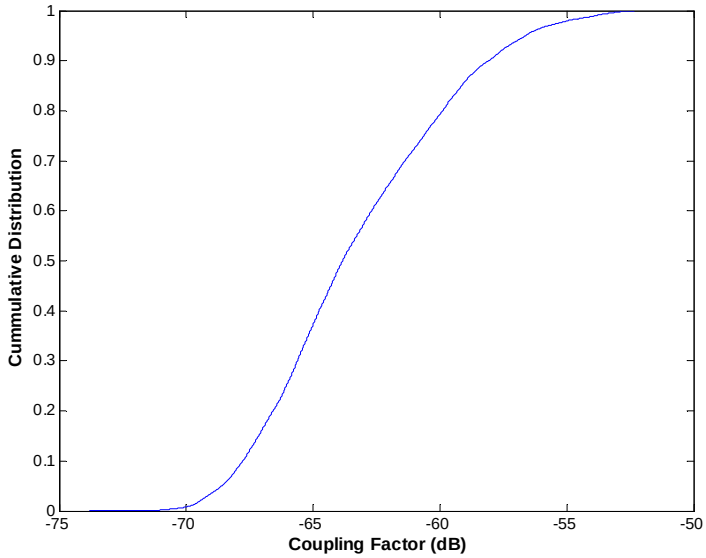

IPC Statistics		
Maximum	-52.4	dB
98 percentile	-54.9	dB
95 percentile	-56.6	dB
90 percentile	-58.1	dB
80 percentile	-59.9	dB
50 percentile	-63.8	dB
Mean	-61.6	dB
No. of Points	28872	
No. of Position Scans	72	
Freqs per Sweep	401	

Figure 4.4-7b: LearJet 35A ATC IPC statistics.

4.4.6 GPS

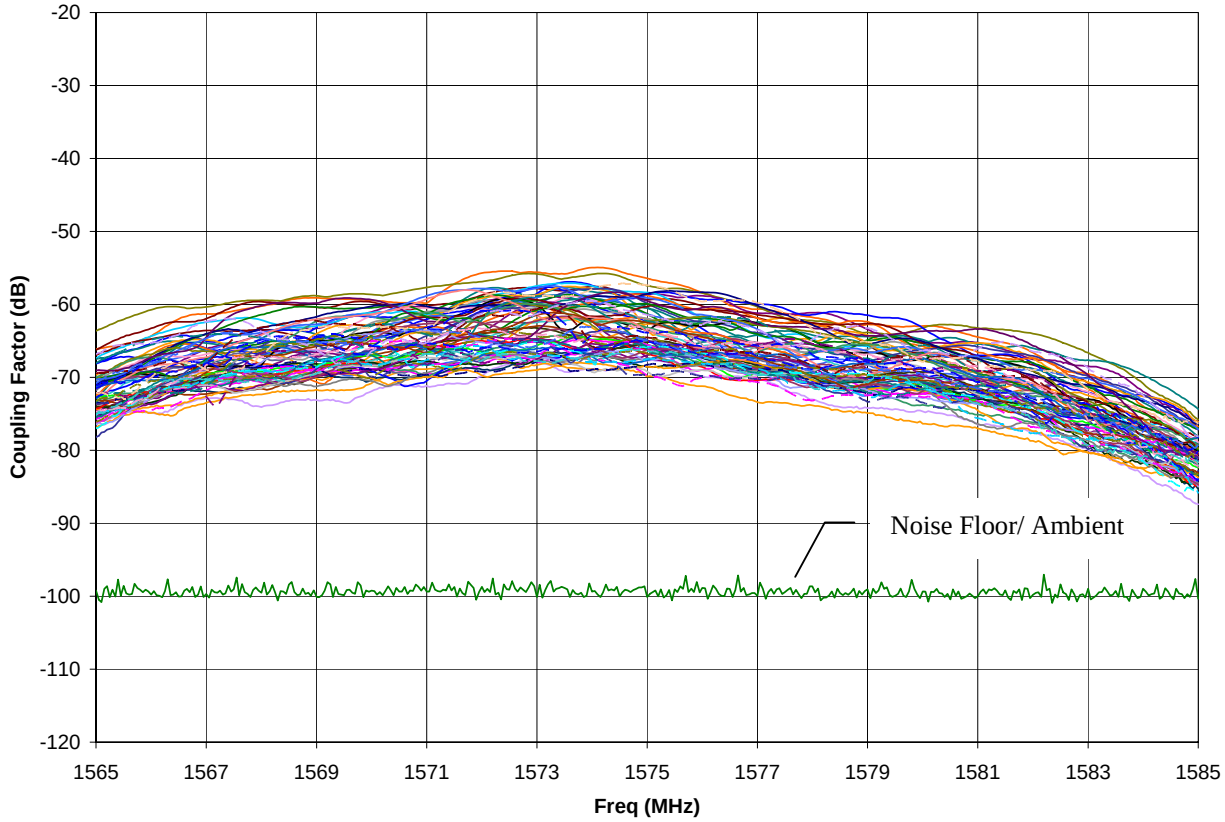

Figure 4.4-8a: LearJet 35A GPS IPC scans at locations within aircraft fuselage.

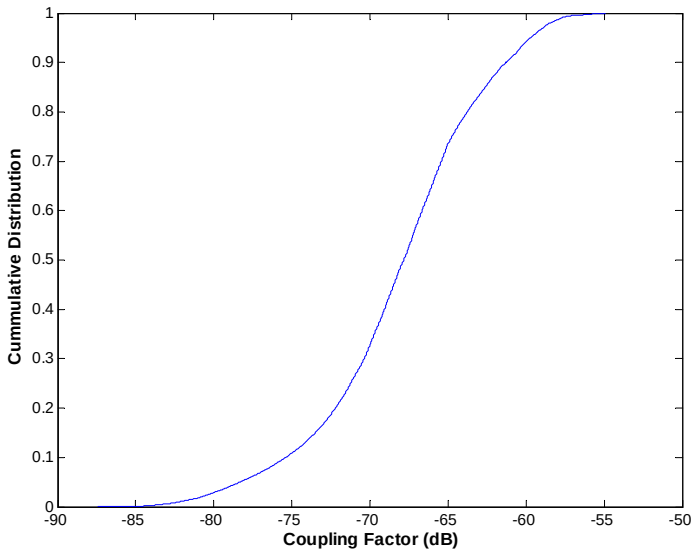

IPC Statistics		
Maximum	-54.9	dB
98 percentile	-58.4	dB
95 percentile	-59.7	dB
90 percentile	-61.3	dB
80 percentile	-63.8	dB
50 percentile	-67.8	dB
Mean	-65.4	dB
No. of Points	28872	
No. of Position Scans	72	
Freqs per Sweep	401	

Figure 4.4-8b: LearJet 35A GPS IPC statistics.

4.5 Sabreliner 65

Figure 4.5-1: Sabreliner 65.

4.5.1 VOR/LOC

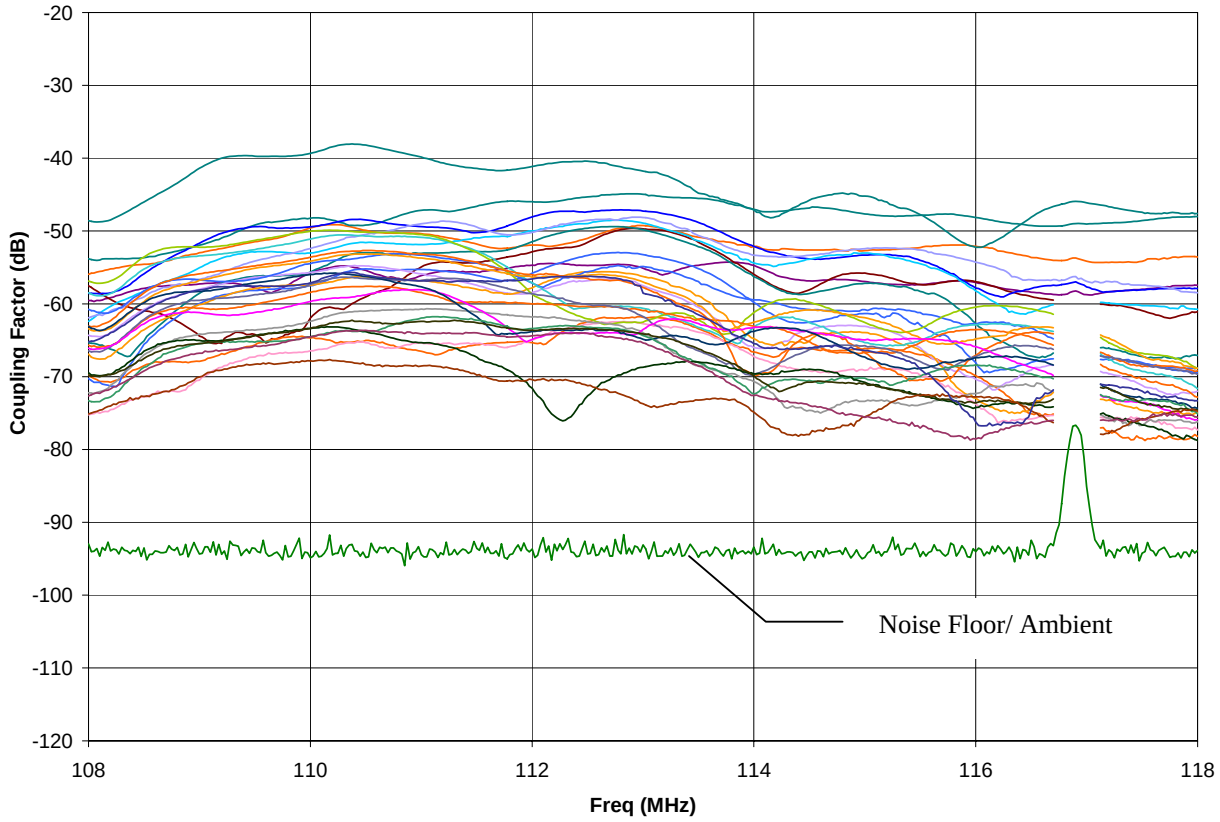

Figure 4.5-2a: Sabreliner 65 VOR/LOC IPC scans at locations within aircraft fuselage.

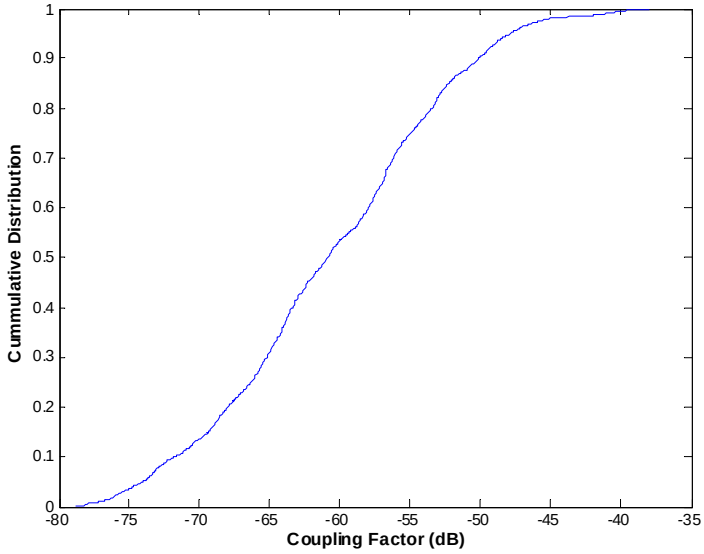

IPC Statistics		
Maximum	-38.1	dB
98 percentile	-45.2	dB
95 percentile	-47.9	dB
90 percentile	-50.1	dB
80 percentile	-53.5	dB
50 percentile	-60.9	dB
Mean	-53.6	dB
No. of Points	11646	
No. of Position Scans	30	
Freqs per Sweep	401	

Figure 4.5-2b: Sabreliner 65 VOR/LOC IPC statistics.

4.5.2 GS

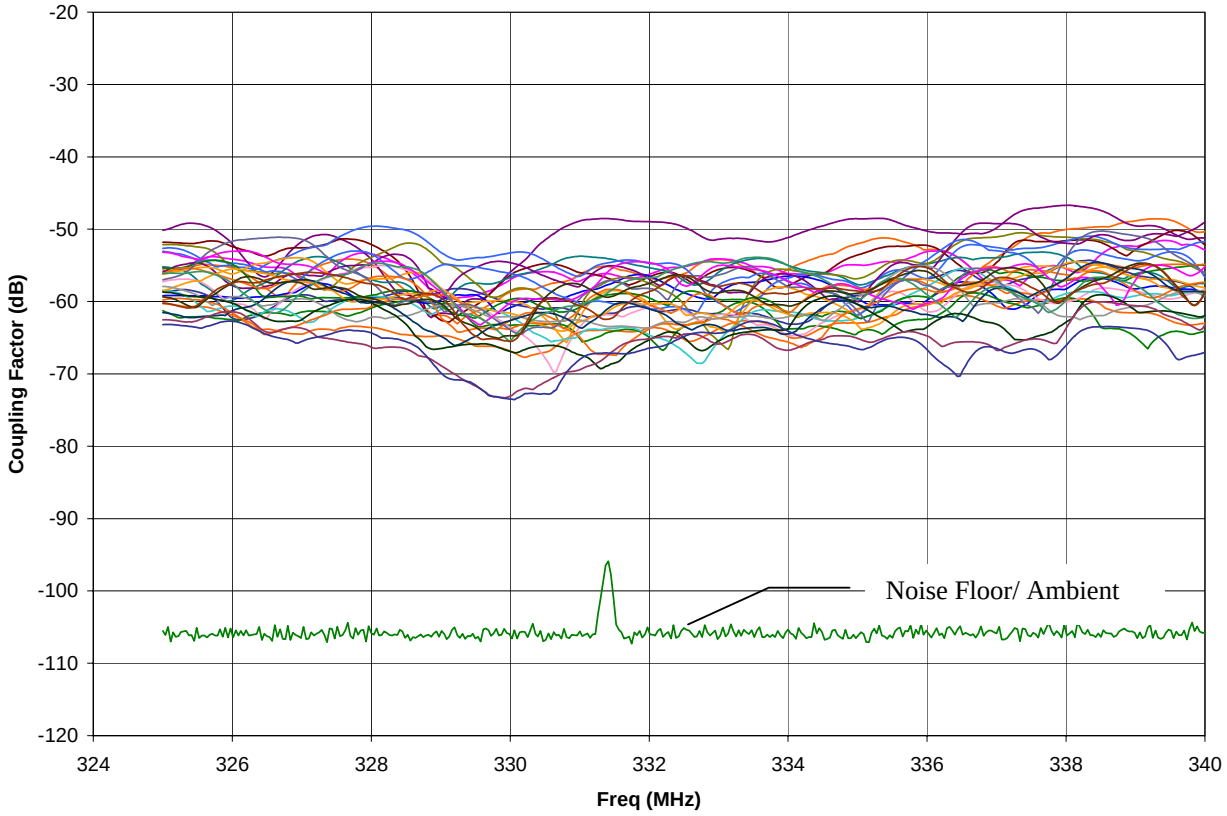

Figure 4.5-3a: Sabreliner 65 GS IPC scans at locations within aircraft fuselage.

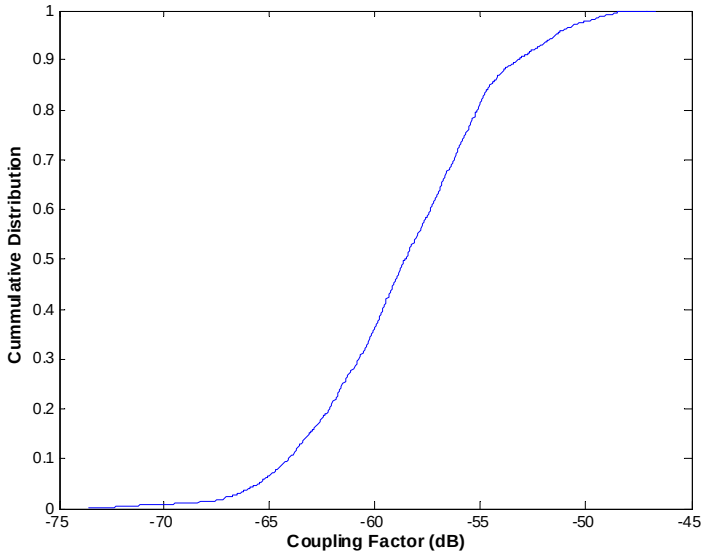

IPC Statistics		
Maximum	-46.7	dB
98 percentile	-49.8	dB
95 percentile	-51.4	dB
90 percentile	-53.2	dB
80 percentile	-55.2	dB
50 percentile	-58.6	dB
Mean	-56.61	dB
No. of Points	12030	
No. of Position Scans	30	
Freqs per Sweep	401	

Figure 4.5-3b: Sabreliner 65 GS IPC statistics.

4.5.3 GPS

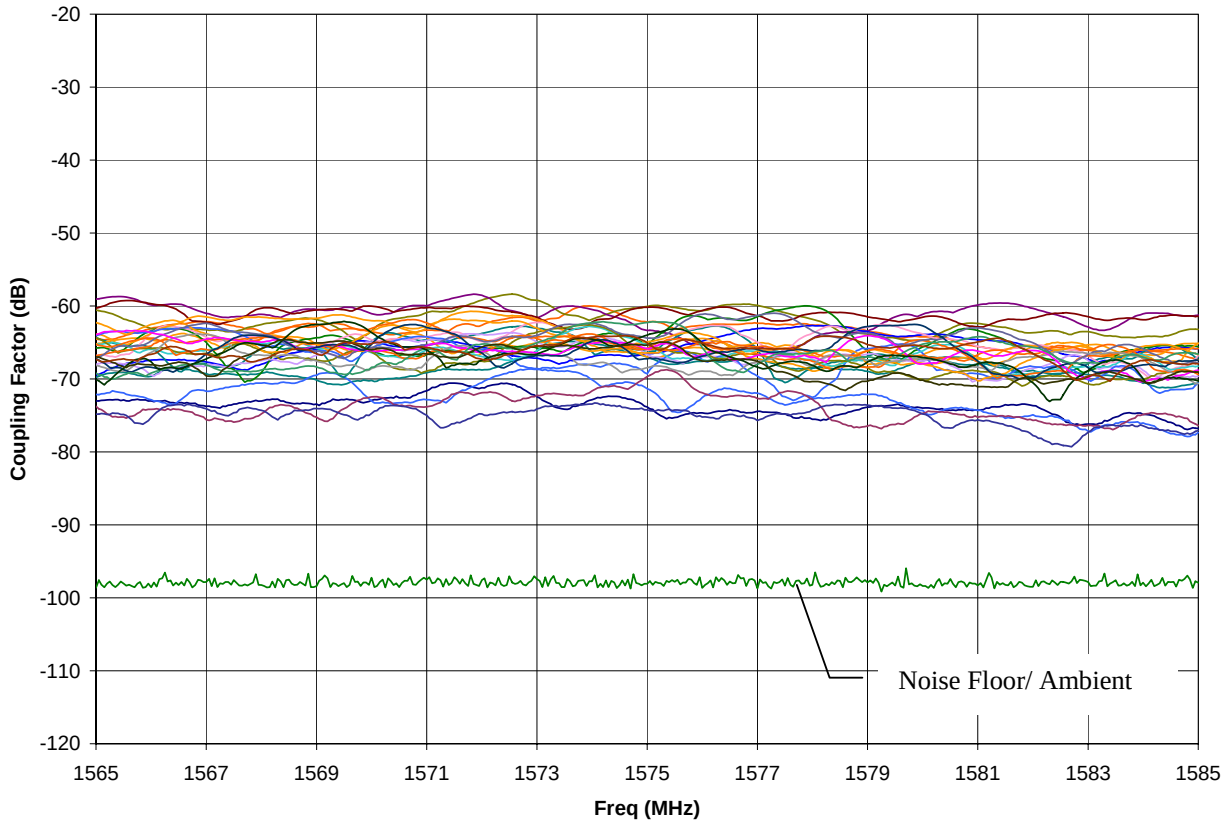

Figure 4.5-4a: Sabreliner 65 GPS IPC scans at locations within aircraft fuselage.

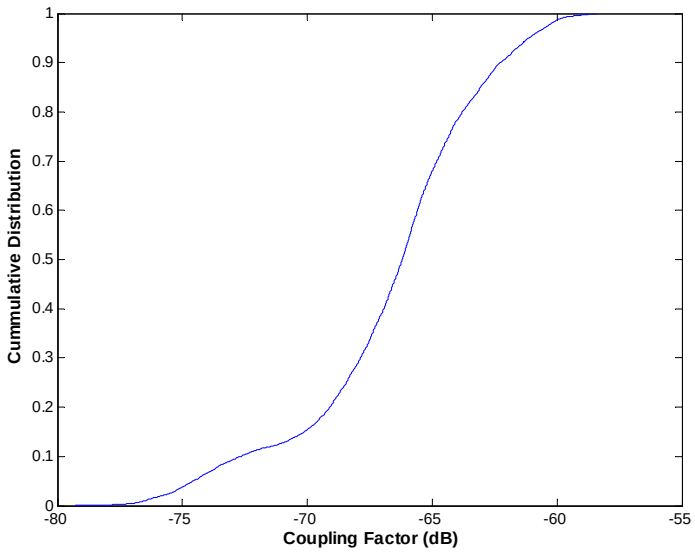

IPC Statistics		
Maximum	-58.4	dB
98 percentile	-60.2	dB
95 percentile	-61.1	dB
90 percentile	-62.3	dB
80 percentile	-63.8	dB
50 percentile	-66.2	dB
Mean	-65.3	dB
No. of Points	12030	
No. of Position Scans	30	
Freqs per Sweep	401	

Figure 4.5-4b: Sabreliner 65 GPS IPC statistics.

4.6 Citation II

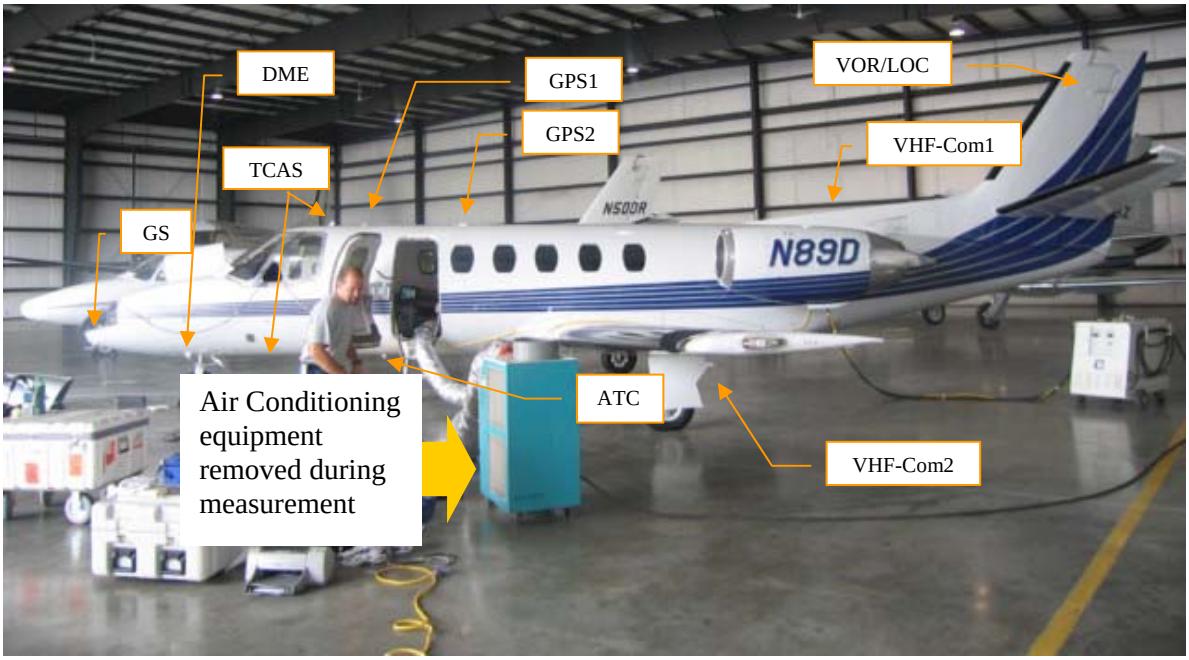

Figure 4.6-1: Citation II.

Figure 4.6-2: Cables to the outsides were taped tightly to the body to minimize re-radiation.

4.6.1 VOR/LOC

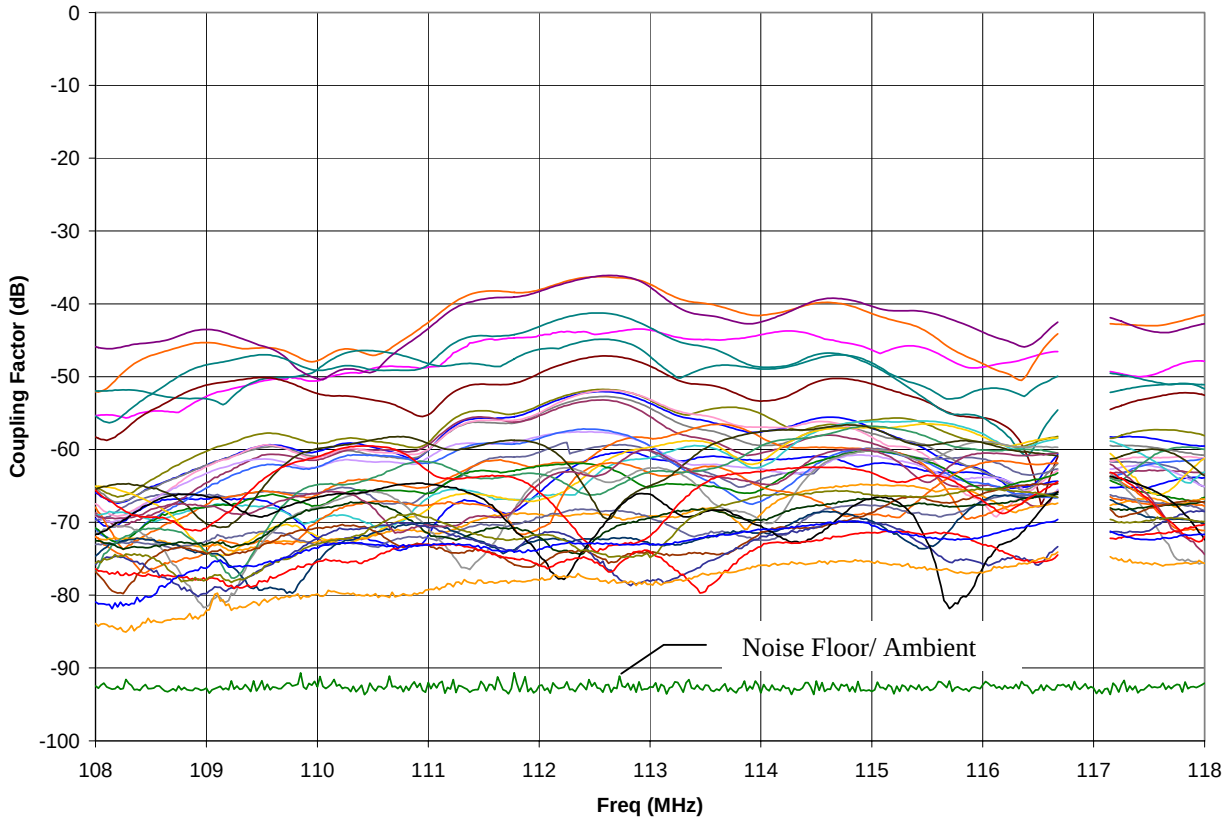

Figure 4.6-3a: Citation II VOR/LOC IPC scans at locations within aircraft fuselage.

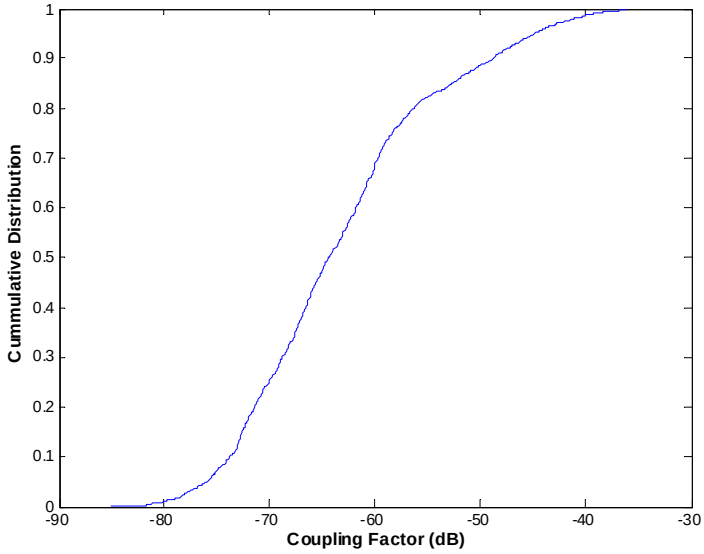

IPC Statistics		
Maximum	-36.1	dB
98 percentile	-41.1	dB
95 percentile	-44.8	dB
90 percentile	-48.7	dB
80 percentile	-56.3	dB
50 percentile	-64.3	dB
Mean	-52.0	dB
No. of Points	13788	
No. of Position Scans	36	
Freqs per Sweep	401	

Figure 4.6-3b: Citation II VOR/LOC IPC statistics.

4.6.2 VHF-Com1

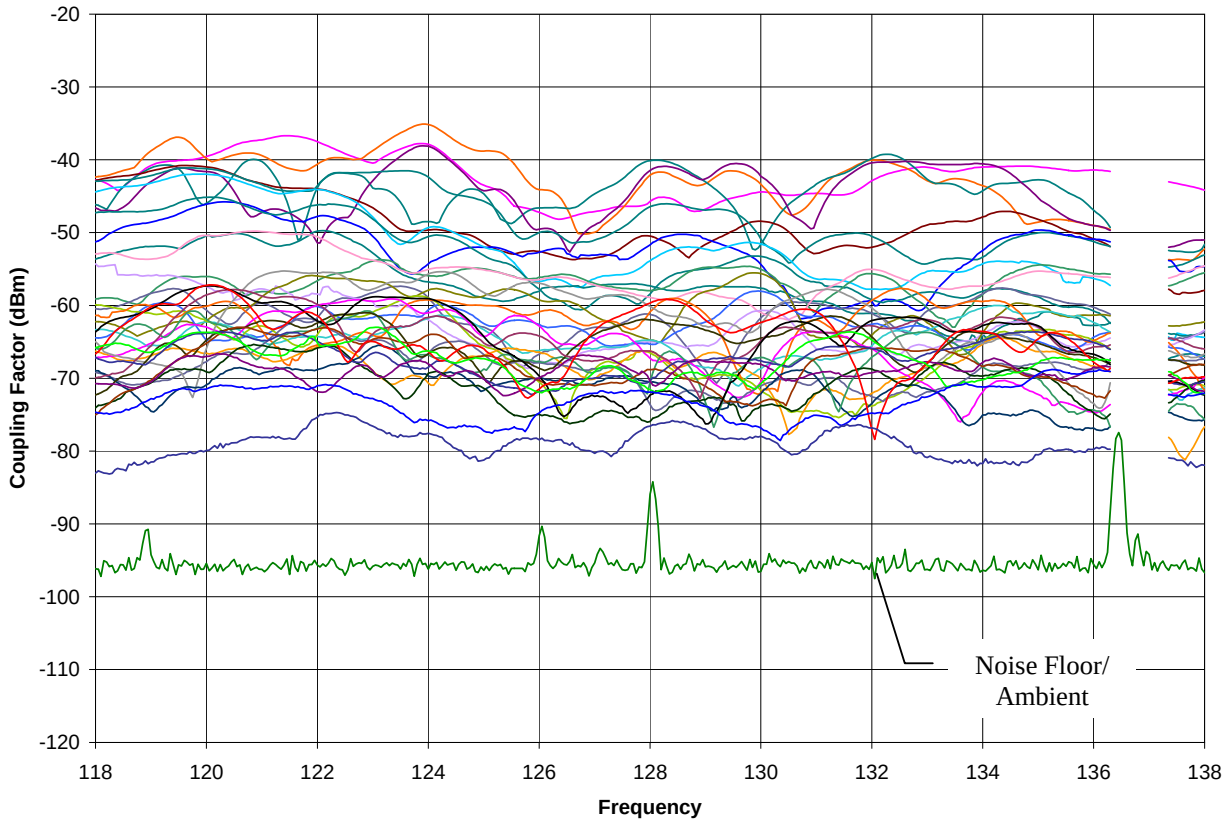

Figure 4.6-4a: Citation II VHF-Com1 IPC scans.

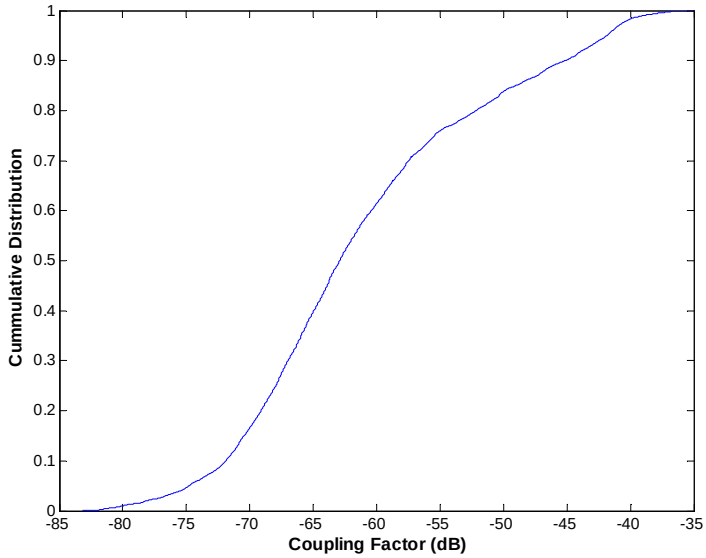

IPC Statistics		
Maximum	-35.1	dB
98 percentile	-40.2	dB
95 percentile	-41.8	dB
90 percentile	-45.1	dB
80 percentile	-52.1	dB
50 percentile	-62.9	dB
Mean	-50.2	dB
No. of Points	13716	
No. of Position Scans	36	
Freqs per Sweep	401	

Figure 4.6-4b: Citation II VHF-Com1 (top of aircraft) IPC statistics.

4.6.3 VHF-Com2

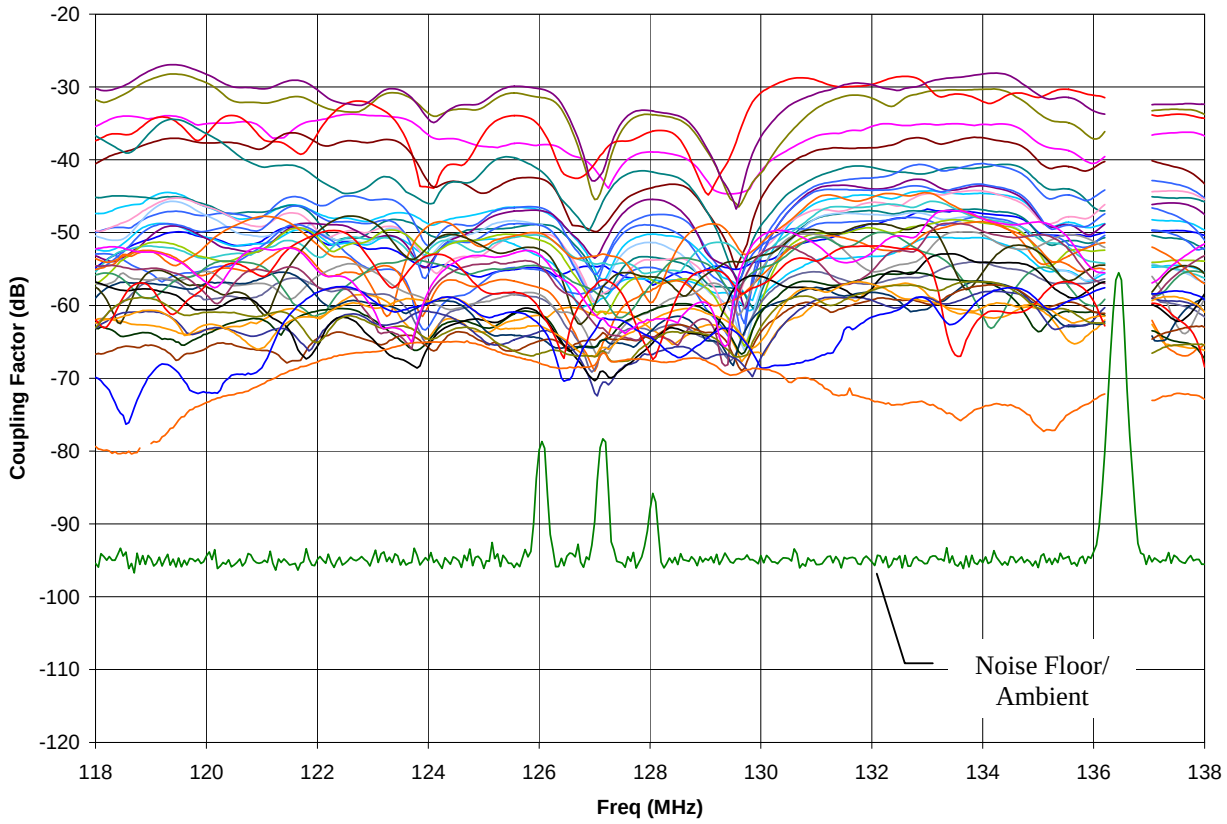

Figure 4.6-5a: Citation II VHF-Com2 IPC scans.

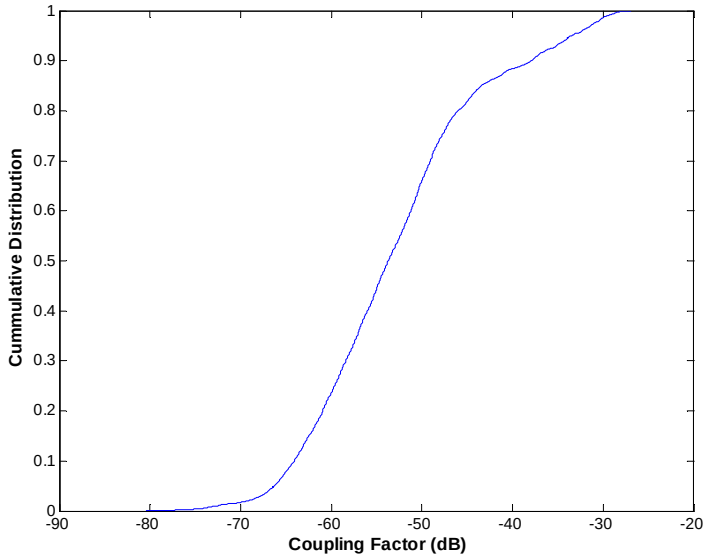

IPC Statistics		
Maximum	-26.9	dB
98 percentile	-30.4	dB
95 percentile	-33.5	dB
90 percentile	-37.9	dB
80 percentile	-45.9	dB
50 percentile	-53.7	dB
Mean	-41.7	dB
No. of Points	14242	
No. of Position Scans	37	
Freqs per Sweep	401	

Figure 4.6-5b: Citation II VHF-Com2 IPC statistics.

4.6.4 GS

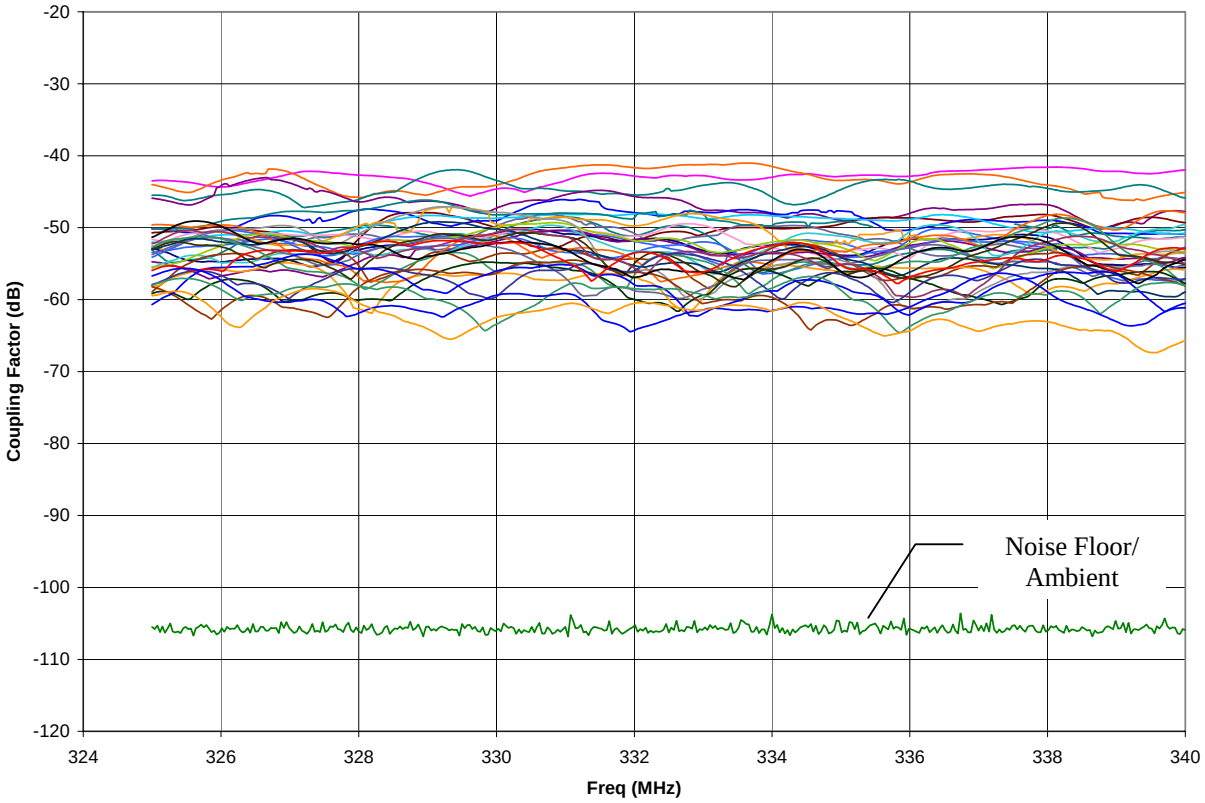

Figure 4.6-6a: Citation II GS IPC scans.

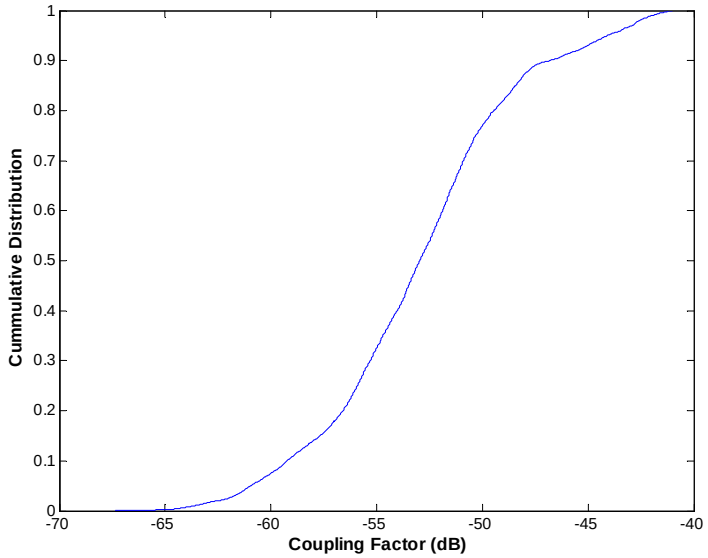

IPC Statistics		
Maximum	-41.0	dB
98 percentile	-42.6	dB
95 percentile	-44.1	dB
90 percentile	-46.8	dB
80 percentile	-49.5	dB
50 percentile	-53.0	dB
Mean	-50.35	dB
No. of Points	14382	
No. of Position Scans	36	
Freqs per Sweep	401	

Figure 4.6-6b: Citation II GS IPC statistics.

4.6.5 DME

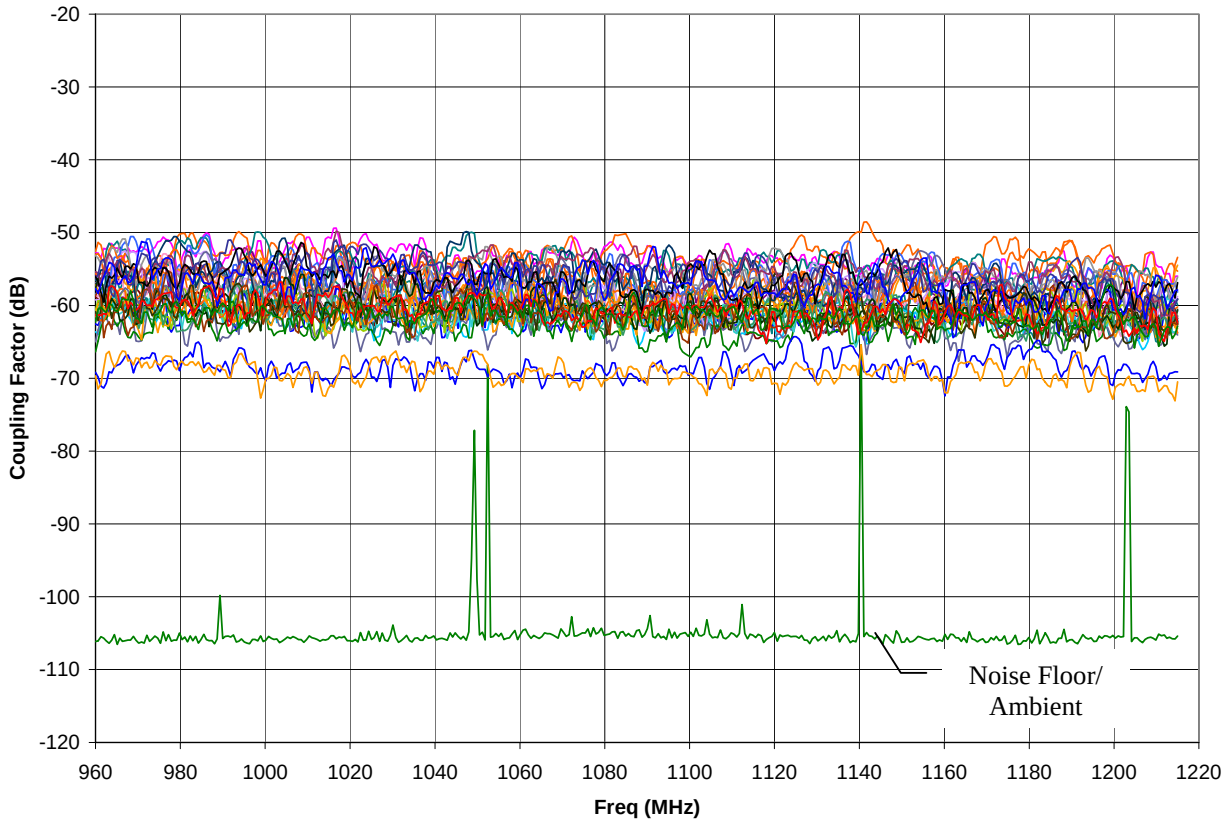

Figure 4.6-7a: Citation II DME IPC scans.

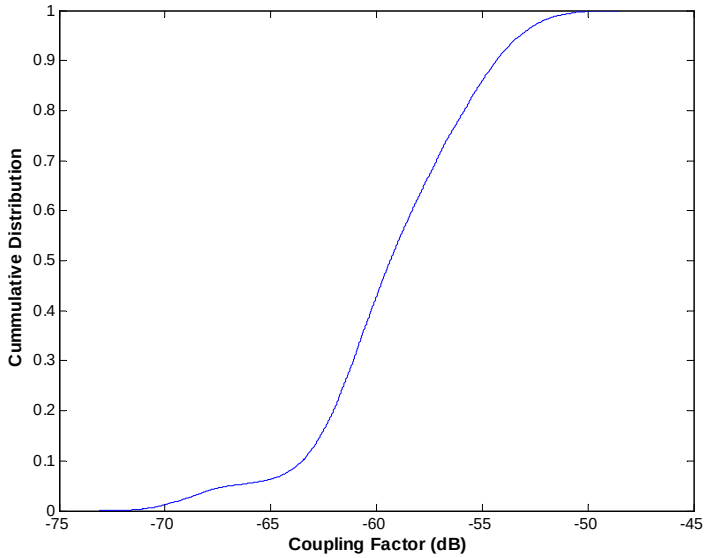

IPC Statistics		
Maximum	-48.5	dB
98 percentile	-52.1	dB
95 percentile	-53.2	dB
90 percentile	-54.3	dB
80 percentile	-55.8	dB
50 percentile	-59.3	dB
Mean	-57.7	dB
No. of Points	14436	
No. of Position Scans	36	
Freqs per Sweep	401	

Figure 4.6-7b: Citation II DME IPC statistics.

4.6.6 ATC

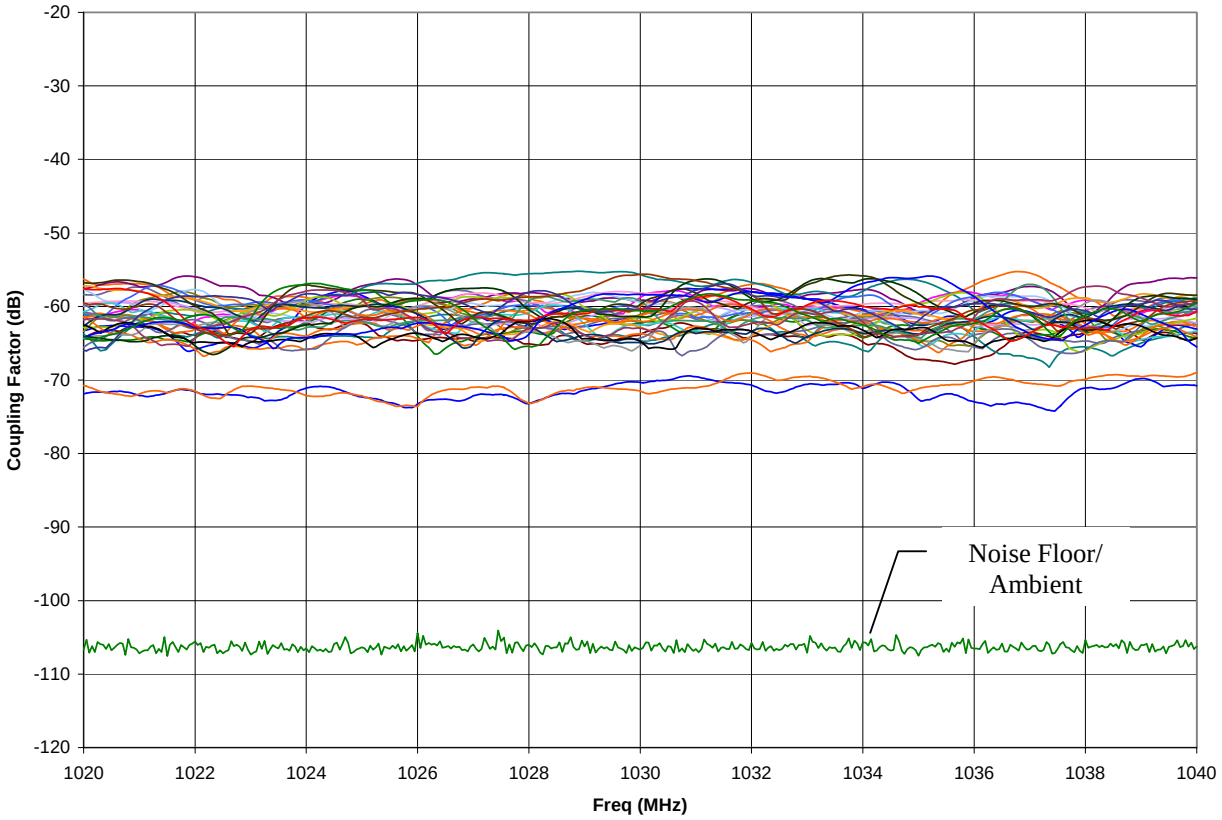

Figure 4.6-8a: Citation II ATC IPC scans.

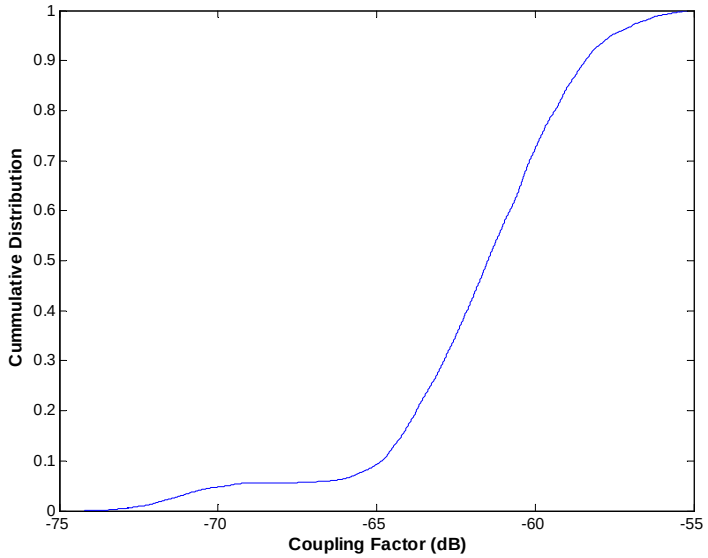

IPC Statistics		
Maximum	-55.2	dB
98 percentile	-56.5	dB
95 percentile	-57.6	dB
90 percentile	-58.4	dB
80 percentile	-59.4	dB
50 percentile	-61.5	dB
Mean	-60.9	dB
No. of Points	14436	
No. of Position Scans	36	
Freqs per Sweep	401	

Figure 4.6-8b: Citation II ATC IPC statistics.

4.6.7 TCAD

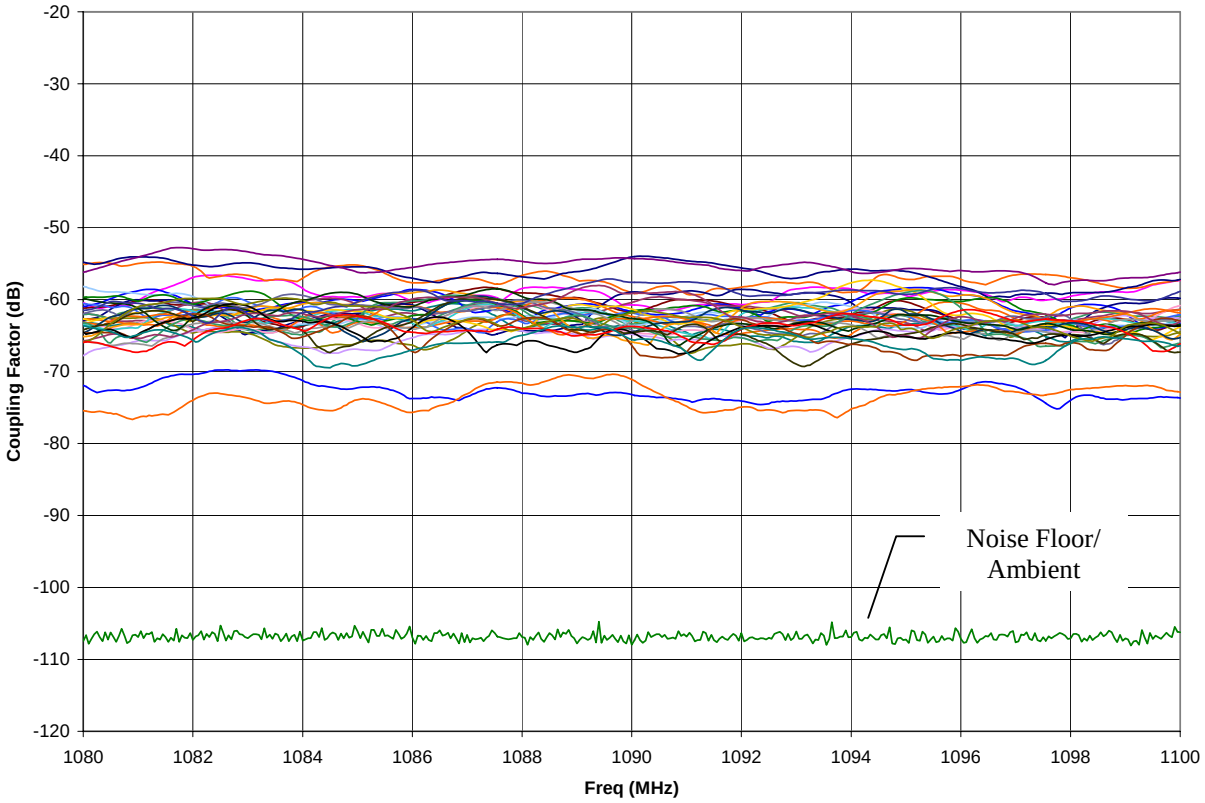

Figure 4.6-9a: Citation II TCAD IPC scans.

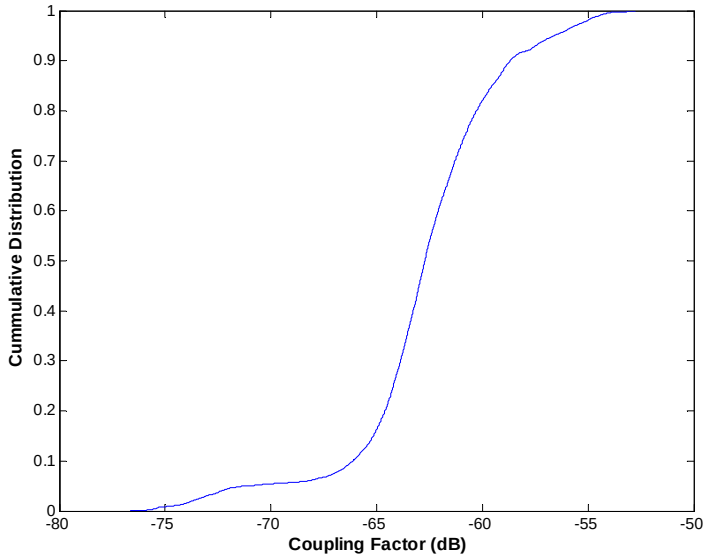

IPC Statistics		
Maximum	-52.8	dB
98 percentile	-55.0	dB
95 percentile	-56.6	dB
90 percentile	-58.7	dB
80 percentile	-60.3	dB
50 percentile	-62.7	dB
Mean	-61.3	dB
No. of Points	14436	
No. of Position Scans	36	
Freqs per Sweep	401	

Figure 4.6-9b: Citation II TCAD IPC statistics.

4.6.8 GPS1

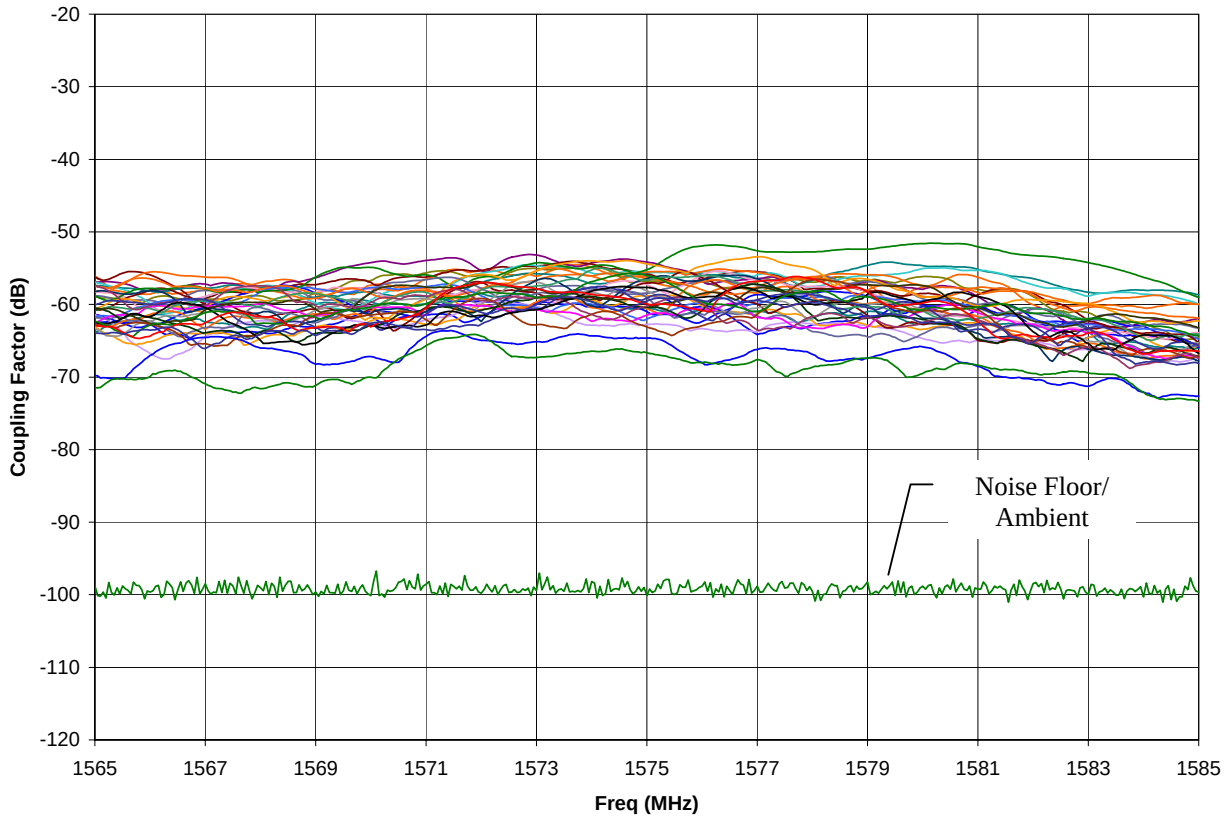

Figure 4.6-10a: Citation II GPS1 IPC scans.

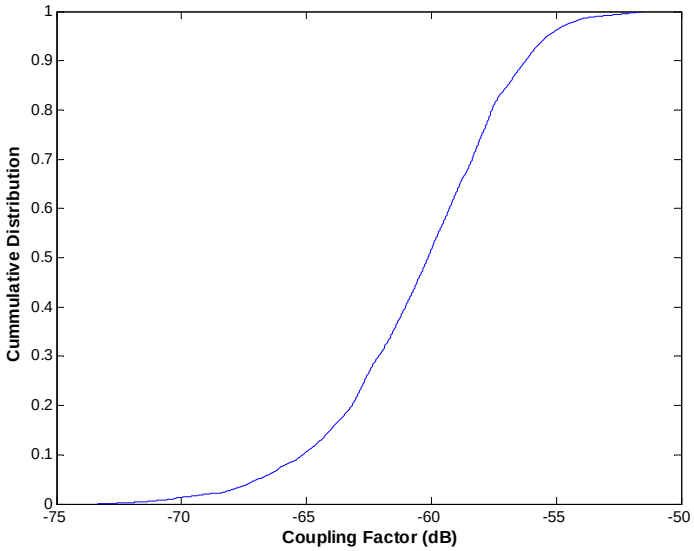

IPC Statistics		
Maximum	-51.6	dB
98 percentile	-54.2	dB
95 percentile	-55.4	dB
90 percentile	-56.2	dB
80 percentile	-57.6	dB
50 percentile	-60.1	dB
Mean	-59.2	dB
No. of Points	14436	
No. of Position Scans	36	
Freqs per Sweep	401	

Figure 4.6-10b: Citation II GPS1 IPC statistics.

4.6.9 GPS2

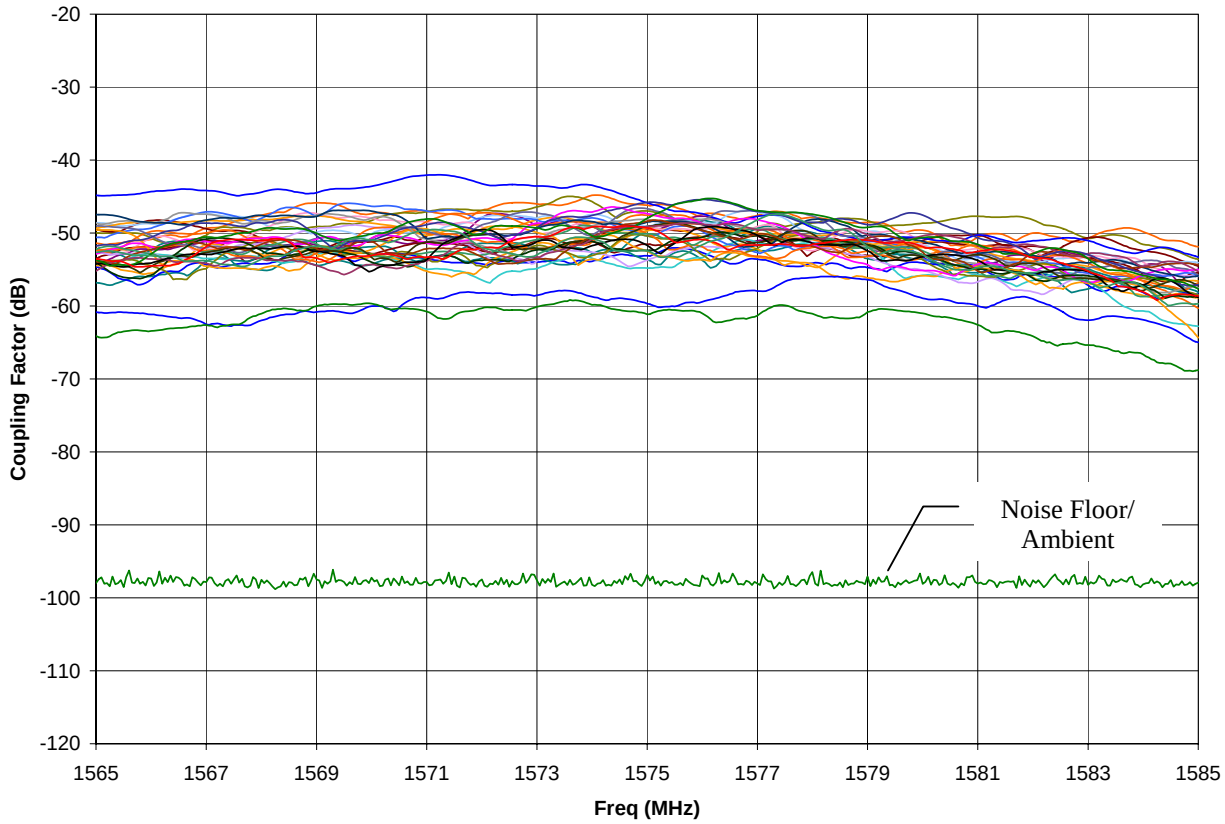

Figure 4.6-11a: Citation II GPS2 IPC scans.

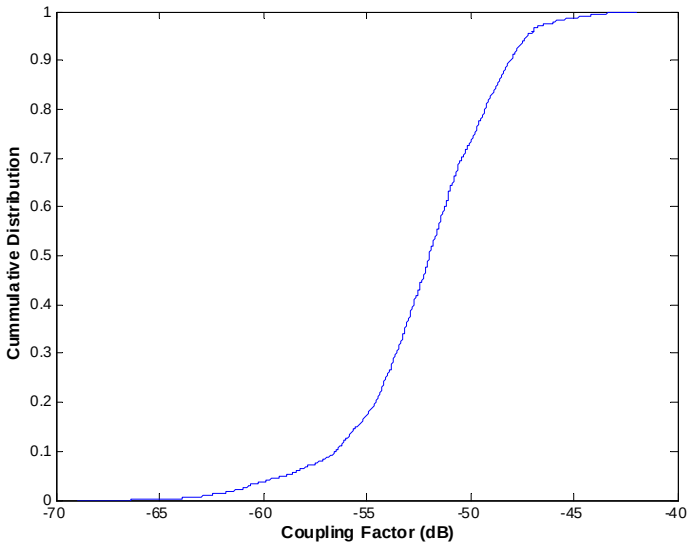

IPC Statistics		
Maximum	-42.0	dB
98 percentile	-45.9	dB
95 percentile	-47.2	dB
90 percentile	-48.1	dB
80 percentile	-49.3	dB
50 percentile	-52.0	dB
Mean	-51.0	dB
No. of Points	14436	
No. of Position Scans	36	
Freqs per Sweep	401	

Figure 4.6-11b: Citation II GPS2 IPC statistics.

4.7 Baron B-58

Figure 4.7-1: Baron B-58.

Figure 4.7-2: Aircraft antennas on top. Power cable routed tightly to the aircraft metal surfaces.

4.7.1 VHF-Com1

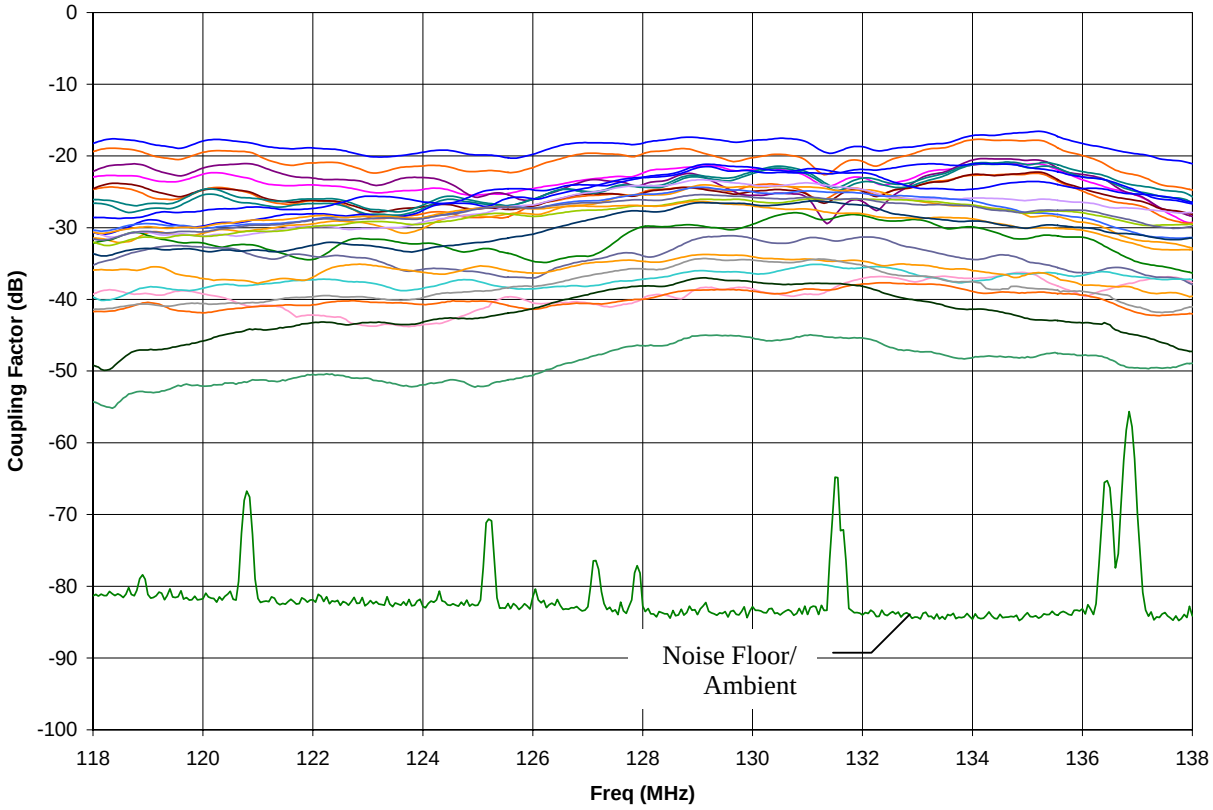

Figure 4.7-3a: Baron B-58 VHF-Com1 IPC scans.

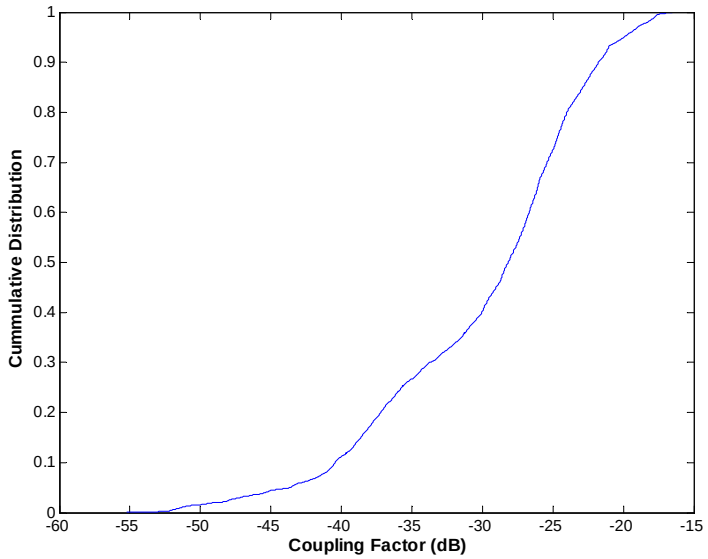

IPC Statistics		
Maximum	-16.6	dB
98 percentile	-18.3	dB
95 percentile	-19.9	dB
90 percentile	-21.8	dB
80 percentile	-24.0	dB
50 percentile	-28.2	dB
Mean	-25.8	dB
No. of Points	10426	
No. of Position Scans	26	
Freqs per Sweep	401	

Figure 4.7-3b: Baron B-58 VHF-Com1 IPC statistics.

4.7.2 VHF-Com2

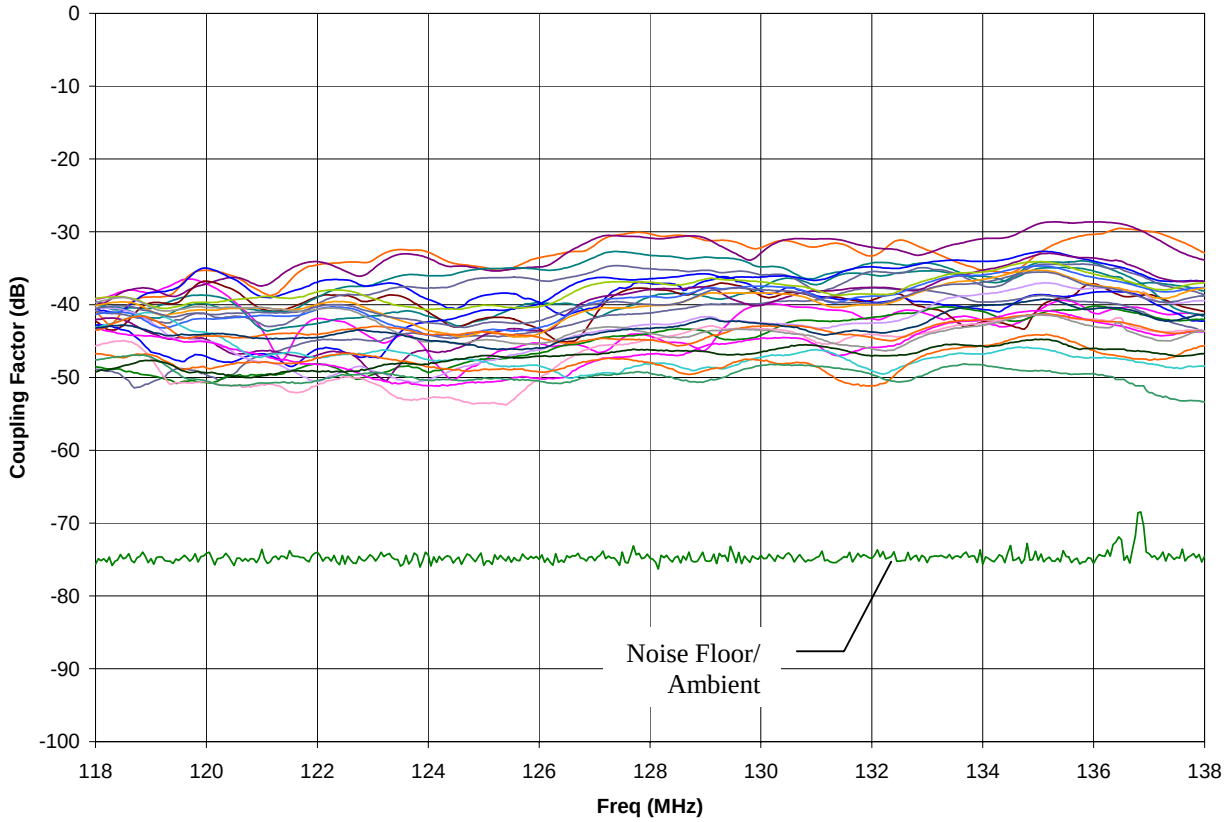

Figure 4.7-4a: Baron B-58 VHF-Com2 IPC scans.

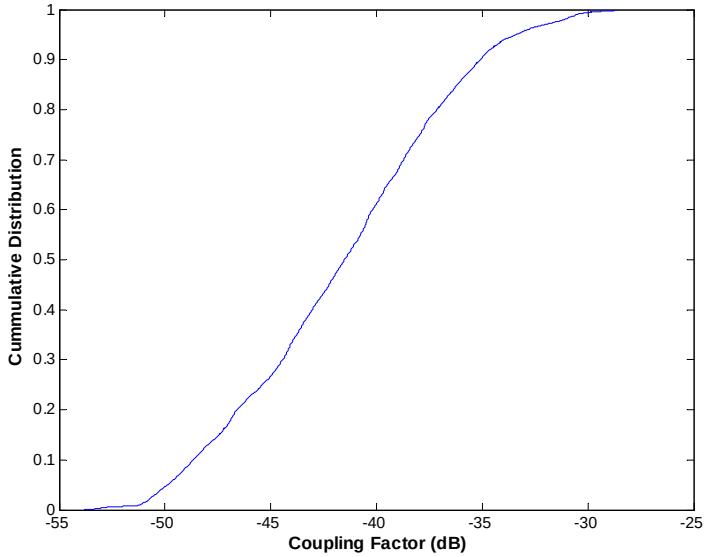

IPC Statistics		
Maximum	-28.6	dB
98 percentile	-31.1	dB
95 percentile	-33.4	dB
90 percentile	-35.1	dB
80 percentile	-37.1	dB
50 percentile	-41.5	dB
Mean	-38.8	dB
No. of Points	10426	
No. of Position Scans	26	
Freqs per Sweep	401	

Figure 4.7-4b: Baron B-58 VHF-Com2 IPC statistics.

4.7.3 GS

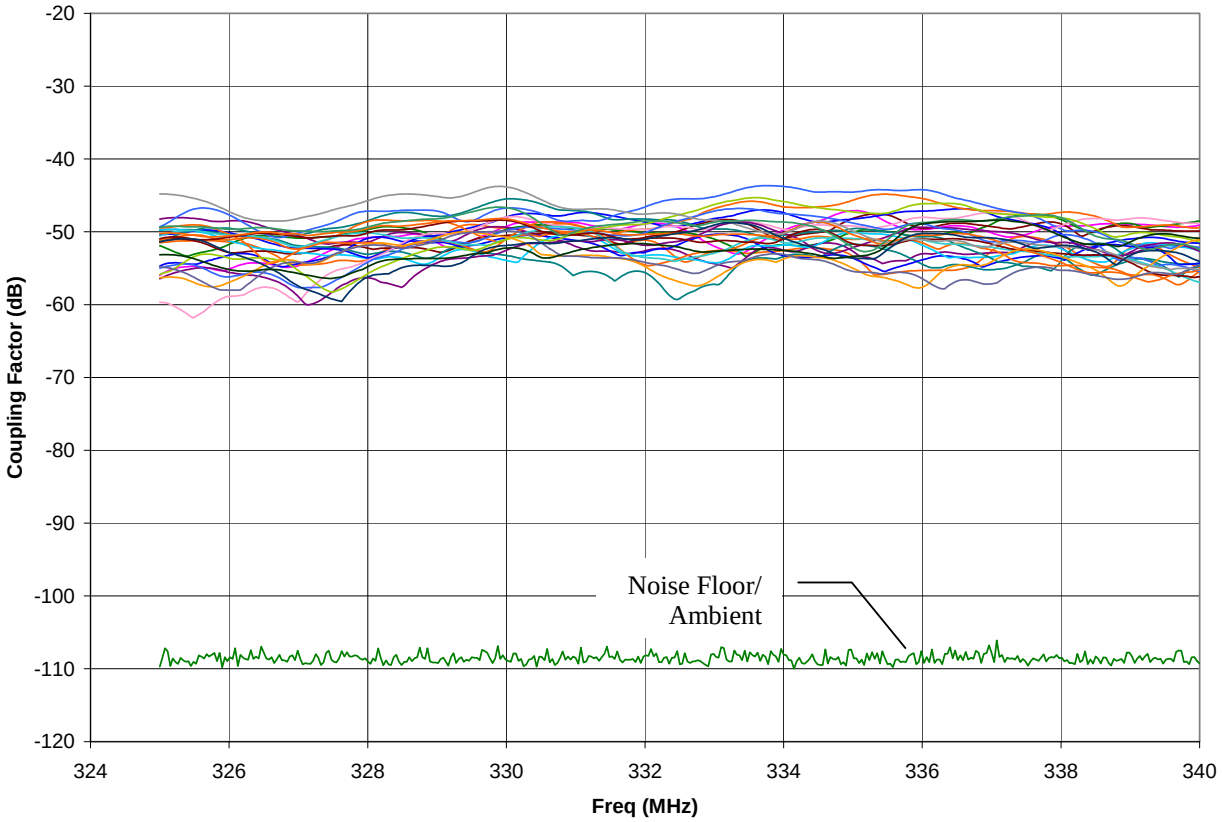

Figure 4.7-5a: Baron B-58 GS IPC scans.

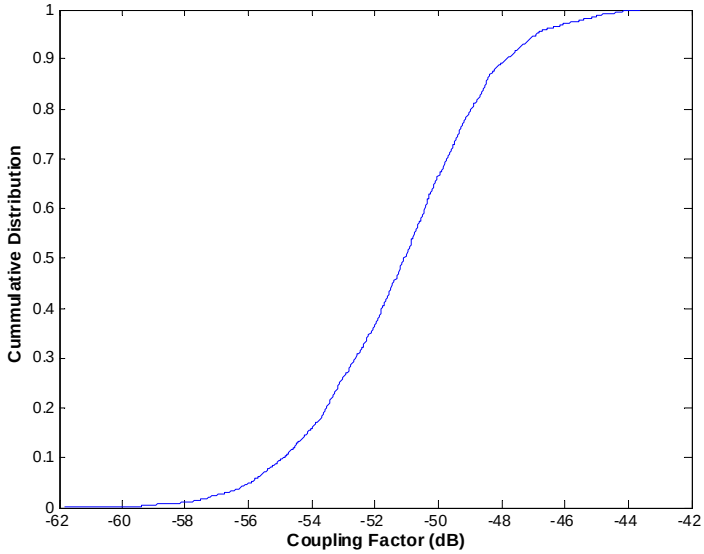

IPC Statistics		
Maximum	-43.7	dB
98 percentile	-45.4	dB
95 percentile	-46.9	dB
90 percentile	-47.8	dB
80 percentile	-49.0	dB
50 percentile	-51.1	dB
Mean	-50.4	dB
No. of Points	10426	
No. of Position Scans	26	
Freqs per Sweep	401	

Figure 4.7-5b: Baron B-58 GS IPC statistics.

4.7.4 ATC

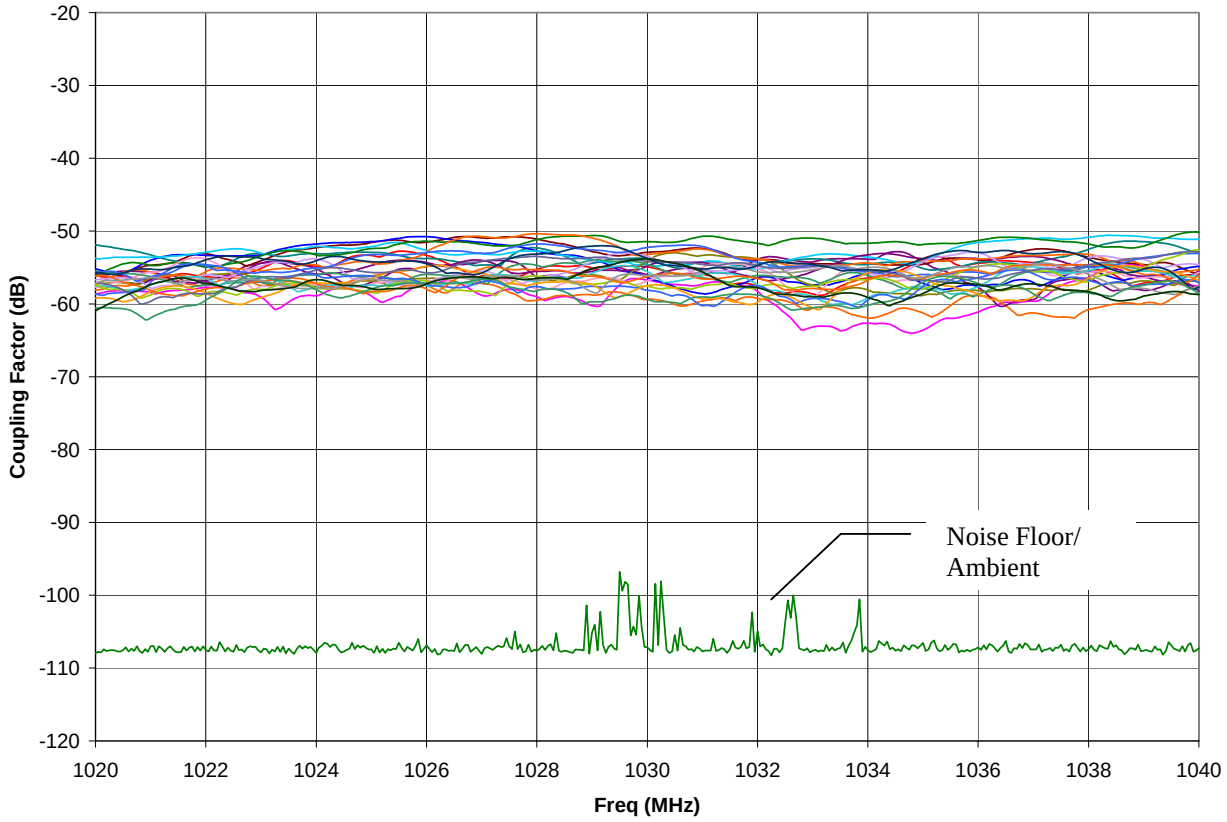

Figure 4.7-6a: Baron B-58 ATC IPC scans.

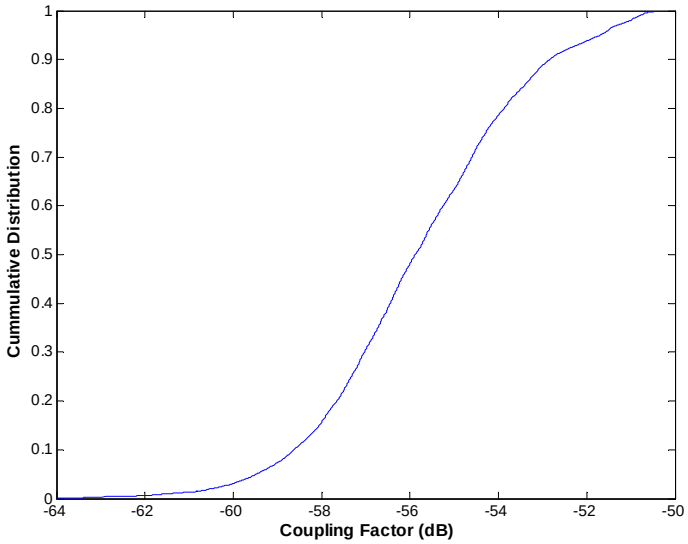

IPC Statistics		
Maximum	-50.1	dB
98 percentile	-51.0	dB
95 percentile	-51.7	dB
90 percentile	-52.8	dB
80 percentile	-53.9	dB
50 percentile	-55.9	dB
Mean	-55.2	dB
No. of Points	10426	
No. of Position Scans	26	
Freqs per Sweep	401	

Figure 4.7-6b: Baron B-58 ATC IPC statistics.

4.7.5 TCAS

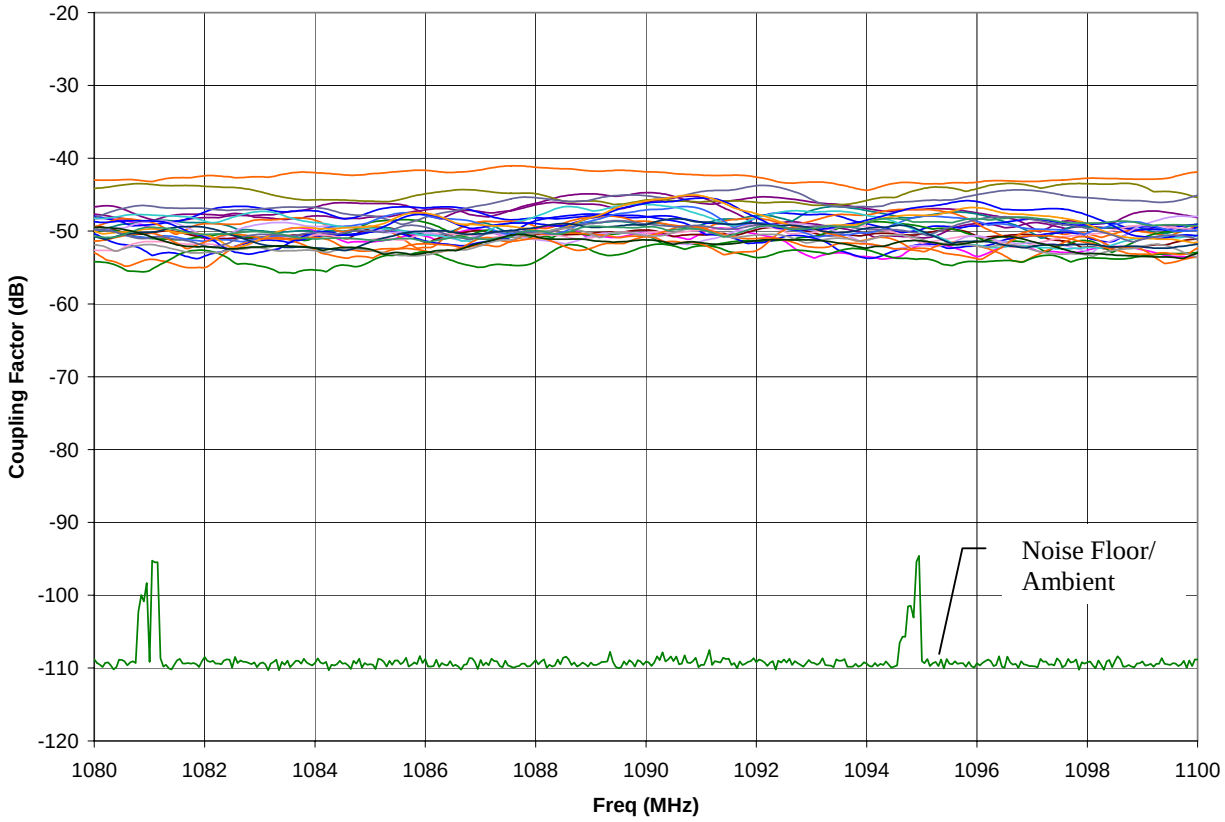

Figure 4.7-7a: Baron B-58 TCAS IPC scans.

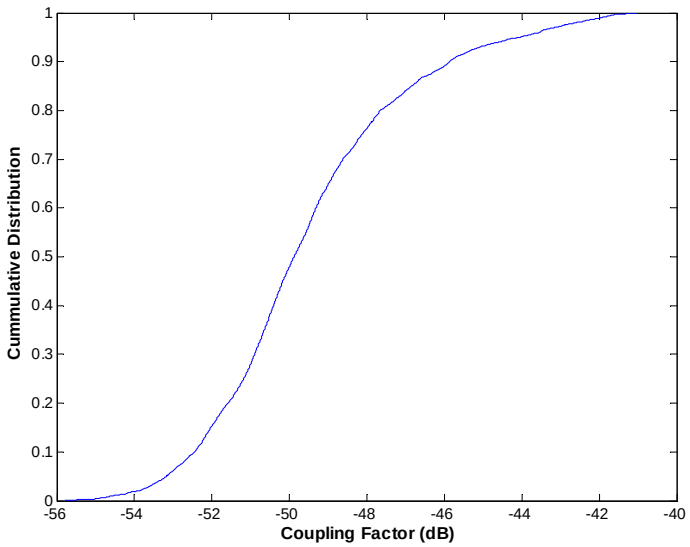

IPC Statistics		
Maximum	-41.0	dB
98 percentile	-42.6	dB
95 percentile	-44.1	dB
90 percentile	-45.9	dB
80 percentile	-47.6	dB
50 percentile	-49.9	dB
Mean	-48.6	dB
No. of Points	10426	
No. of Position Scans	26	
Freqs per Sweep	401	

Figure 4.7-7b: Baron B-58 TCAS IPC statistics.

4.7.6 GPS

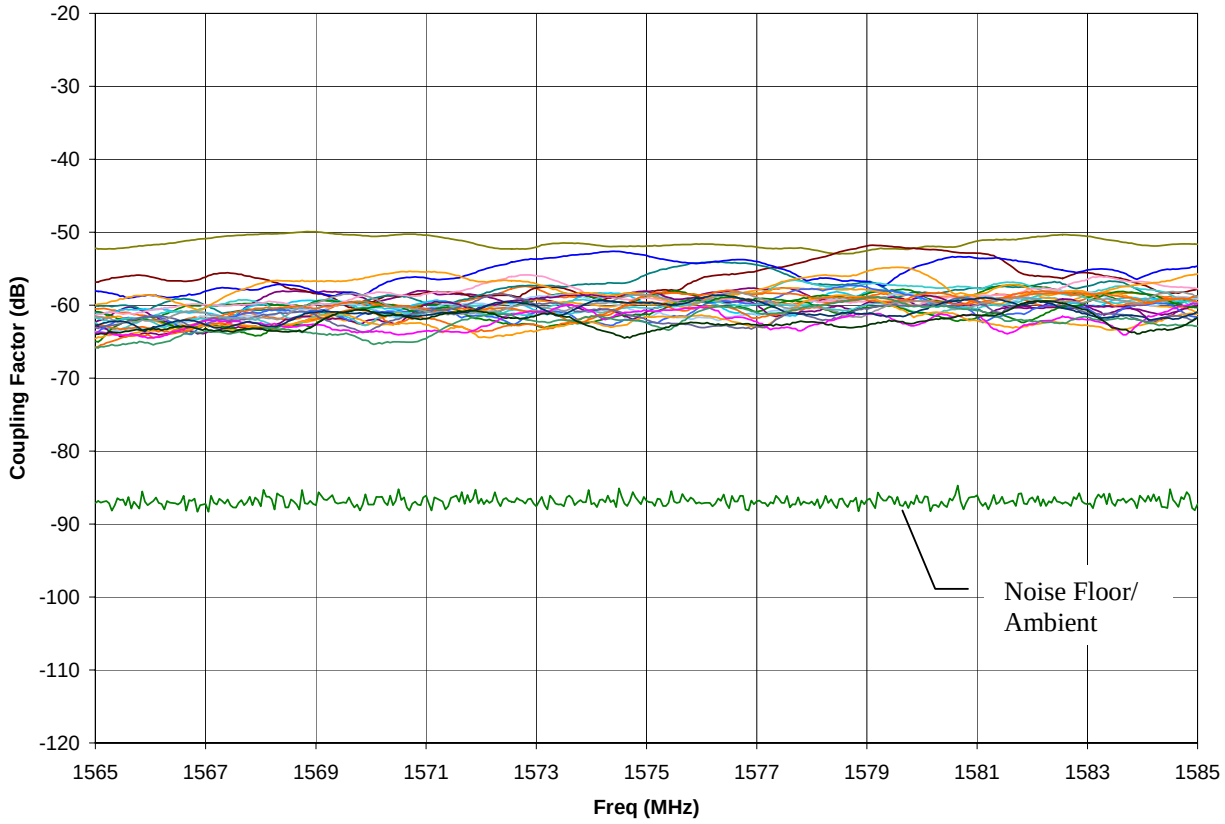

Figure 4.7-8a: Baron B-58 GPS IPC scans.

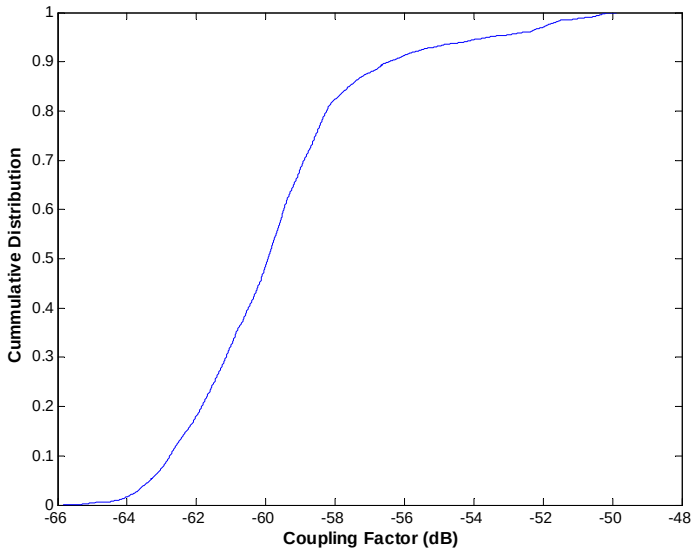

IPC Statistics		
Maximum	-49.9	dB
98 percentile	-51.7	dB
95 percentile	-53.6	dB
90 percentile	-56.4	dB
80 percentile	-58.2	dB
50 percentile	-59.9	dB
Mean	-58.6	dB
No. of Points	10426	
No. of Position Scans	26	
Freqs per Sweep	401	

Figure 4.7-8b: Baron B-58 GPS IPC statistics.

4.8 Piper Saratoga

Figure 4.8-1: Piper Saratoga

Figure 4.8-2: Internal setup with seats removed.

4.8.1 VOR/LOC

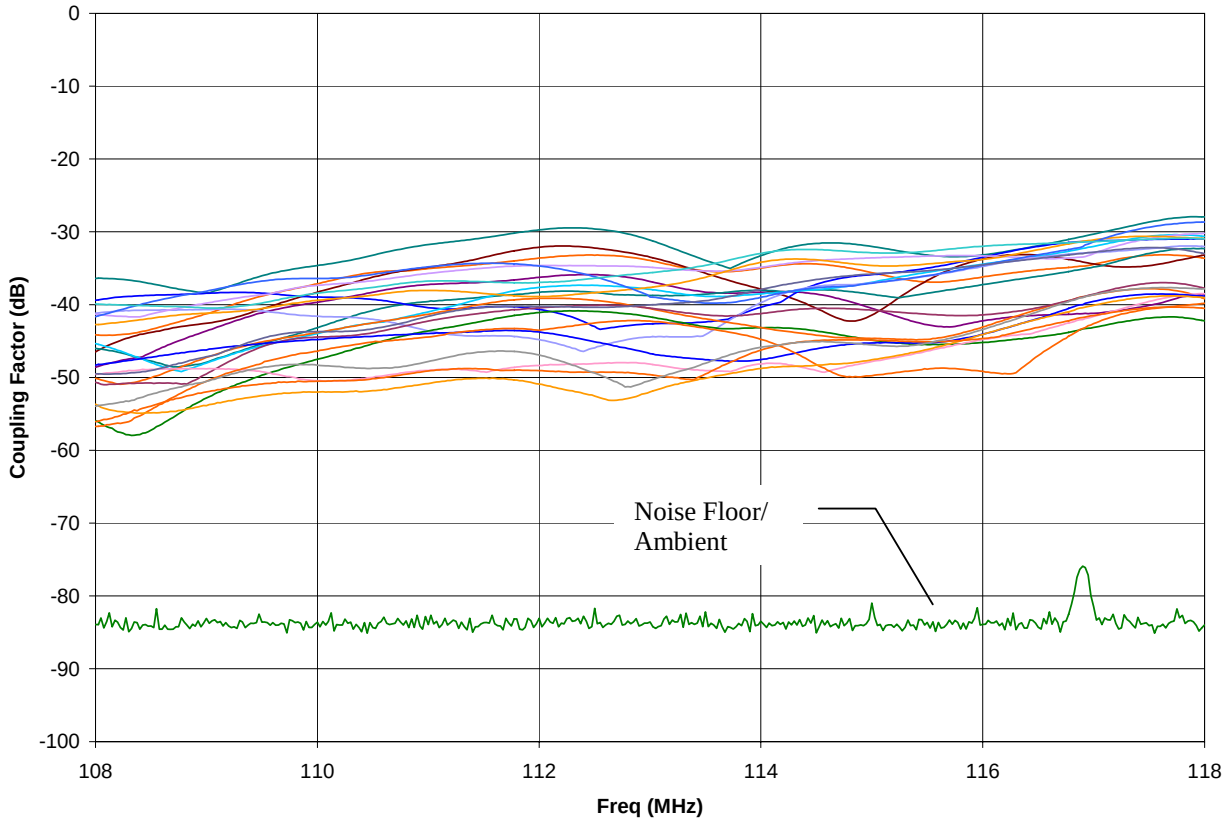

Figure 4.8-3a: Piper Saratoga VOR/LOC IPC scans.

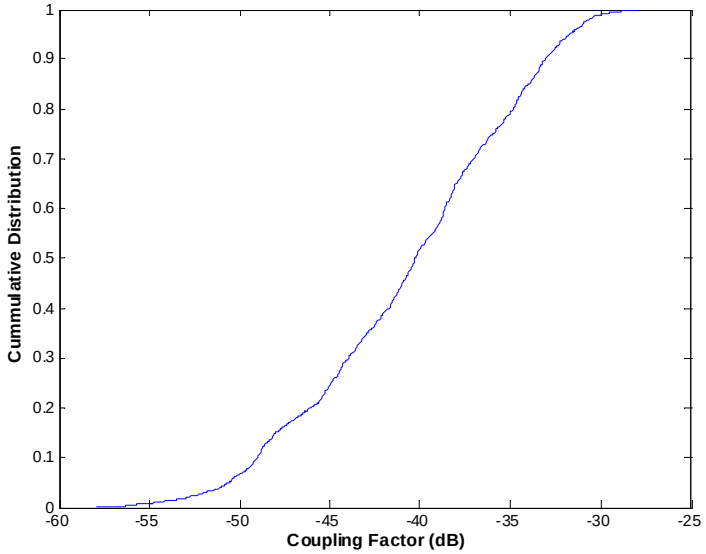

IPC Statistics		
Maximum	-27.9	dB
98 percentile	-30.6	dB
95 percentile	-31.7	dB
90 percentile	-33.1	dB
80 percentile	-34.9	dB
50 percentile	-40.3	dB
Mean	-37.3	dB
No. of Points	8822	
No. of Position Scans	22	
Freqs per Sweep	401	

Figure 4.8-3b: Piper Saratoga VOR/LOC IPC statistics.

4.8.2 VHF-Com1

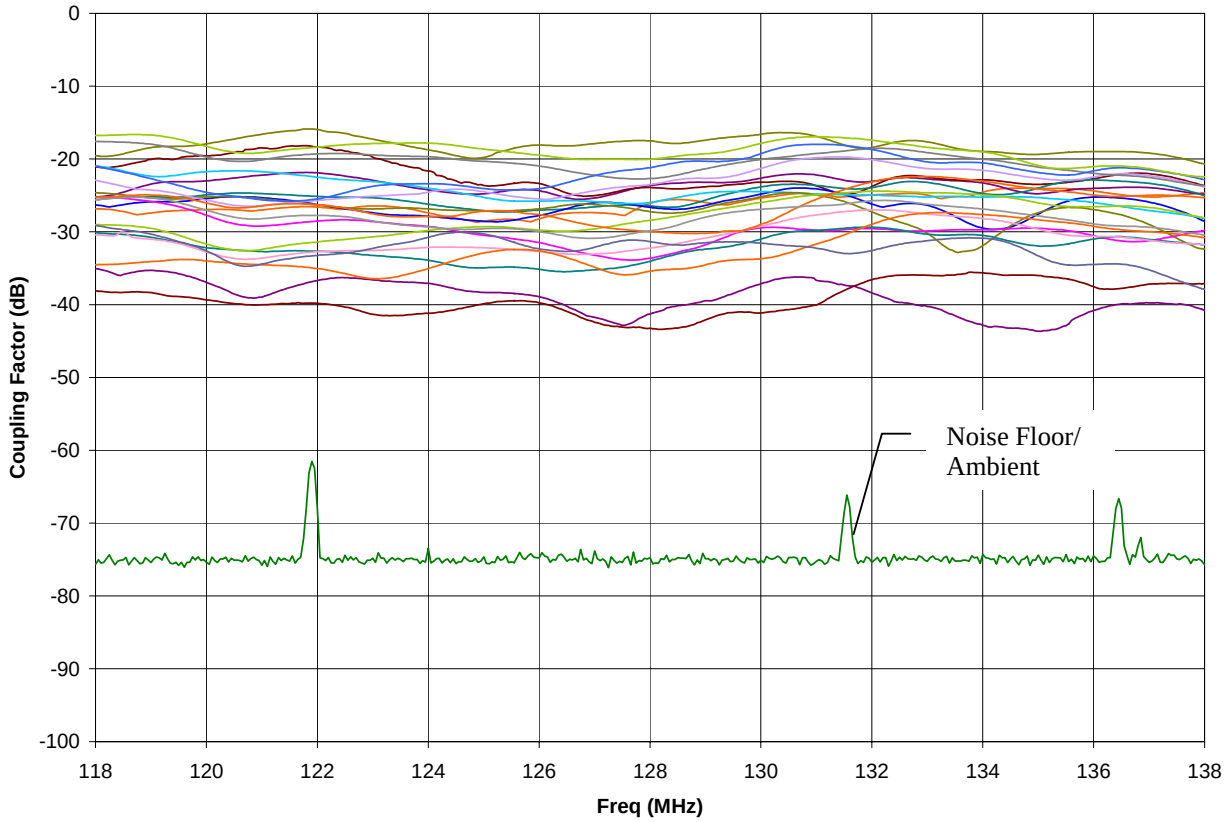

Figure 4.8-4a: Piper Saratoga VHF-Com1 IPC scans.

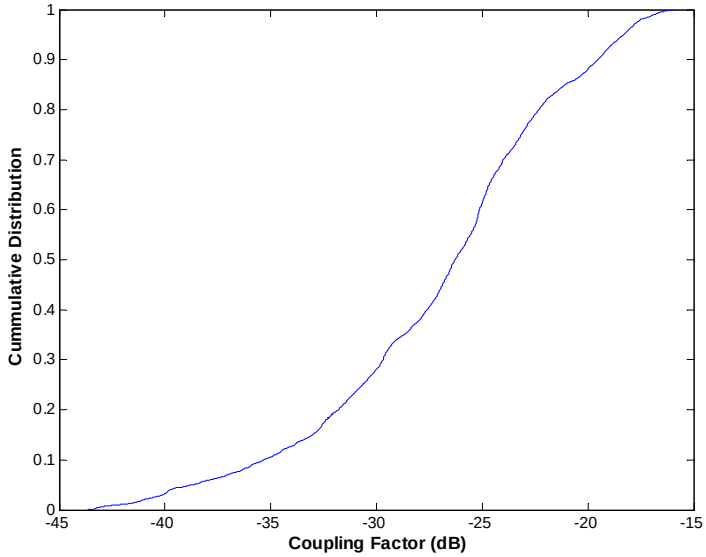

IPC Statistics		
Maximum	-15.9	dB
98 percentile	-17.5	dB
95 percentile	-18.3	dB
90 percentile	-19.5	dB
80 percentile	-22.3	dB
50 percentile	-26.3	dB
Mean	-24.0	dB
No. of Points	8822	
No. of Position Scans	22	
Freqs per Sweep	401	

Figure 4.8-4b: Piper Saratoga VHF-Com1 IPC statistics.

4.8.3 VHF-Com2

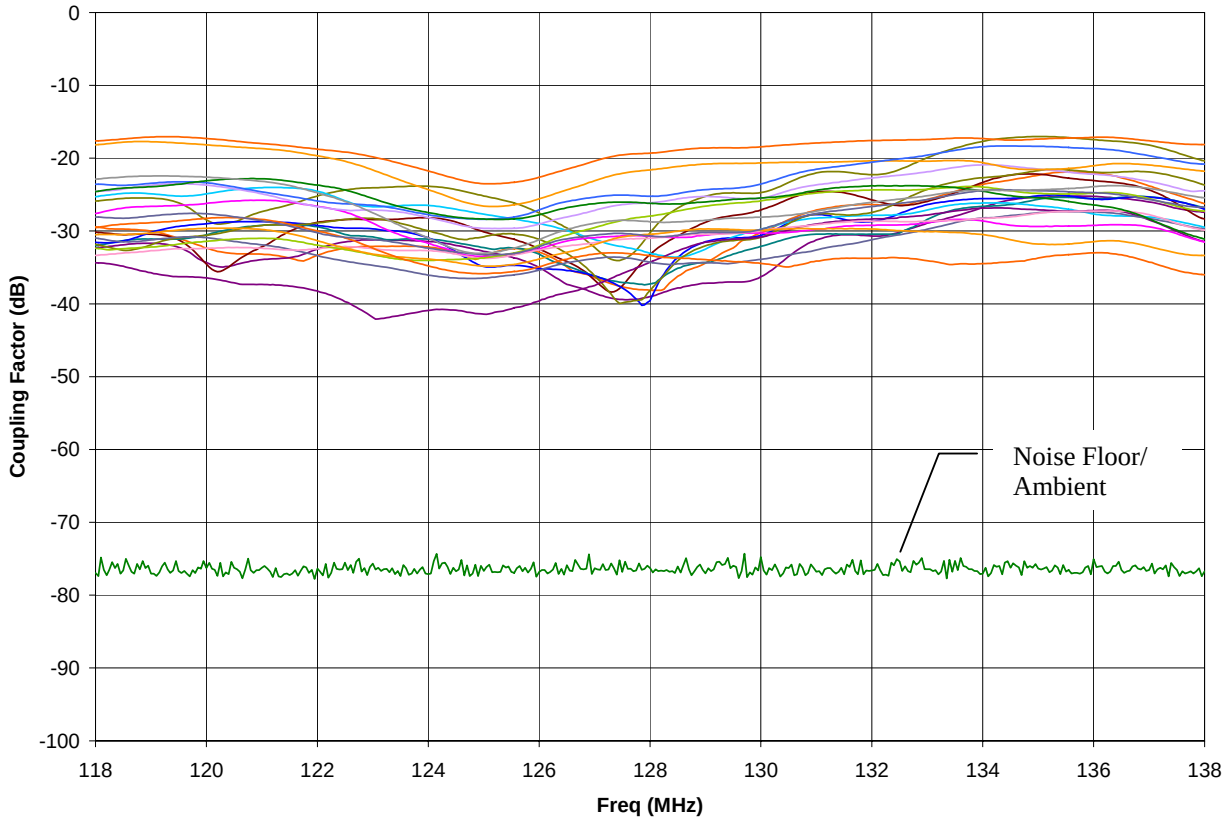

Figure 4.8-5a: Piper Saratoga VHF-Com2 IPC scans.

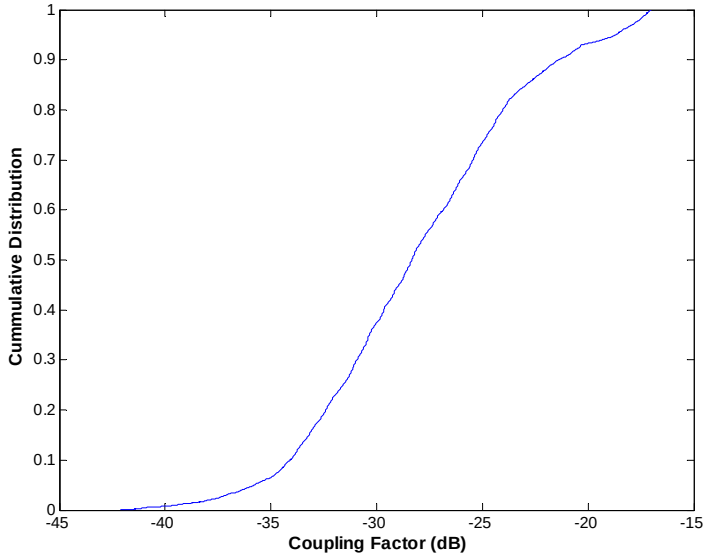

IPC Statistics		
Maximum	-17.0	dB
98 percentile	-17.5	dB
95 percentile	-18.7	dB
90 percentile	-21.4	dB
80 percentile	-24.0	dB
50 percentile	-28.3	dB
Mean	-25.3	dB
No. of Points	8822	
No. of Position Scans	22	
Freqs per Sweep	401	

Figure 4.8-5b: Piper Saratoga VHF-Com2 IPC statistics

4.8.4 GS

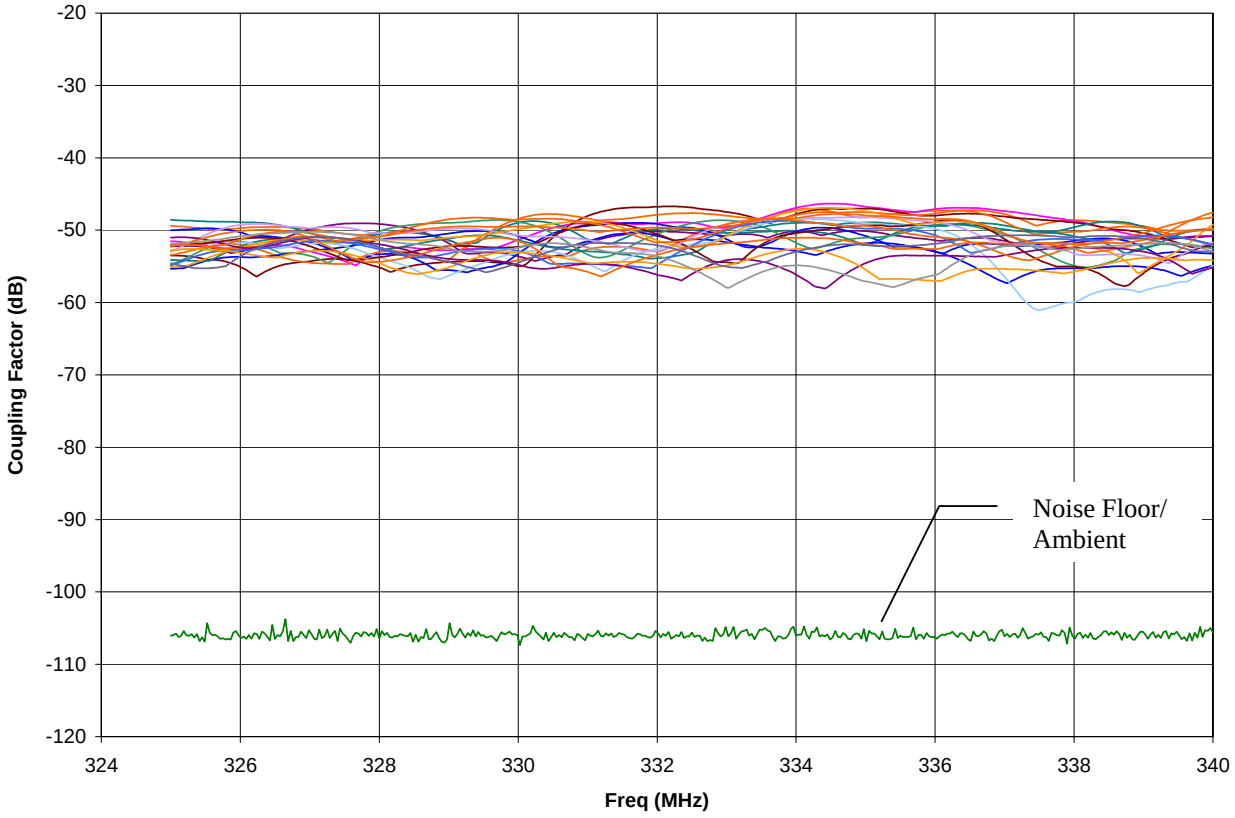

Figure 4.8-6a: Piper Saratoga GS IPC scans.

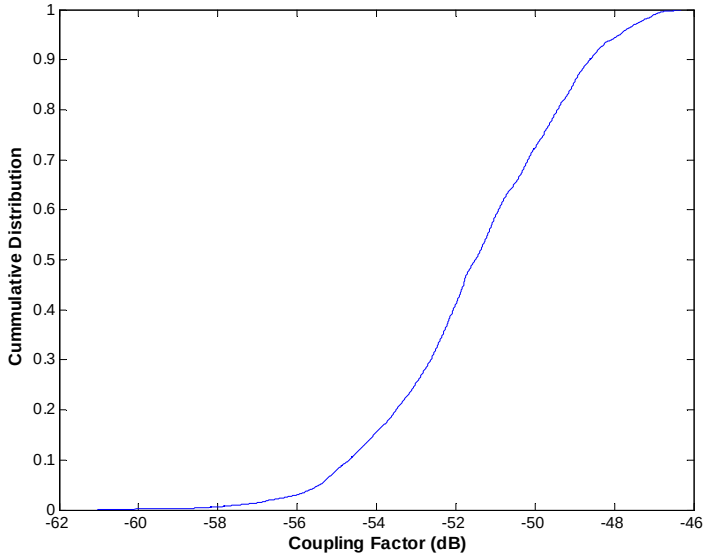

IPC Statistics		
Maximum	-46.3	dB
98 percentile	-47.2	dB
95 percentile	-47.9	dB
90 percentile	-48.6	dB
80 percentile	-49.4	dB
50 percentile	-51.5	dB
Mean	-51.0	dB
No. of Points	8822	
No. of Position Scans	22	
Freqs per Sweep	401	

Figure 4.8-6b: Piper Saratoga GS IPC statistics

4.8.5 DME

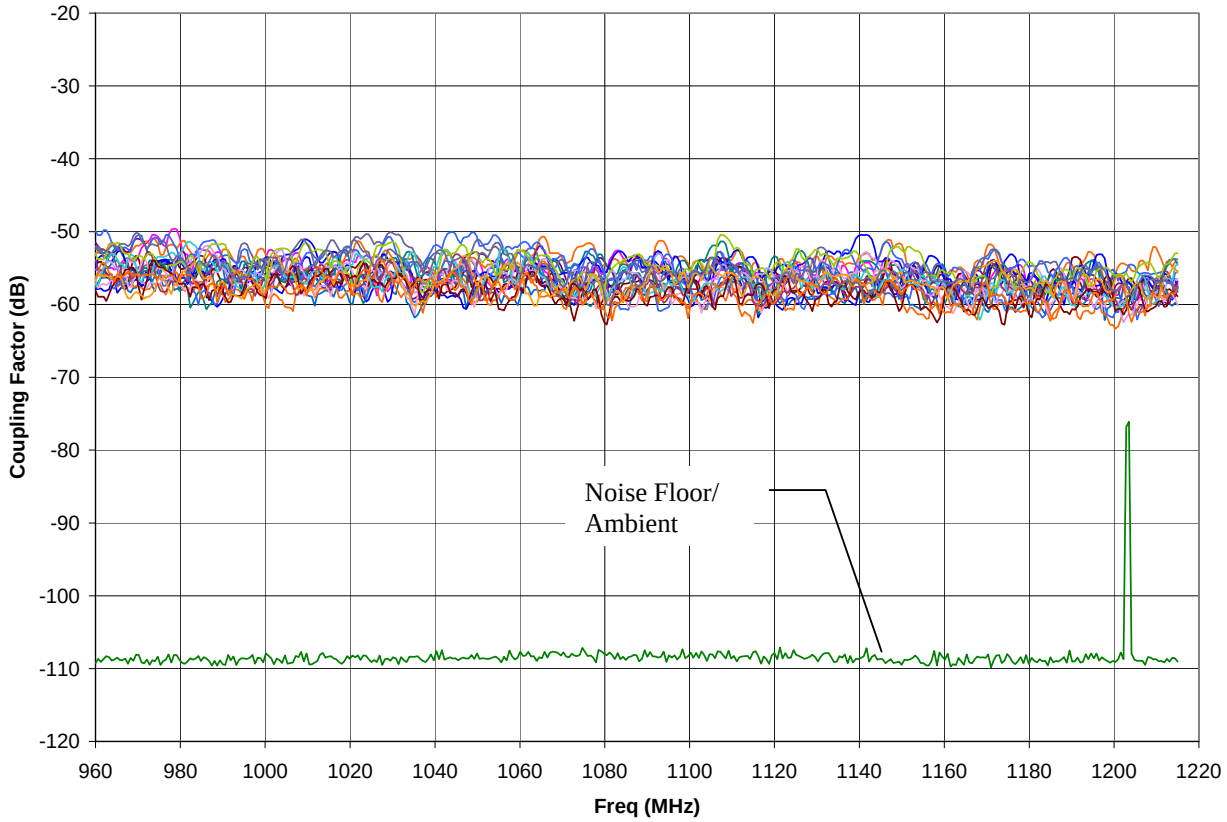

Figure 4.8-7a: Piper Saratoga DME IPC scans.

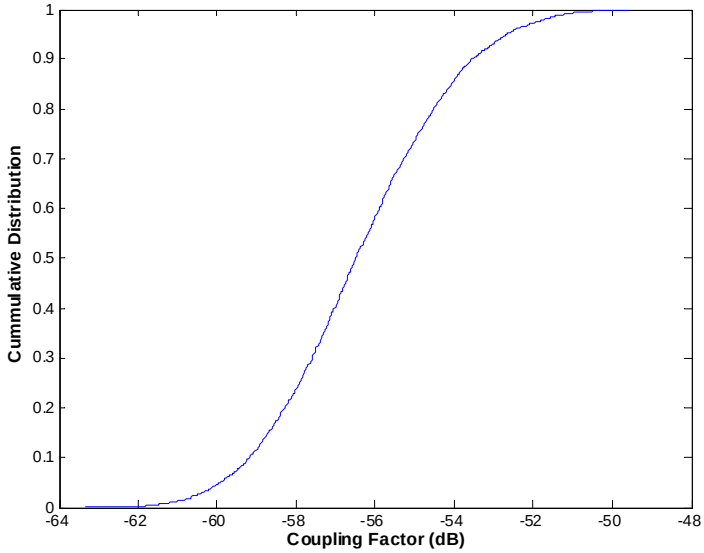

IPC Statistics		
Maximum	-49.6	dB
98 percentile	-51.7	dB
95 percentile	-52.7	dB
90 percentile	-53.5	dB
80 percentile	-54.5	dB
50 percentile	-56.5	dB
Mean	-56.4	dB
No. of Points	8822	
No. of Position Scans	22	
Freqs per Sweep	401	

Figure 4.8-7b: Piper Saratoga DME IPC statistics

4.8.6 ATC

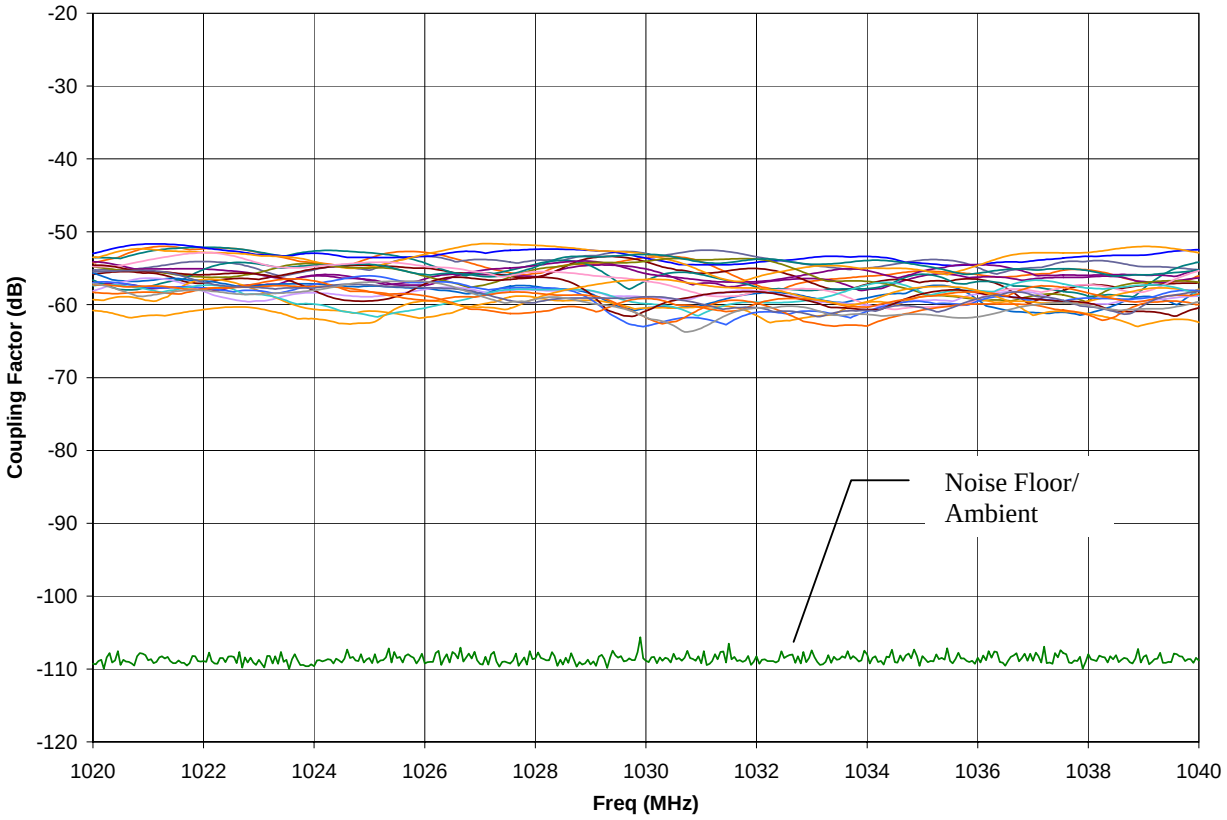

Figure 4.8-8a: Piper Saratoga ATC IPC scans.

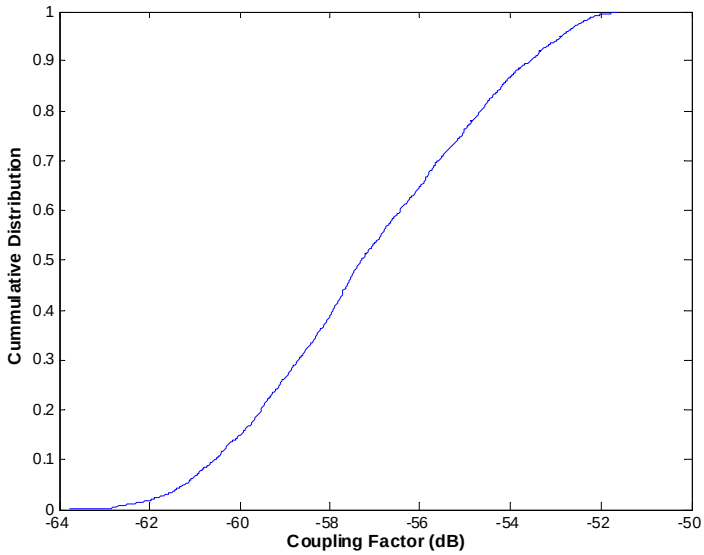

IPC Statistics		
Maximum	-51.6	dB
98 percentile	-52.4	dB
95 percentile	-52.9	dB
90 percentile	-53.5	dB
80 percentile	-54.6	dB
50 percentile	-57.3	dB
Mean	-56.4	dB
No. of Points	8822	
No. of Position Scans	22	
Freqs per Sweep	401	

Figure 4.8-8b: Piper Saratoga ATC IPC statistics

4.8.7 GPS

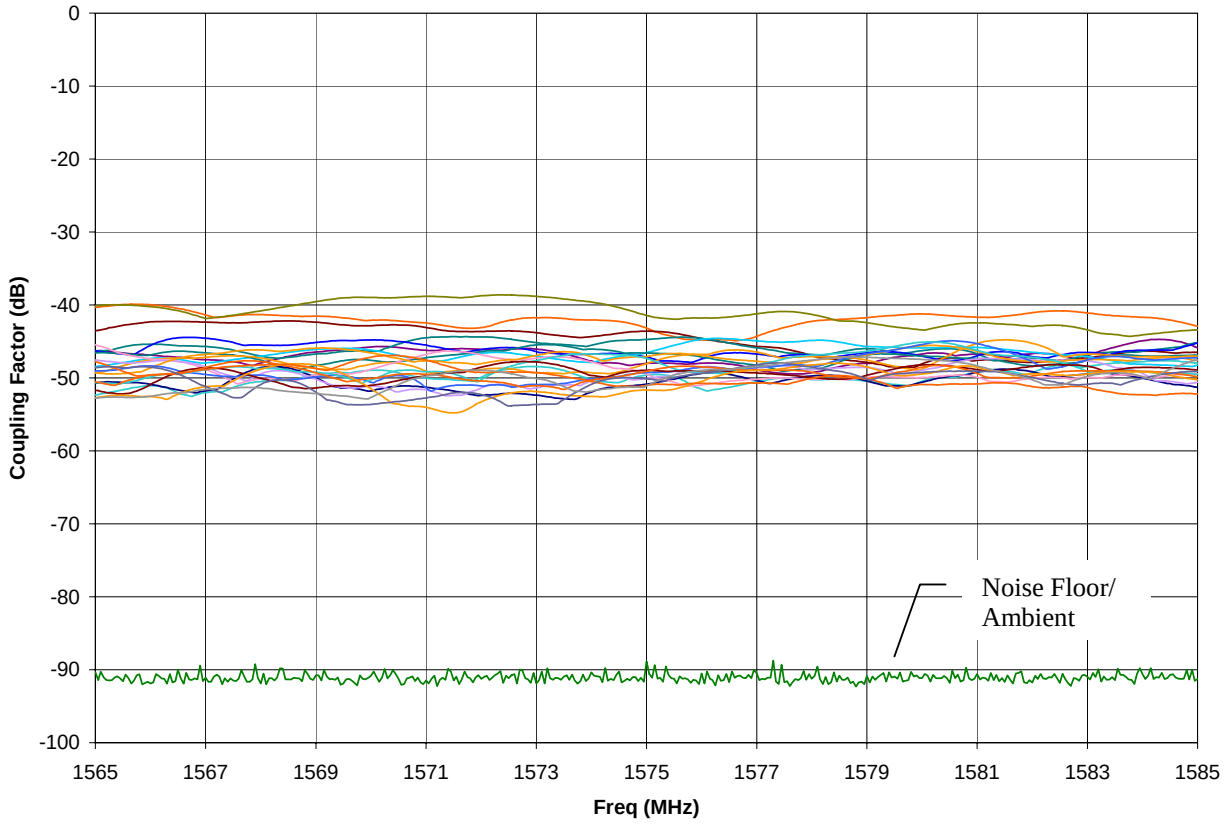

Figure 4.8-9a: Piper Saratoga GPS IPC scans.

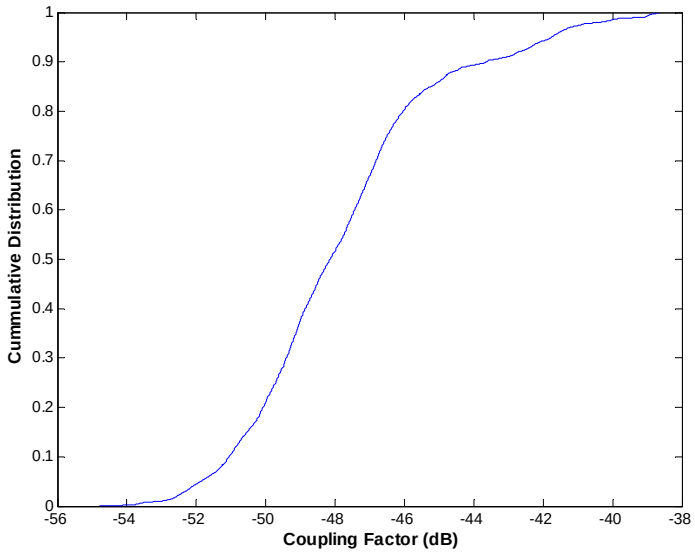

IPC Statistics		
Maximum	-38.6	dB
98 percentile	-40.4	dB
95 percentile	-41.8	dB
90 percentile	-43.6	dB
80 percentile	-46.0	dB
50 percentile	-48.2	dB
Mean	-46.7	dB
No. of Points	8822	
No. of Position Scans	22	
Freqs per Sweep	401	

Figure 4.8-9b: Piper Saratoga GPS IPC statistics

4.9 Gulfstream GII

Figure 4.9-1: Gulfstream GII.

Figure 4.9-2: Samples of Gulfstream GII external antennas.

4.9.1 VOR/LOC

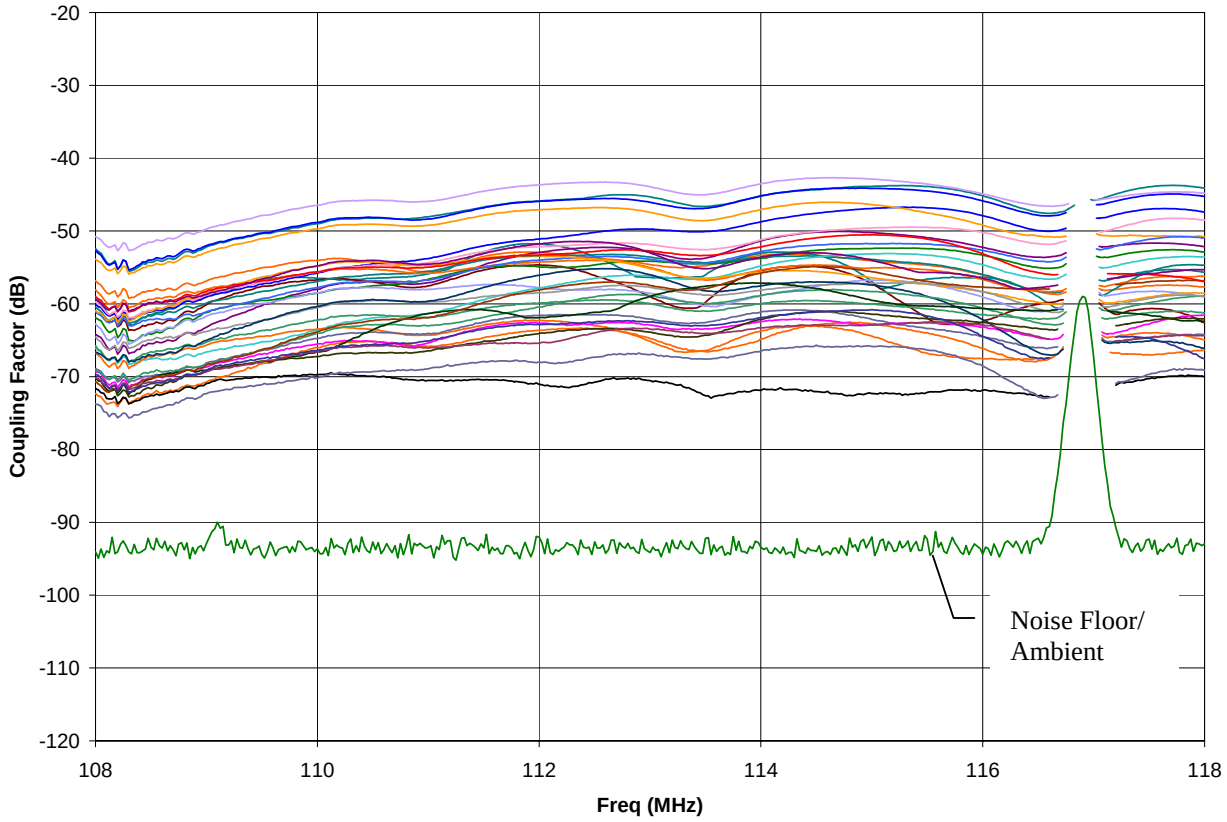

Figure 4.9-3a: Gulfstream GII VOR/LOC IPC scans.

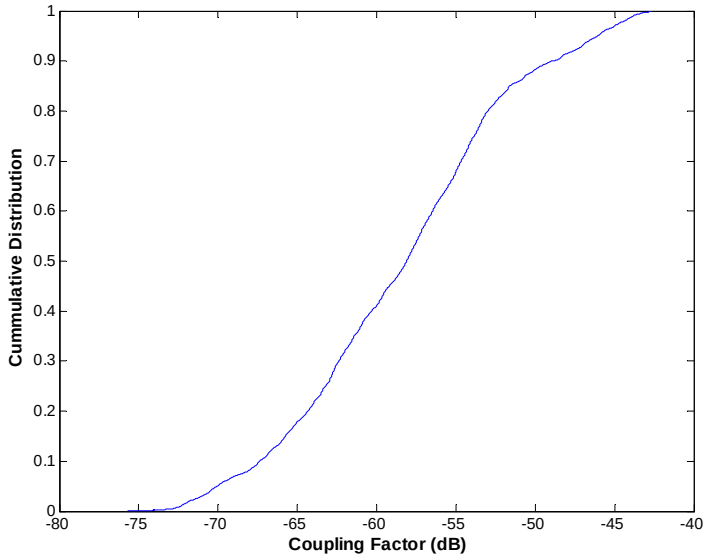

IPC Statistics		
Maximum	-42.7	dB
98 percentile	-44.3	dB
95 percentile	-46.1	dB
90 percentile	-48.9	dB
80 percentile	-53.0	dB
50 percentile	-58.1	dB
Mean	-53.4	dB
No. of Points	13162	
No. of Position Scans	34	
Freqs per Sweep	401	

Figure 4.9-3b: Gulfstream GII VOR/LOC IPC statistics.

4.9.2 VHF-Com1

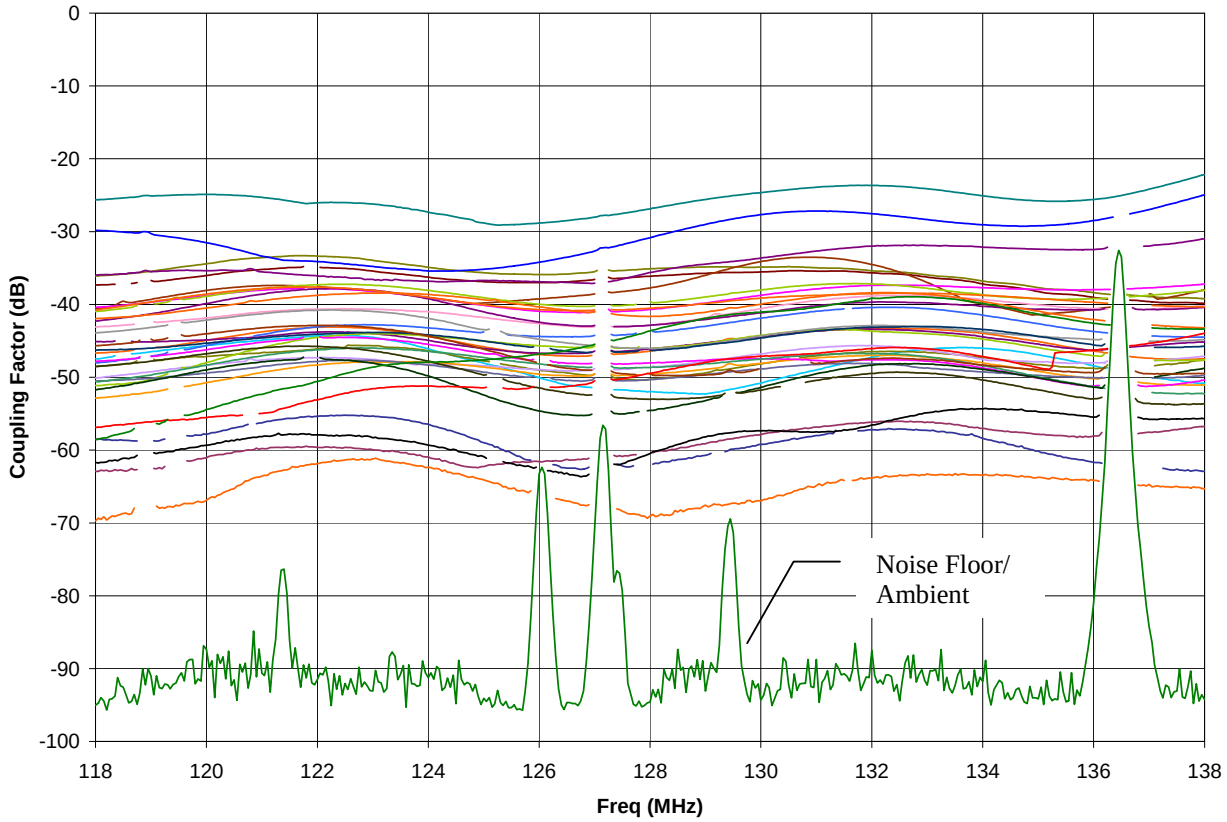

Figure 4.9-4a: Gulfstream GII VHF-Com1 IPC scans.

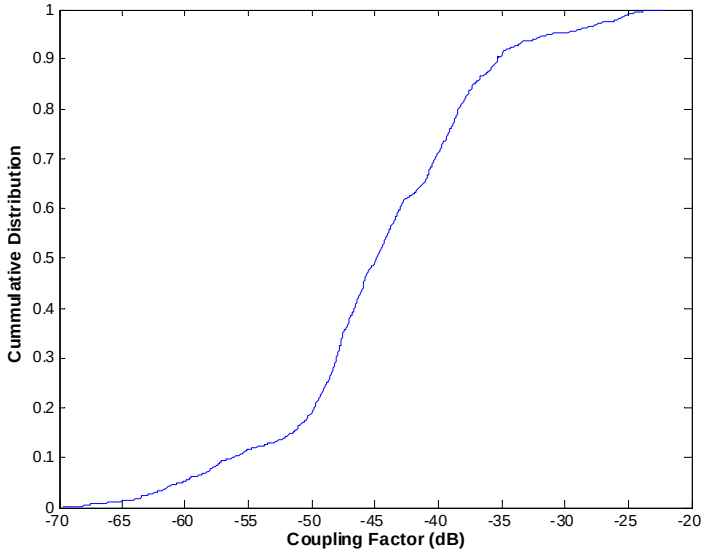

IPC Statistics		
Maximum	-22.2	dB
98 percentile	-25.8	dB
95 percentile	-31.1	dB
90 percentile	-35.3	dB
80 percentile	-38.4	dB
50 percentile	-44.9	dB
Mean	-37.2	dB
No. of Points	12733	
No. of Position Scans	34	
Freqs per Sweep	401	

Figure 4.9-4b: Gulfstream GII VHF-Com1 IPC statistics.

4.9.3 VHF-Com2

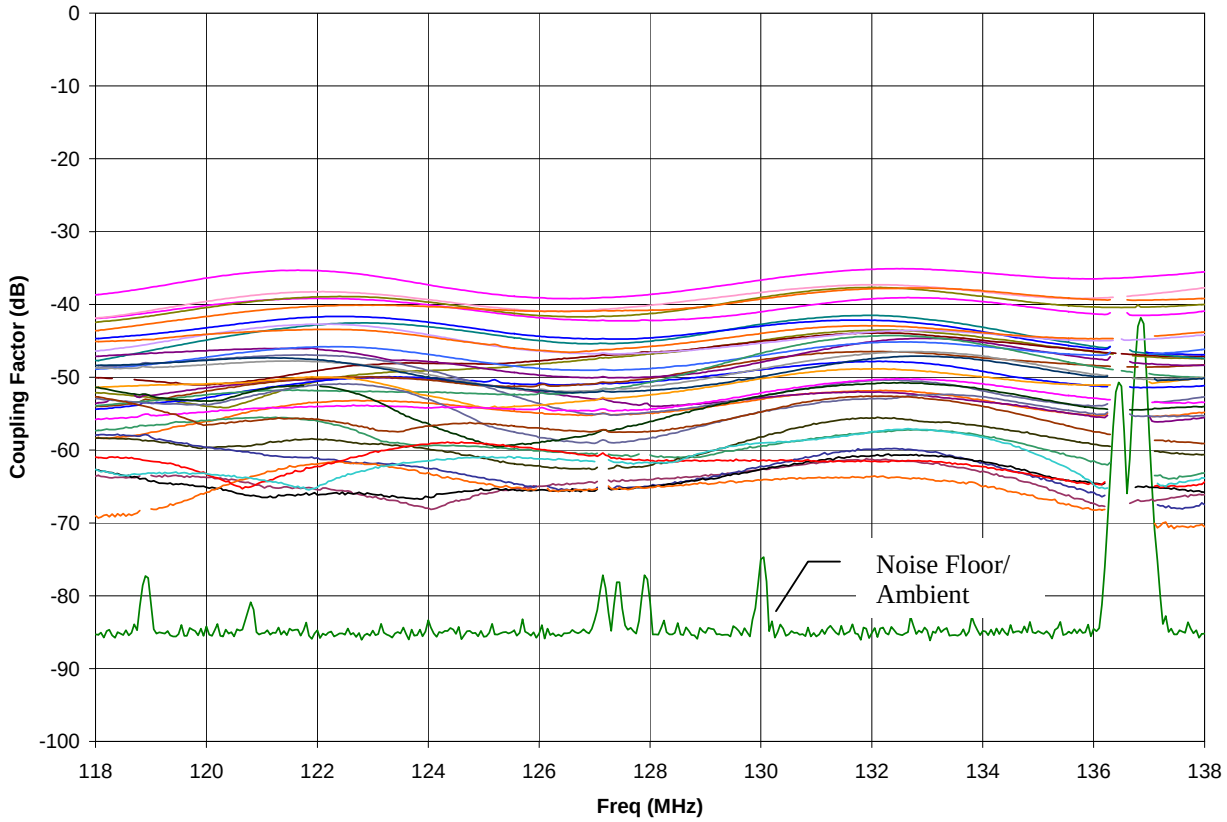

Figure 4.9-5a: Gulfstream GII VHF-Com2 IPC scans.

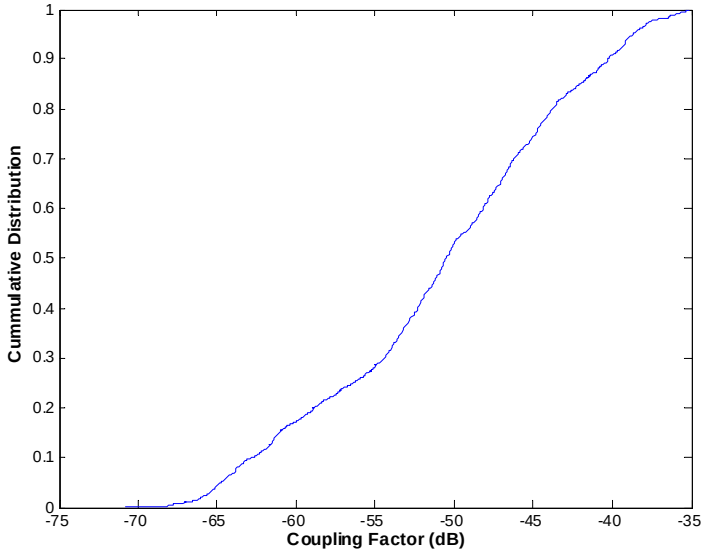

IPC Statistics		
Maximum	-35.1	dB
98 percentile	-37.3	dB
95 percentile	-38.7	dB
90 percentile	-40.2	dB
80 percentile	-43.8	dB
50 percentile	-50.5	dB
Mean	-45.2	dB
No. of Points	13240	
No. of Position Scans	34	
Freqs per Sweep	401	

Figure 4.9-5b: Gulfstream GII VHF-Com2 IPC statistics.

4.9.4 GS

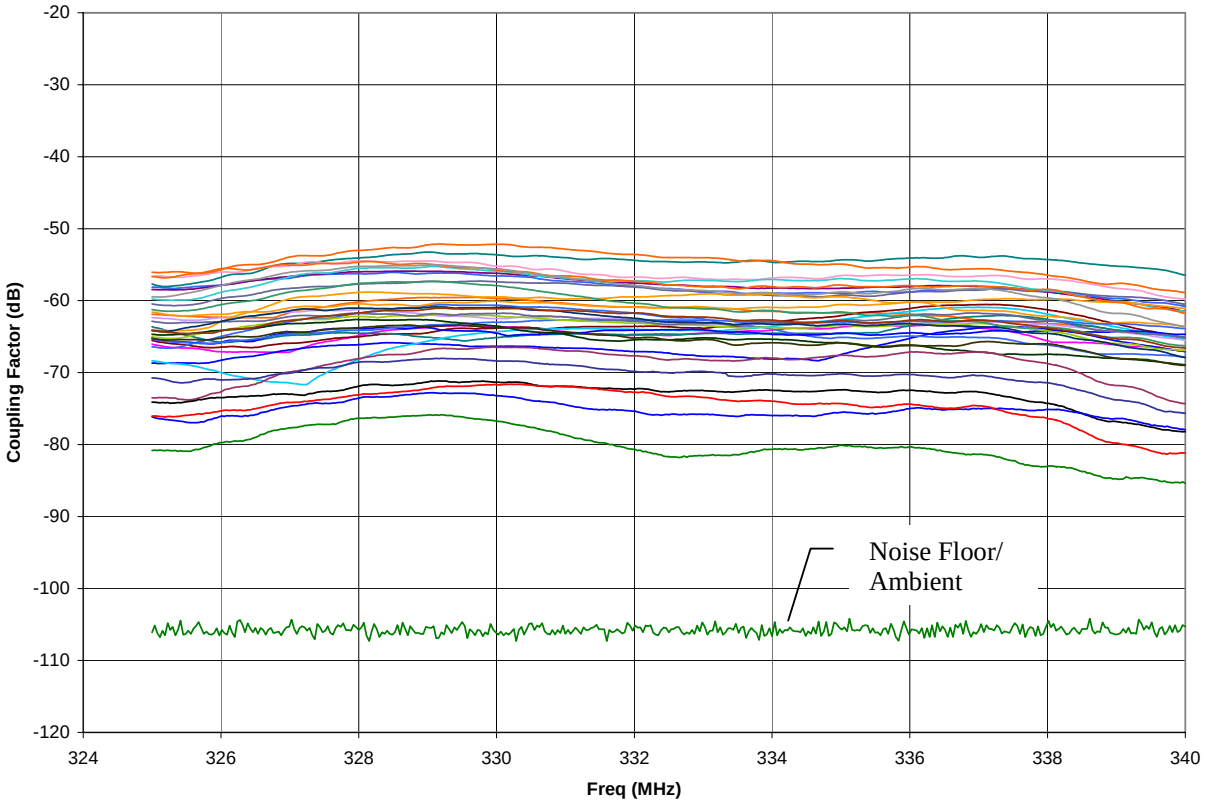

Figure 4.9-6a: Gulfstream GII GS IPC scans.

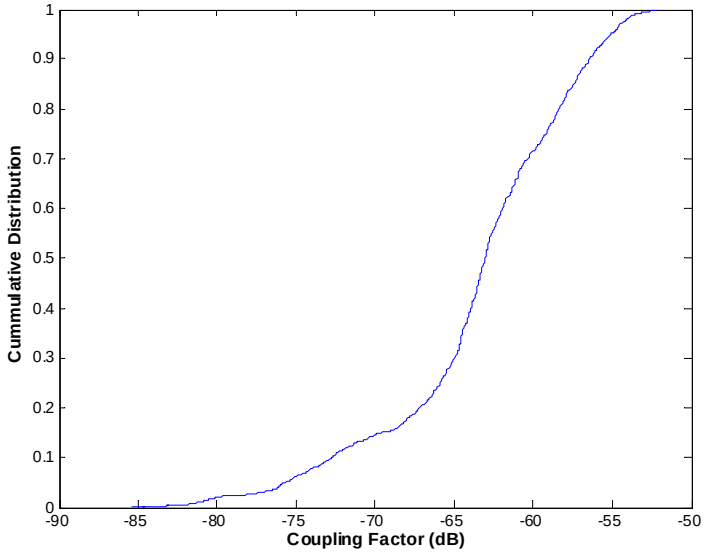

IPC Statistics		
Maximum	-52.1	dB
98 percentile	-54.1	dB
95 percentile	-55.0	dB
90 percentile	-56.4	dB
80 percentile	-58.3	dB
50 percentile	-63.0	dB
Mean	-60.5	dB
No. of Points	13634	
No. of Position Scans	34	
Freqs per Sweep	401	

Figure 4.9-6b: Gulfstream GII GS IPC statistics.

4.9.5 DME

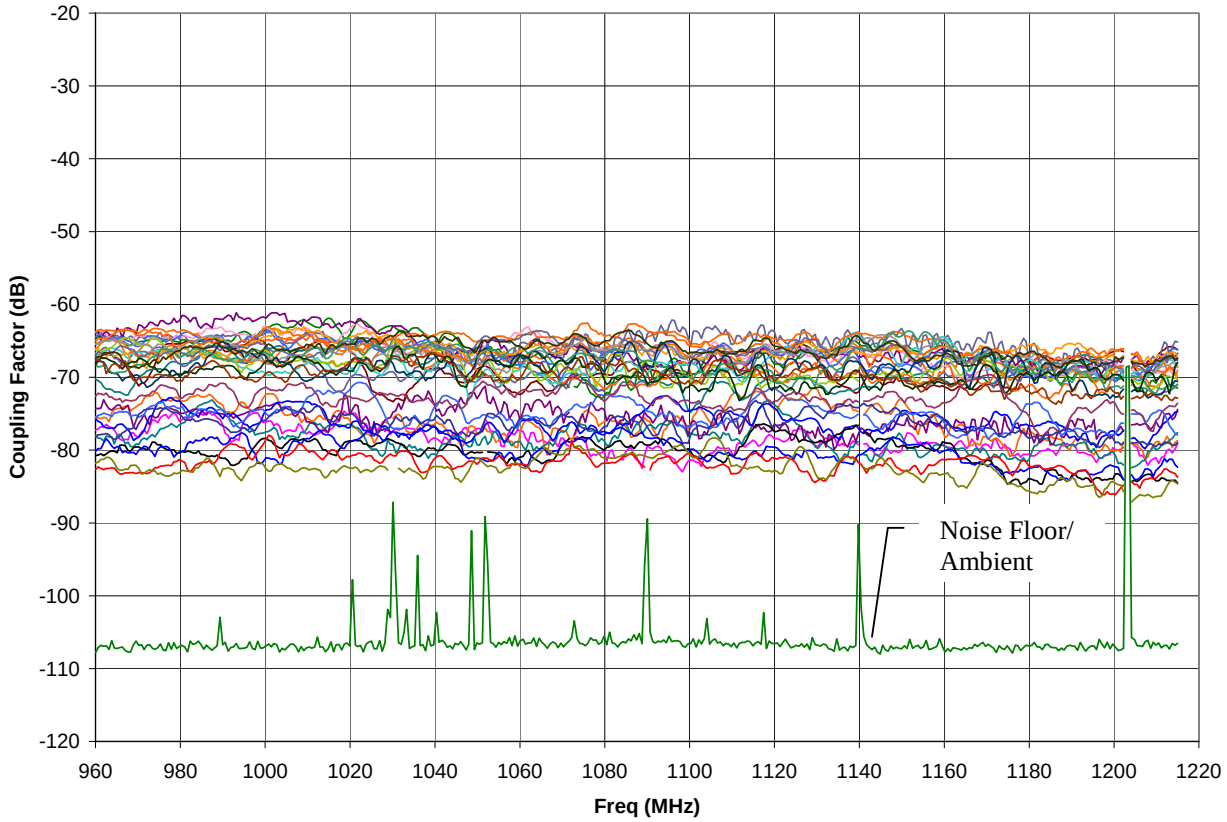

Figure 4.9-7a: Gulfstream GII DME IPC scans.

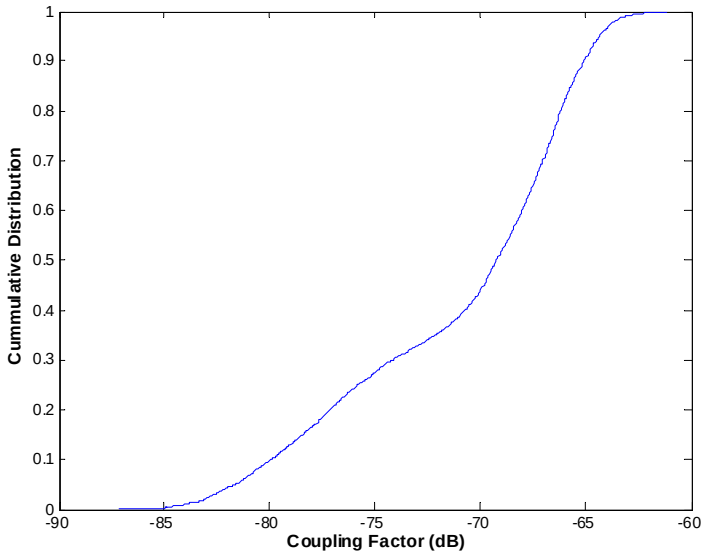

IPC Statistics		
Maximum	-61.1	dB
98 percentile	-63.6	dB
95 percentile	-64.3	dB
90 percentile	-65.1	dB
80 percentile	-66.2	dB
50 percentile	-69.2	dB
Mean	-68.5	dB
No. of Points	13516	
No. of Position Scans	34	
Freqs per Sweep	401	

Figure 4.9-7b: Gulfstream GII DME IPC statistics

4.9.6 ATC

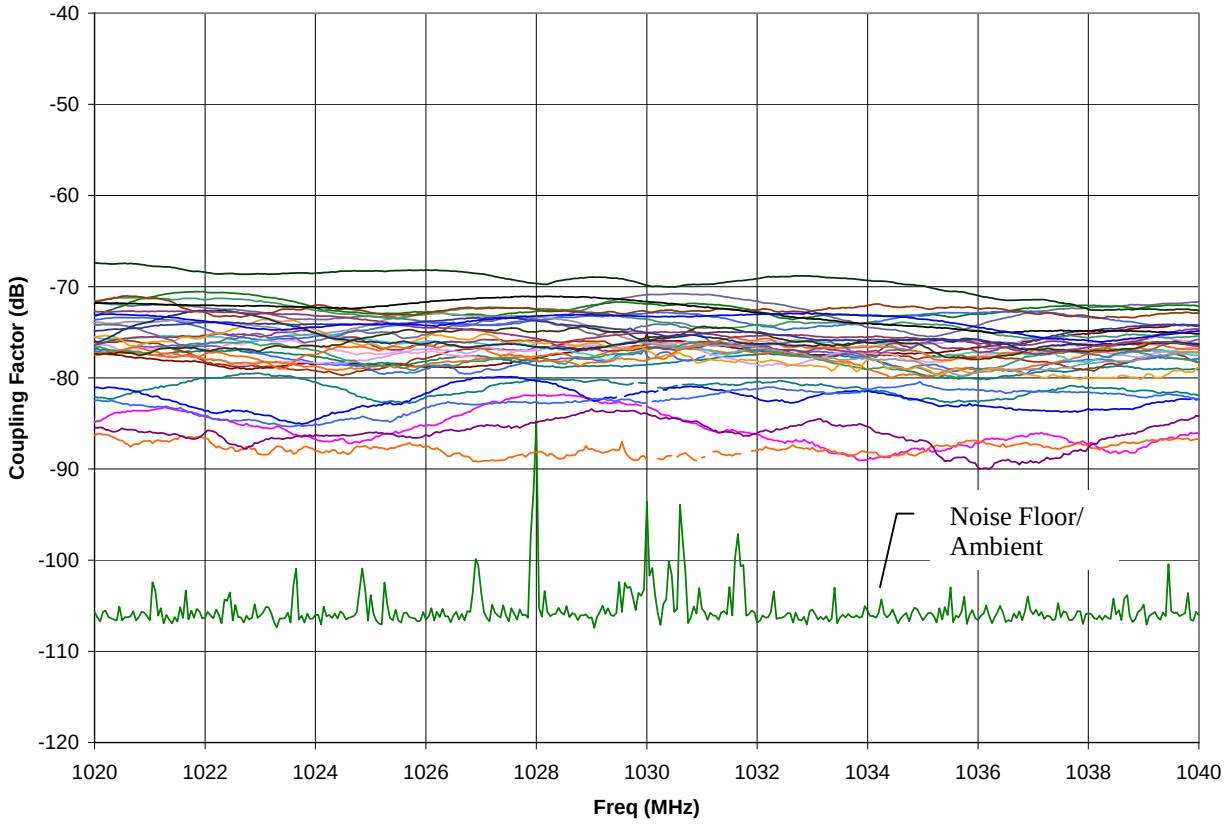

Figure 4.9-8a: Gulfstream GII ATC IPC scans.

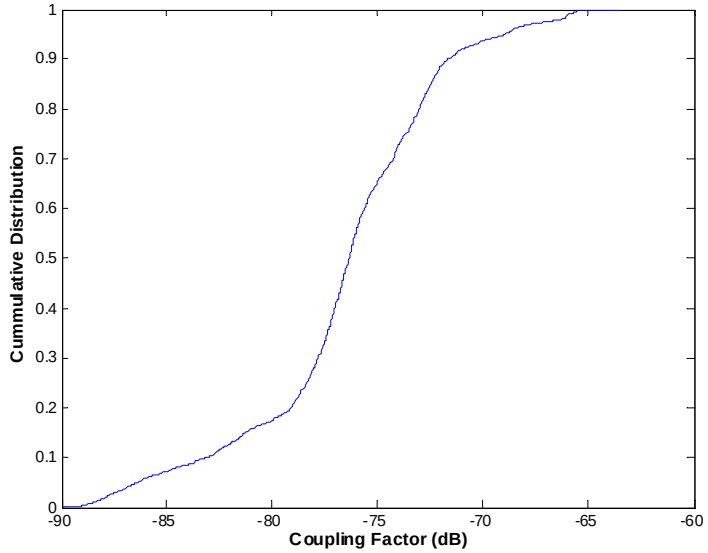

IPC Statistics		
Maximum	-63.5	dB
98 percentile	-66.3	dB
95 percentile	-69.0	dB
90 percentile	-71.6	dB
80 percentile	-73.1	dB
50 percentile	-76.3	dB
Mean	-74.31	dB
No. of Points	13613	
No. of Position Scans	34	
Freqs per Sweep	401	

Figure 4.9-8b: Gulfstream GII ATC IPC statistics

4.9.7 TCAS

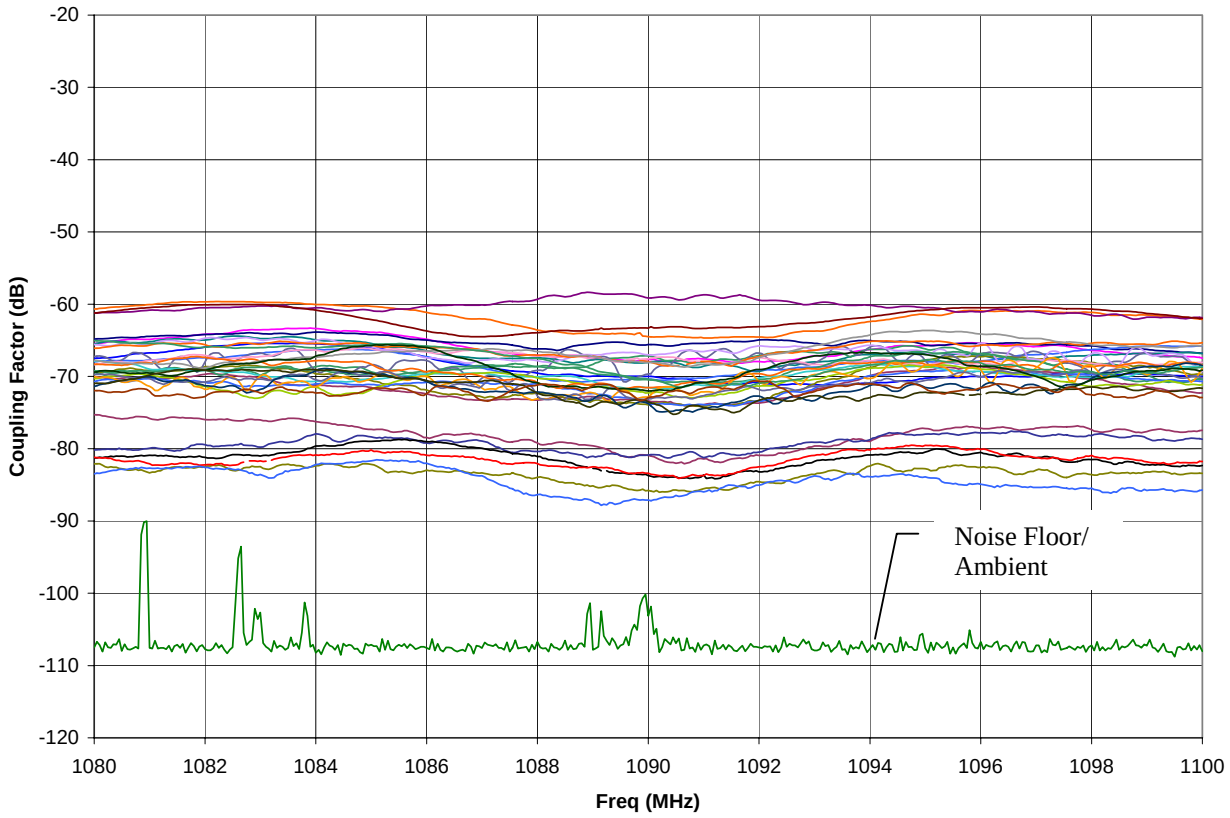

Figure 4.9-9a: Gulfstream GII TCAS IPC scans.

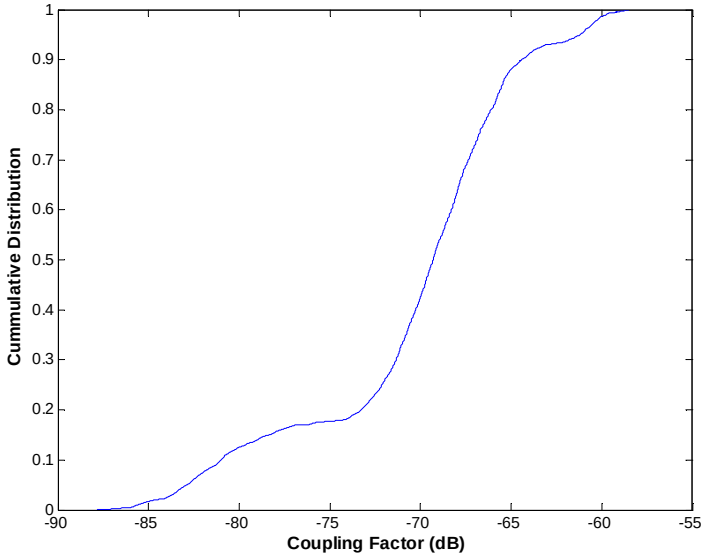

IPC Statistics		
Maximum	-58.4	dB
98 percentile	-60.2	dB
95 percentile	-61.2	dB
90 percentile	-64.4	dB
80 percentile	-66.1	dB
50 percentile	-69.3	dB
Mean	-67.4	dB
No. of Points	13615	
No. of Position Scans	34	
Freqs per Sweep	401	

Figure 4.9-9b: Gulfstream GII TCAS IPC statistics

4.9.8 GPS1

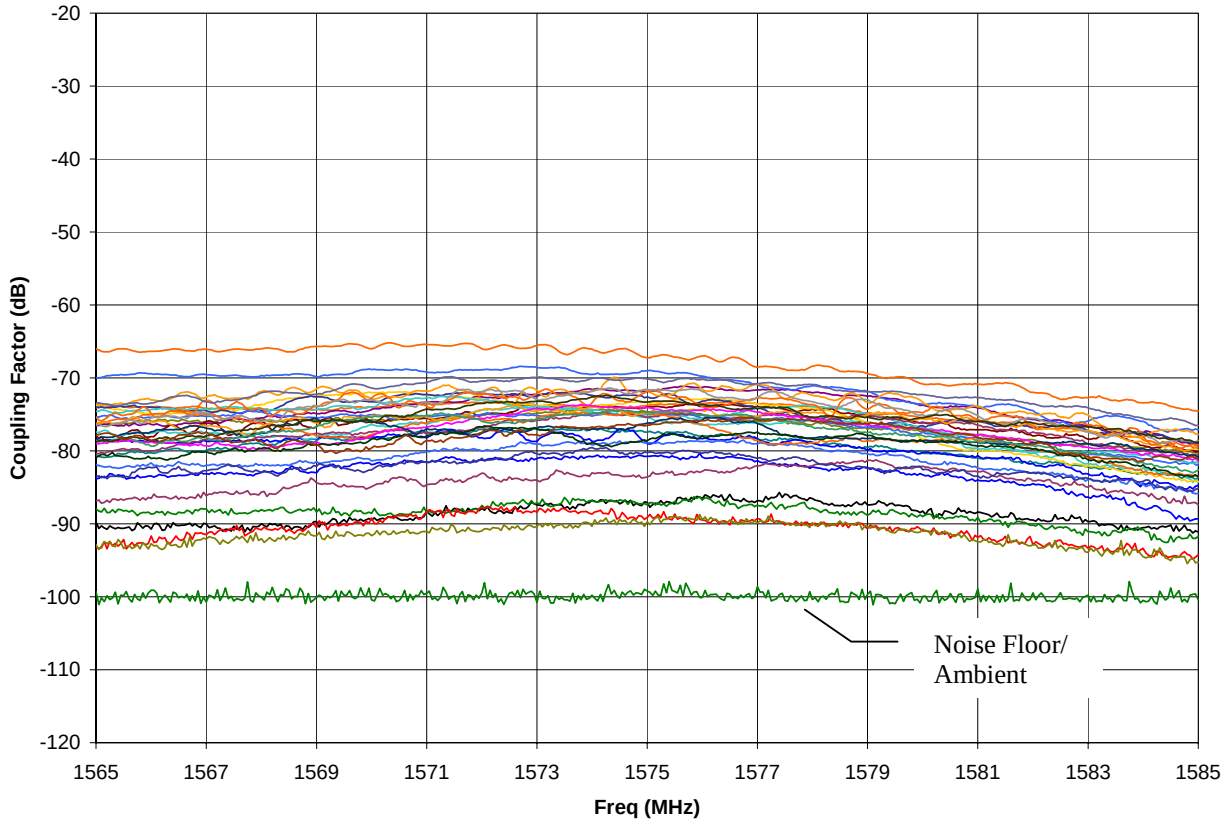

Figure 4.9-10a: Gulfstream GII GPS IPC scans.

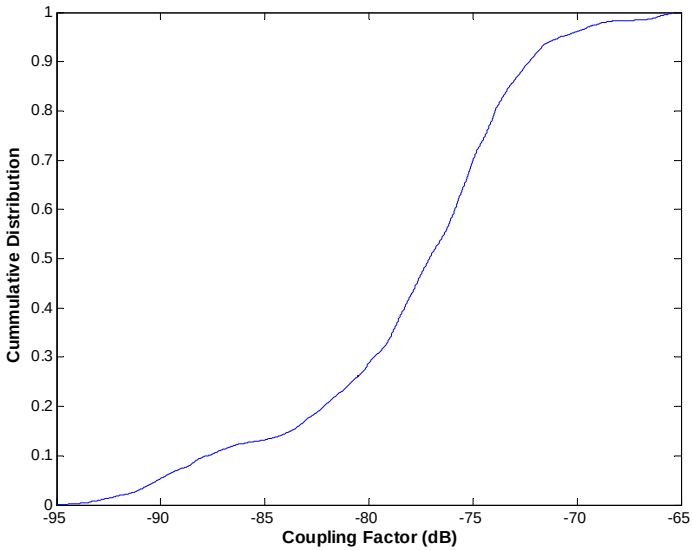

IPC Statistics		
Maximum	-65.2	dB
98 percentile	-68.6	dB
95 percentile	-70.8	dB
90 percentile	-72.3	dB
80 percentile	-73.9	dB
50 percentile	-77.1	dB
Mean	-75.4	dB
No. of Points	13634	
No. of Position Scans	34	
Freqs per Sweep	401	

Figure 4.9-10b: Gulfstream GII GPS1 IPC statistics.

4.10 King Air 200

Figure 4.10-1: King Air 200.

4.10.1 VOR/LOC

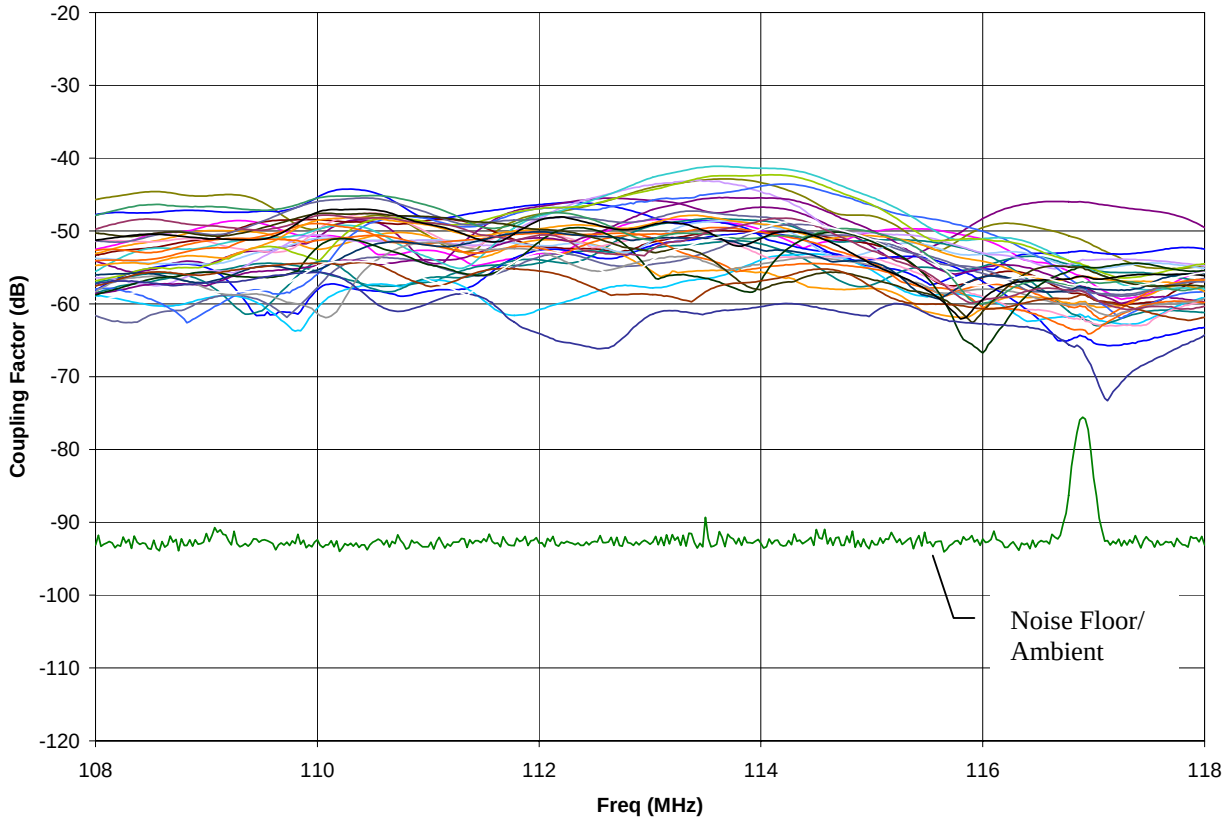

Figure 4.10-2a: King Air 200 VOR/LOC IPC scans.

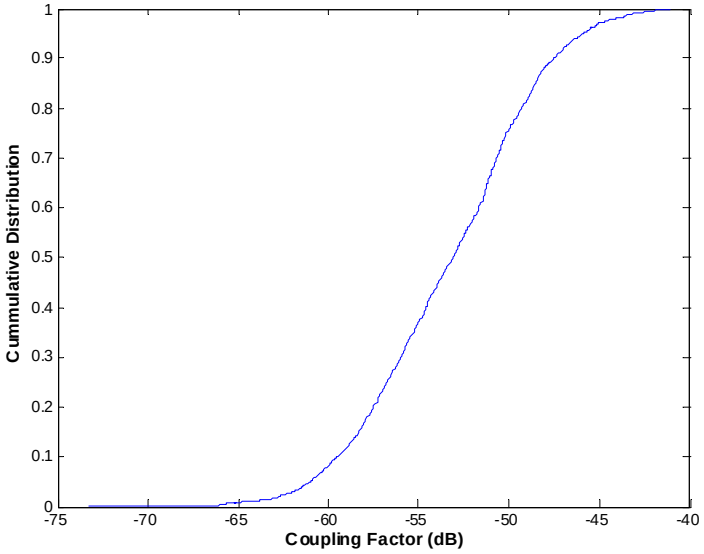

IPC Statistics		
Maximum	-41.1	dB
98 percentile	-44.2	dB
95 percentile	-45.9	dB
90 percentile	-47.5	dB
80 percentile	-49.3	dB
50 percentile	-53.1	dB
Mean	-51.0	dB
No. of Points	12832	
No. of Position Scans	32	
Freqs per Sweep	401	

Figure 4.10-2b: King Air 200 VOR/LOC IPC statistics.

4.10.2 VHF-Com1

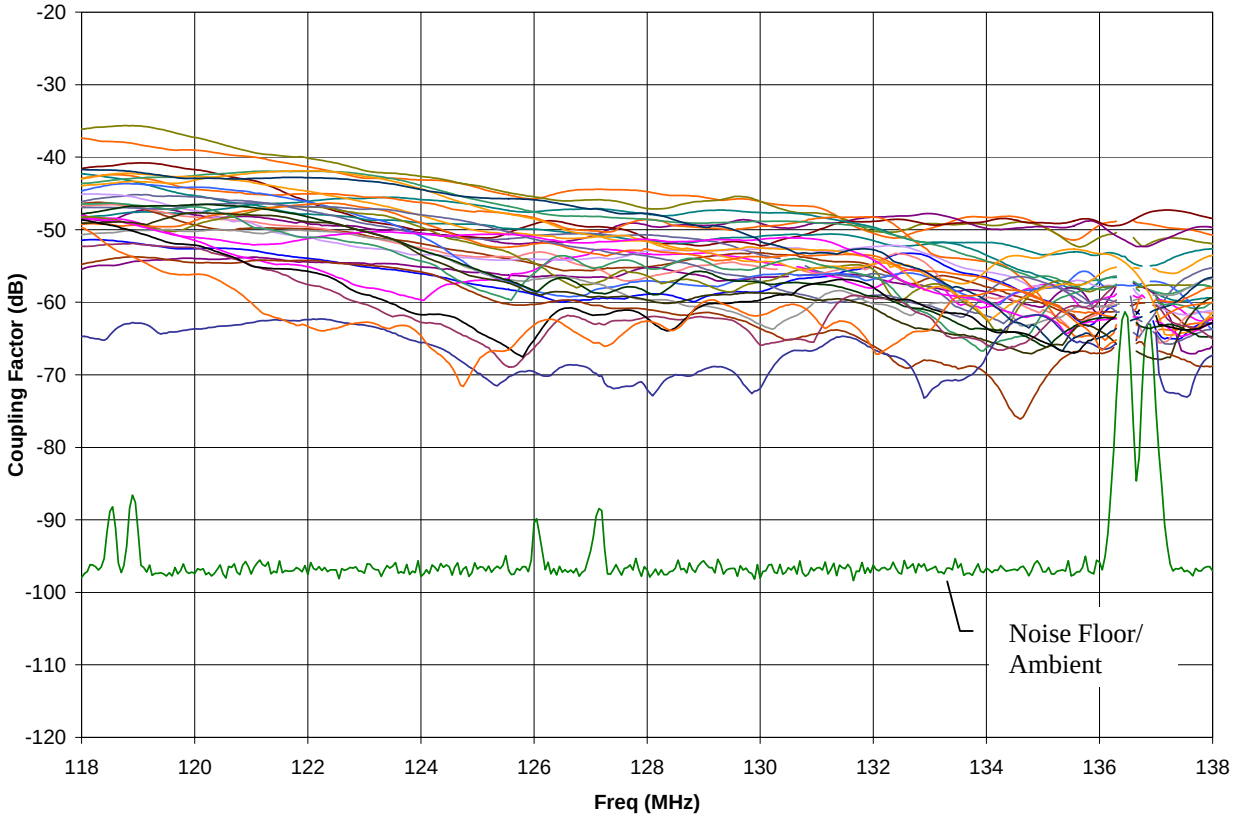

Figure 4.10-3a: King Air 200 VHF-Com1 IPC scans.

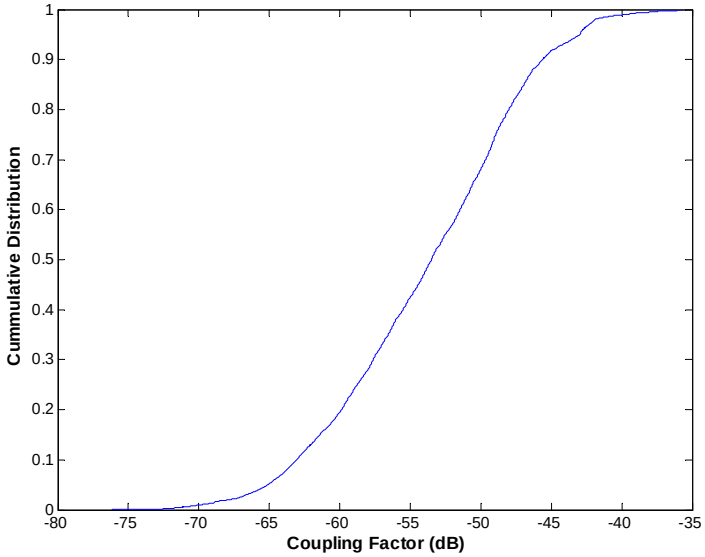

IPC Statistics		
Maximum	-35.6	dB
98 percentile	-41.9	dB
95 percentile	-43.0	dB
90 percentile	-45.6	dB
80 percentile	-48.0	dB
50 percentile	-53.5	dB
Mean	-49.3	dB
No. of Points	12585	
No. of Position Scans	32	
Freqs per Sweep	401	

Figure 4.10-3b: King Air 200 VHF-Com1 IPC statistics.

4.10.3 VHF-Com2

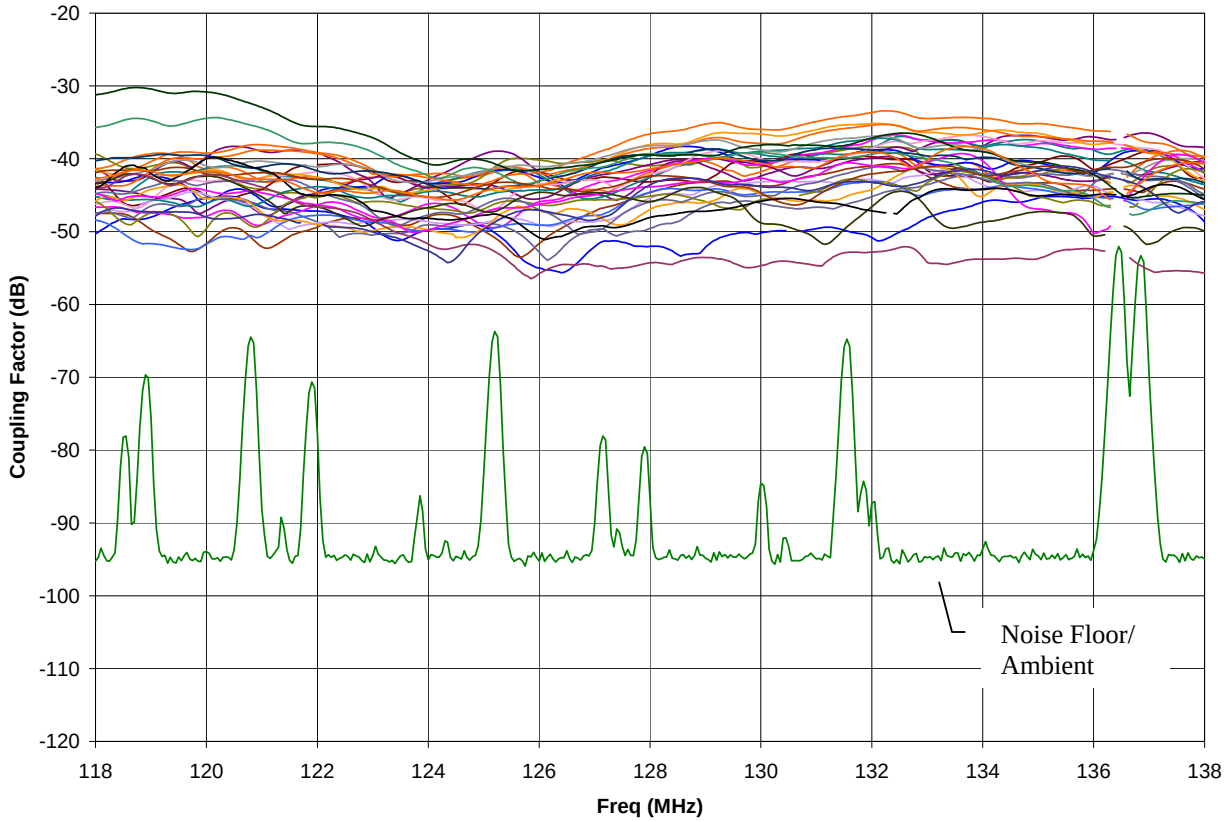

Figure 4.10-4a: King Air 200 VHF-Com2 IPC scans.

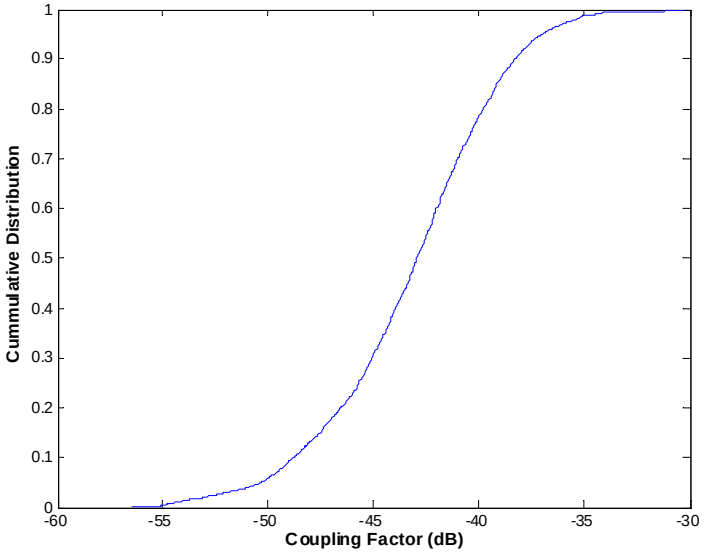

IPC Statistics		
Maximum	-30.2	dB
98 percentile	-35.4	dB
95 percentile	-37.0	dB
90 percentile	-38.3	dB
80 percentile	-39.8	dB
50 percentile	-42.9	dB
Mean	-41.4	dB
No. of Points	12702	
No. of Position Scans	32	
Freqs per Sweep	401	

Figure 4.10-4b: King Air 200 VHF-Com2 IPC statistics.

4.10.4 GS

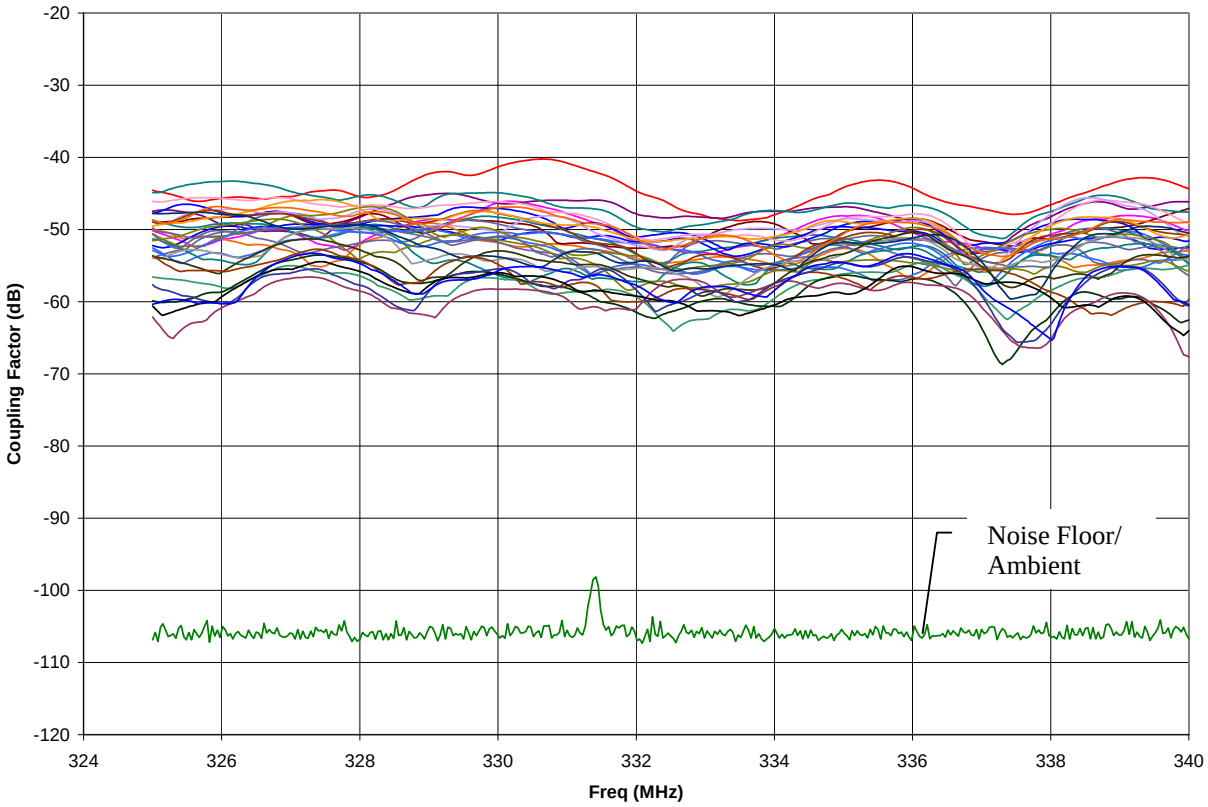

Figure 4.10-5a: King Air 200 GS IPC scans.

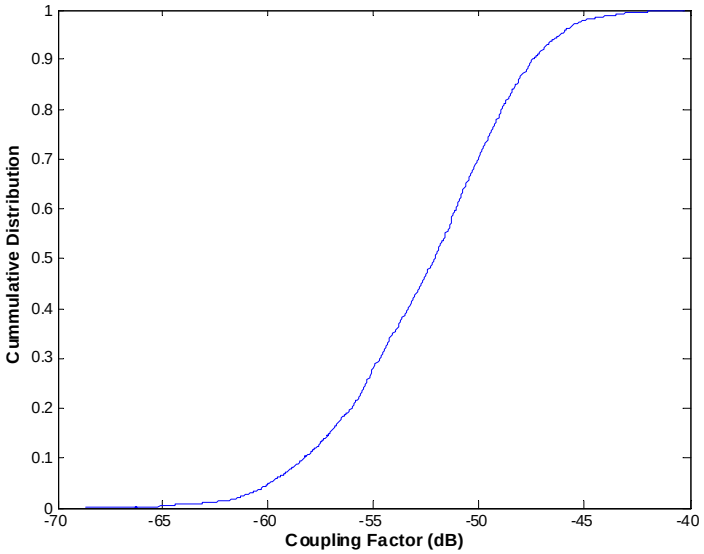

IPC Statistics		
Maximum	-40.2	dB
98 percentile	-44.9	dB
95 percentile	-46.1	dB
90 percentile	-47.4	dB
80 percentile	-48.9	dB
50 percentile	-52.1	dB
Mean	-50.7	dB
No. of Points	12832	
No. of Position Scans	32	
Freqs per Sweep	401	

Figure 4.10-5b: King Air 200 GS IPC statistics.

4.10.5 DME1

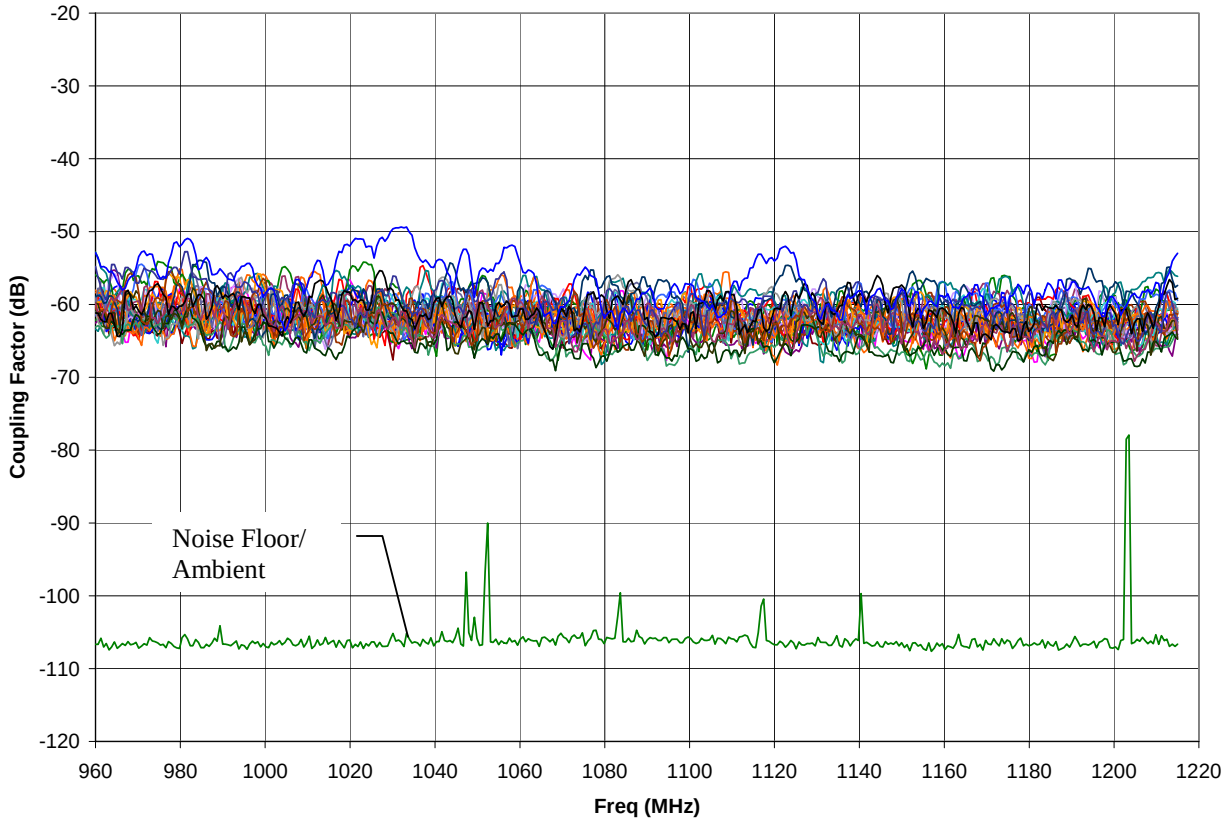

Figure 4.10-6a: King Air 200 DME1 IPC scans.

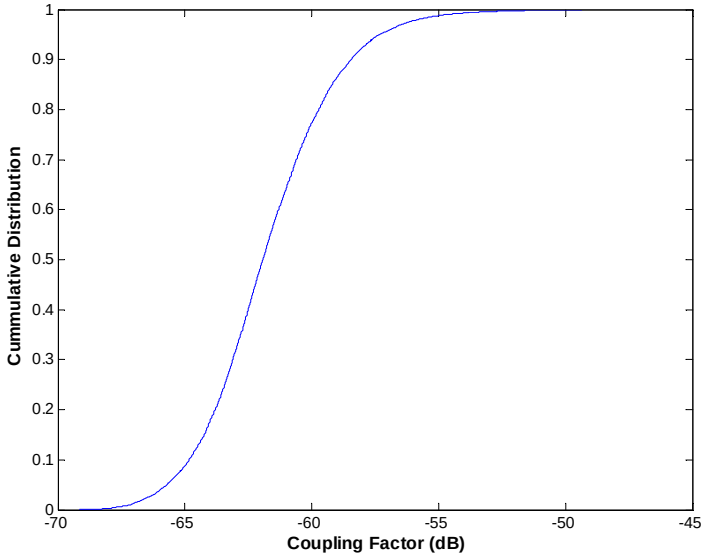

IPC Statistics		
Maximum	-49.4	dB
98 percentile	-55.8	dB
95 percentile	-57.3	dB
90 percentile	-58.4	dB
80 percentile	-59.7	dB
50 percentile	-61.9	dB
Mean	-60.9	dB
No. of Points	12832	
No. of Position Scans	32	
Freqs per Sweep	401	

Figure 4.10-6b: King Air 200 DME1 IPC statistics.

4.10.6 DME2

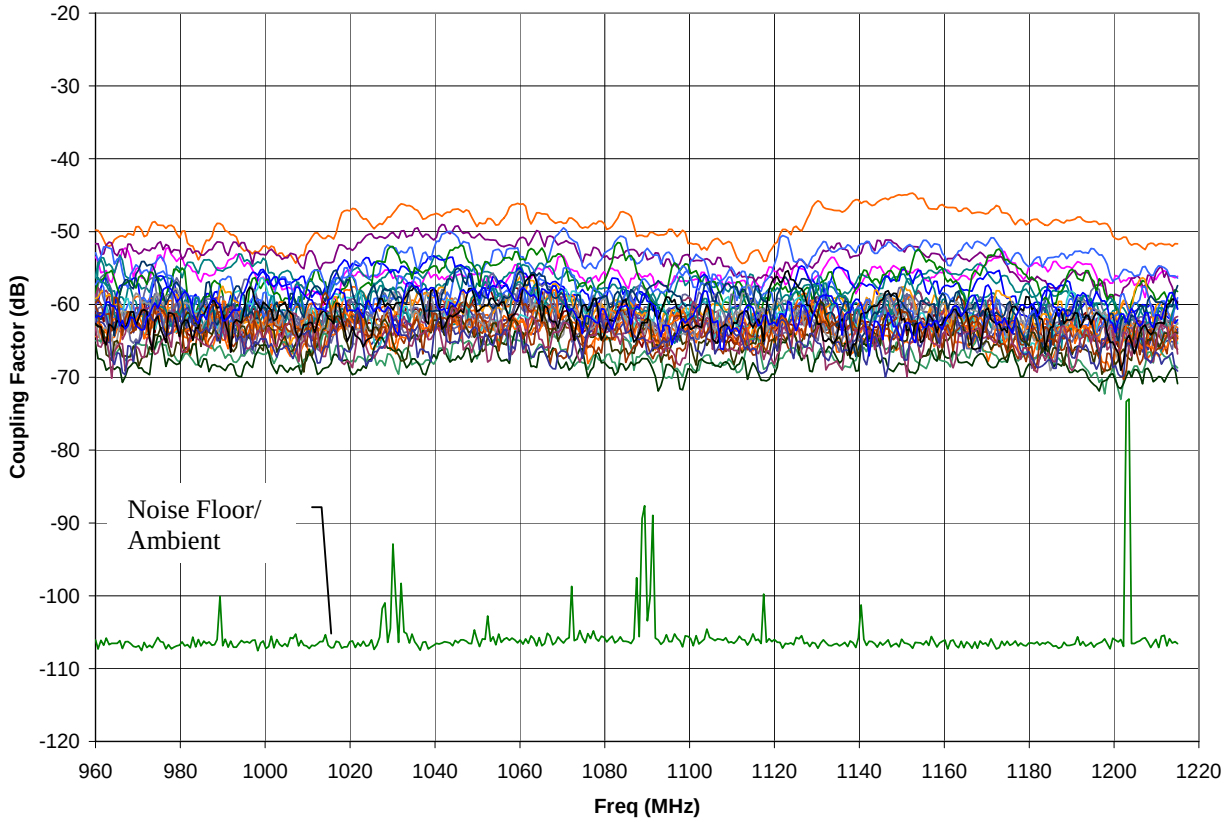

Figure 4.10-7a: King Air 200 DME2 IPC scans.

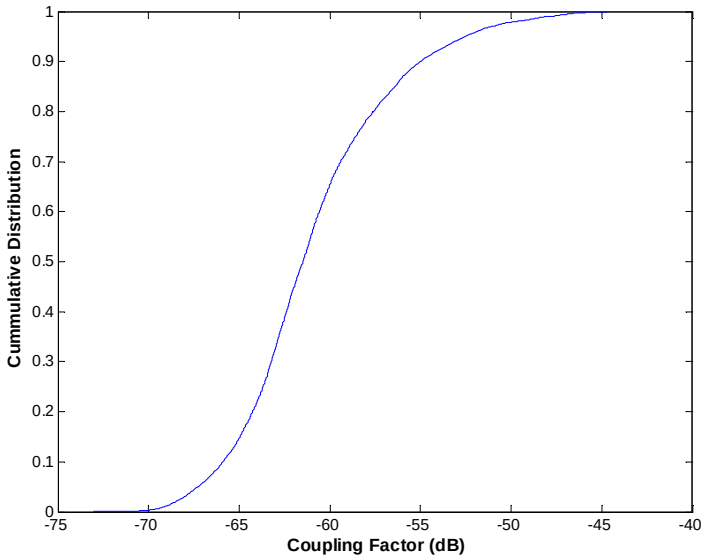

IPC Statistics		
Maximum	-44.7	dB
98 percentile	-49.8	dB
95 percentile	-52.5	dB
90 percentile	-55.0	dB
80 percentile	-57.6	dB
50 percentile	-61.5	dB
Mean	-58.1	dB
No. of Points	12832	
No. of Position Scans	32	
Freqs per Sweep	401	

Figure 4.10-7b: King Air 200 DME2 IPC statistics.

4.10.7 ATC

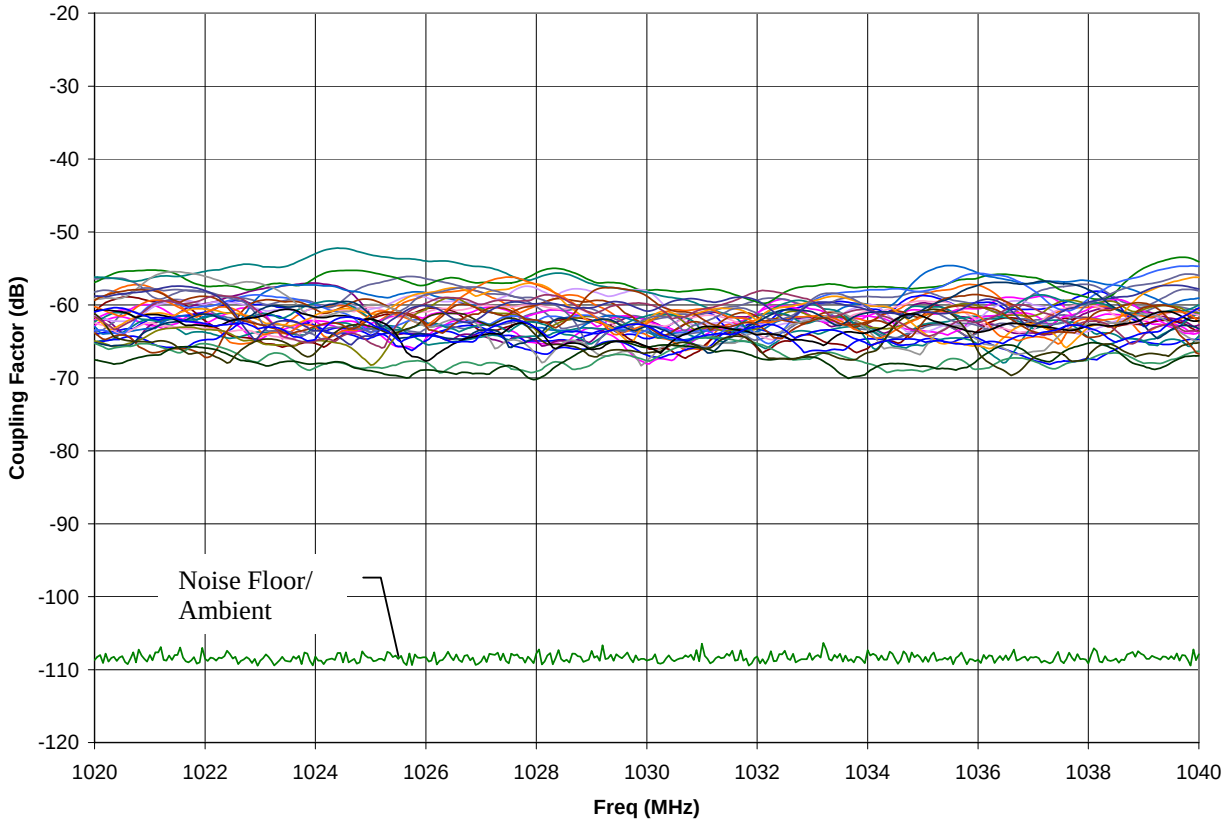

Figure 4.10-8a: King Air 200 ATC IPC scans.

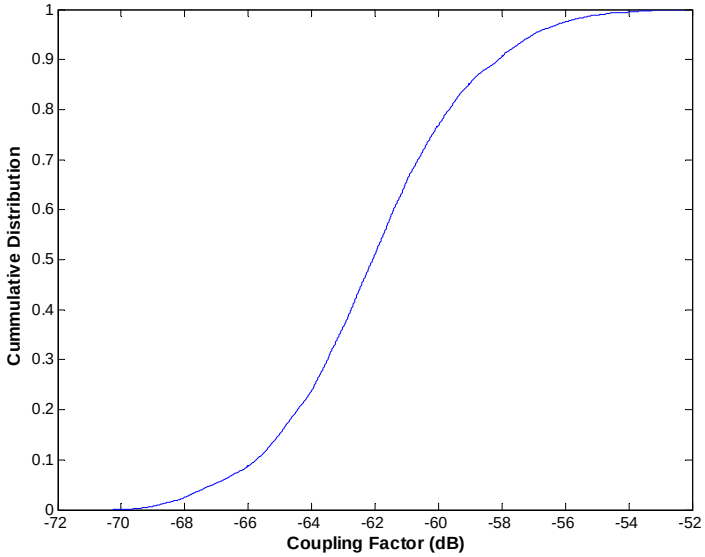

IPC Statistics		
Maximum	-52.2	dB
98 percentile	-55.7	dB
95 percentile	-57.0	dB
90 percentile	-58.1	dB
80 percentile	-59.7	dB
50 percentile	-62.1	dB
Mean	-61.0	dB
No. of Points	12832	
No. of Position Scans	32	
Freqs per Sweep	401	

Figure 4.10-8b: King Air 200 ATC IPC statistics.

4.10.8 GPS

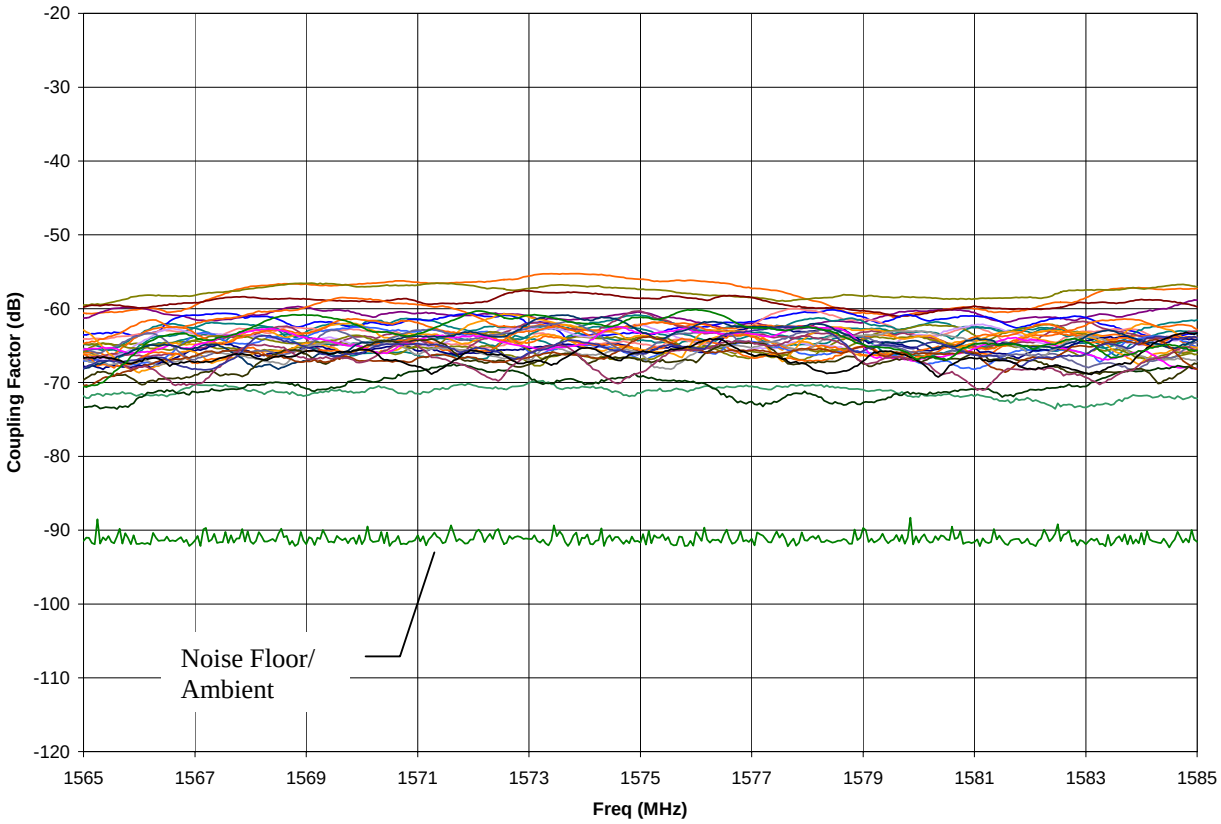

Figure 4.10-9a: King Air 200 GPS IPC scans.

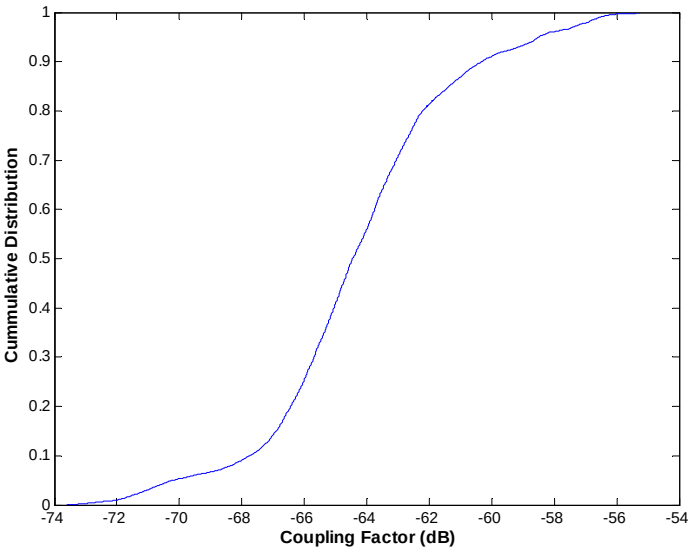

IPC Statistics		
Maximum	-55.3	dB
98 percentile	-56.9	dB
95 percentile	-58.5	dB
90 percentile	-60.3	dB
80 percentile	-62.2	dB
50 percentile	-64.5	dB
Mean	-63.1	dB
No. of Points	12832	
No. of Position Scans	32	
Freqs per Sweep	401	

Figure 4.10-9b: King Air 200 GPS IPC statistics.

5 Observations and Results Summary

Figures 5-1 to 5-7 summarize the IPC cumulative distribution curves presented in Section 4 for different aircraft. These consolidated charts enable easy comparison between different installations.

The CDF curves potentially have applications in interference risk assessment and optimization. CDF curves for the individual *source – path loss – victim threshold* elements may be combined to yield overall interference risk factors. Optimization may then be performed by making trade-offs in each element's test and qualification levels to achieve an overall interference risk target. Measurement and utilization of CDF data are not included in current test processes [5].

Tables 5-1a and 5-1b summarize the maximum IPC data by tabulating the worst case coupling of all locations and frequencies measured. This type of worst case presentation is typical in the past efforts illustrated in [1][3][5], except the data were typically in IPL form. IPL and IPC are simply the negative of one another. The IPL term is more widely recognized, while plots of IPC data are often more intuitive. By reporting the statistics of the data, additional insights may be gained in interference risk assessment.

The charts show significant data variations between different aircraft models. However, it can be seen that the data cumulative distribution curves are similar in shape for several different aircraft models. Appendix B shows similar plots but with the data normalized to the traces' average (mean) IPC values. The trace's average IPC value was chosen arbitrarily as the normalization factor; however, other normalization factors may be chosen to determine the best fit model. The normalized comparisons in Appendix B confirm that many IPC cumulative distribution curves are indeed similar in shape. Further analysis is needed to validate and utilize this characteristic to improve future measurements and analysis.

Comparing with previously measured larger aircraft, including the Boeing 737, 747 and 757 [1], these small aircraft's peak IPC data are generally higher by 15 dB or more. The difference with large aircraft data can be significant depending on the specific aircraft and systems being compared. Higher IPC data potentially means higher interference risks for the smaller aircraft considered. A summary of large aircraft IPC can be found in Appendix C.

The worst case coupling location for each aircraft system depends on a number of factors that could affect the interference signal propagation path. These factors include aircraft skin material, size, antenna location, door location, window location and size, internal structure and external structure. Determining analytically the peak coupling location can be complex. Upon examination of the measured data, the peak IPC locations are documented in Appendix D. Several general observations can be made.

- Windshield and cockpit are consistently among locations with the highest IPC values (Citation II, LearJet 35A, Piper Saratoga, King Air 200). Though this is expected for aircraft antennas located near the cockpit, it is also often the case for antenna locations further away, i.e. the tail. Large windshield and cockpit windows (relative to the remaining windows) coupled with small aircraft size are possible explanations.

- Windows and doors can provide the highest IPC value if they are close to the victim aircraft antenna

- For antennas located in the aircraft's vertical tail (typically VOR/LOC and GS), windows closest to the tail often are not the strongest coupling locations. Rather, windows further toward the front and windshield often provided the highest IPC values.

- For many aircraft and systems, the spread of IPC values is not large. This means strong coupling can occur for many locations within the aircraft, and the levels are close to the peak value. Small aircraft volume and lack of shielded partitions within the cabin may be the cause.

- As a result of the composite fiberglass skin, the Cirrus SR-22 model provided little shielding between the inside and the aircraft top-mounted antennas. Very strong coupling was achieved by positioning the transmit antenna directly underneath the base of aircraft antennas.

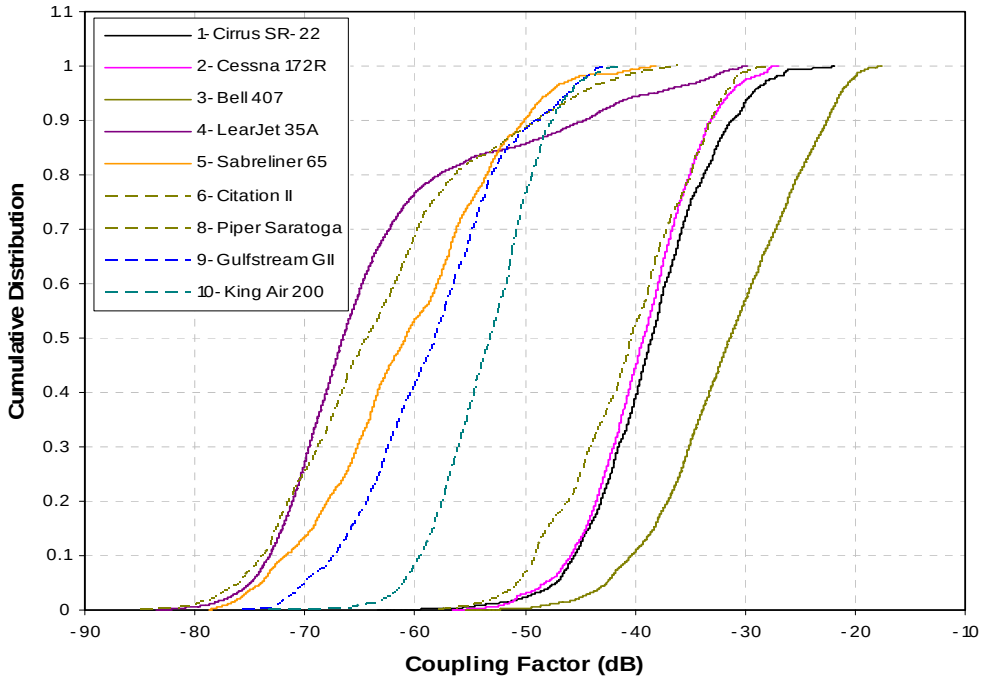

Figure 5-1: VOR/LOC IPC cumulative distribution comparison.

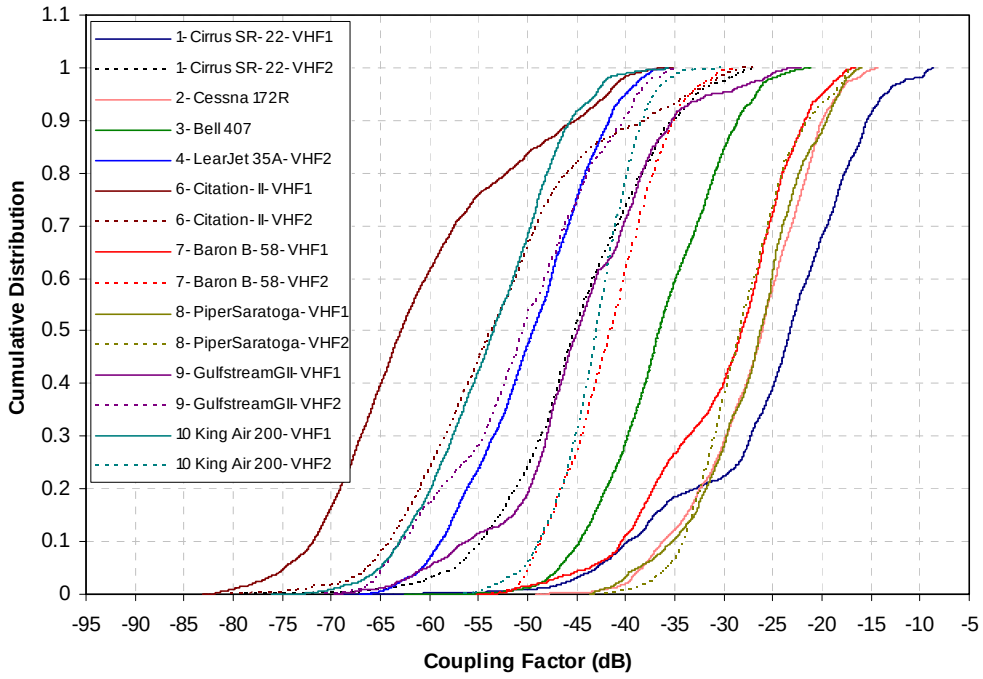

Figure 5-2: VHF-Com IPC cumulative distribution comparison.

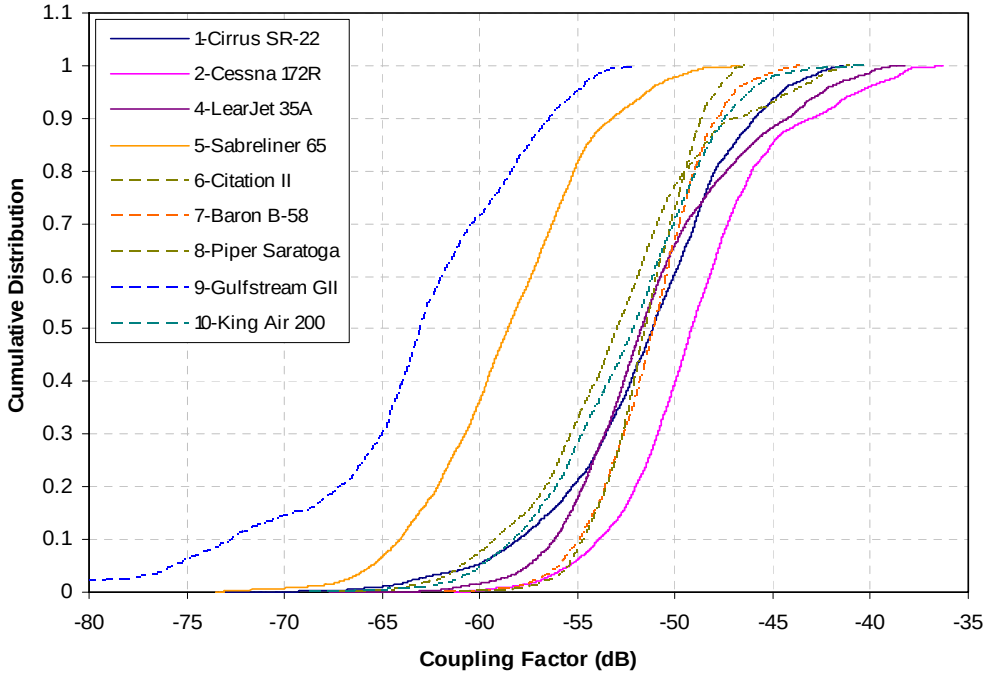

Figure 5-3: GS IPC cumulative distribution comparison.

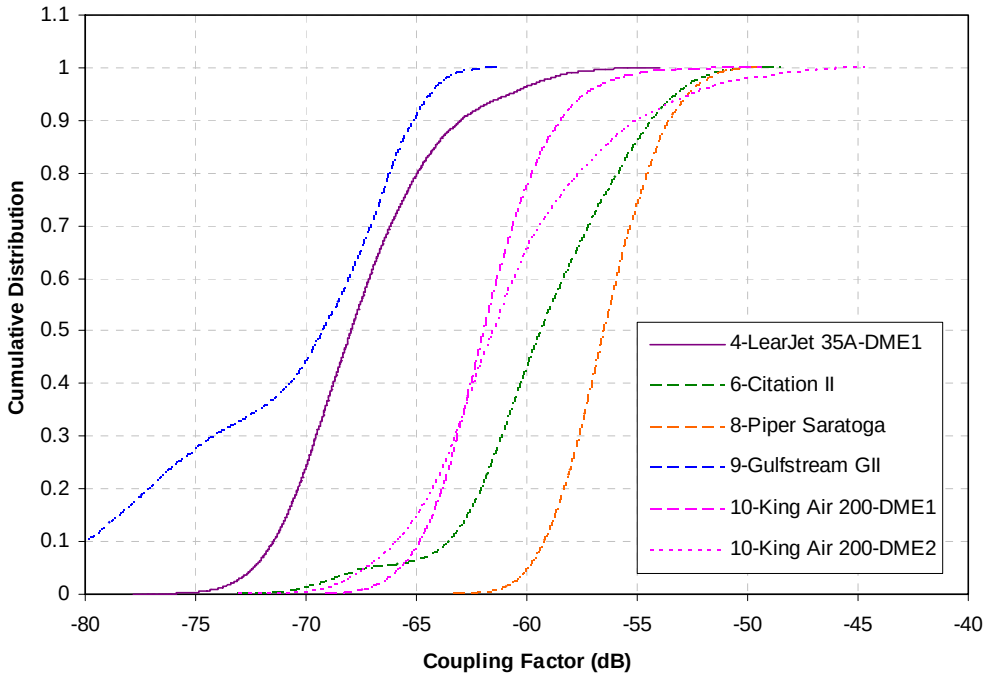

Figure 5-4: DME IPC cumulative distribution comparison.

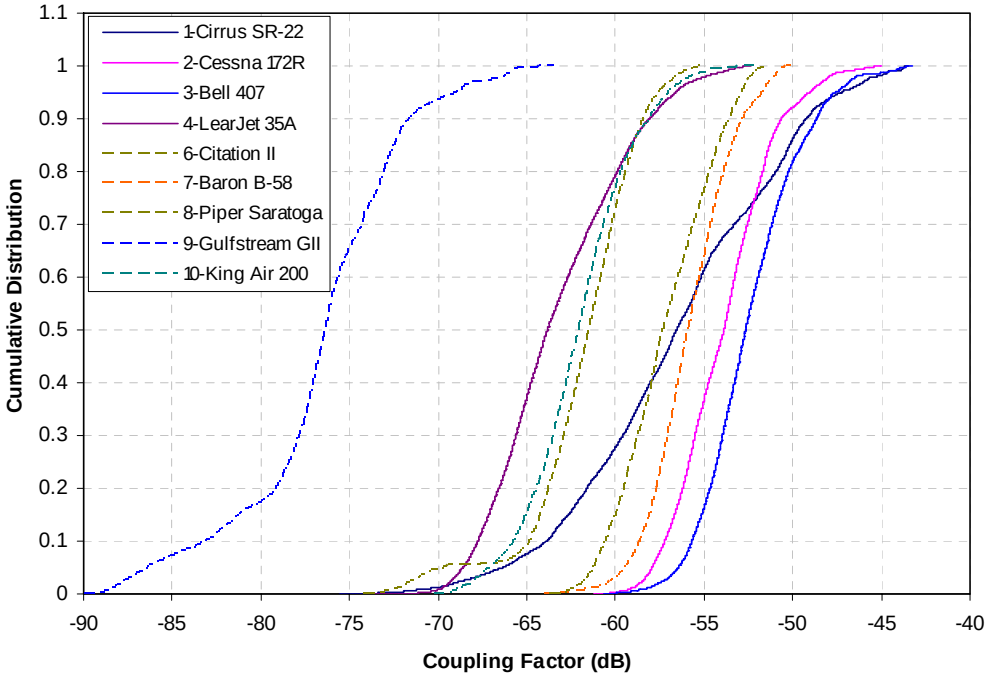

Figure 5-5: ATC IPC cumulative distribution comparison.

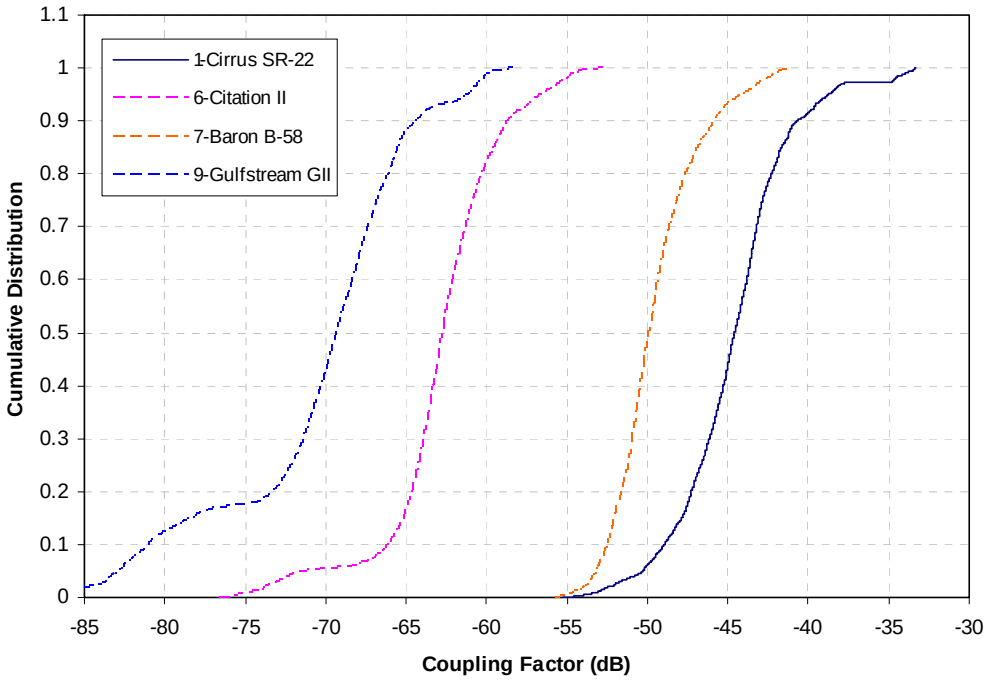

Figure 5-6: TCAS (and TCAD) cumulative distribution comparison.

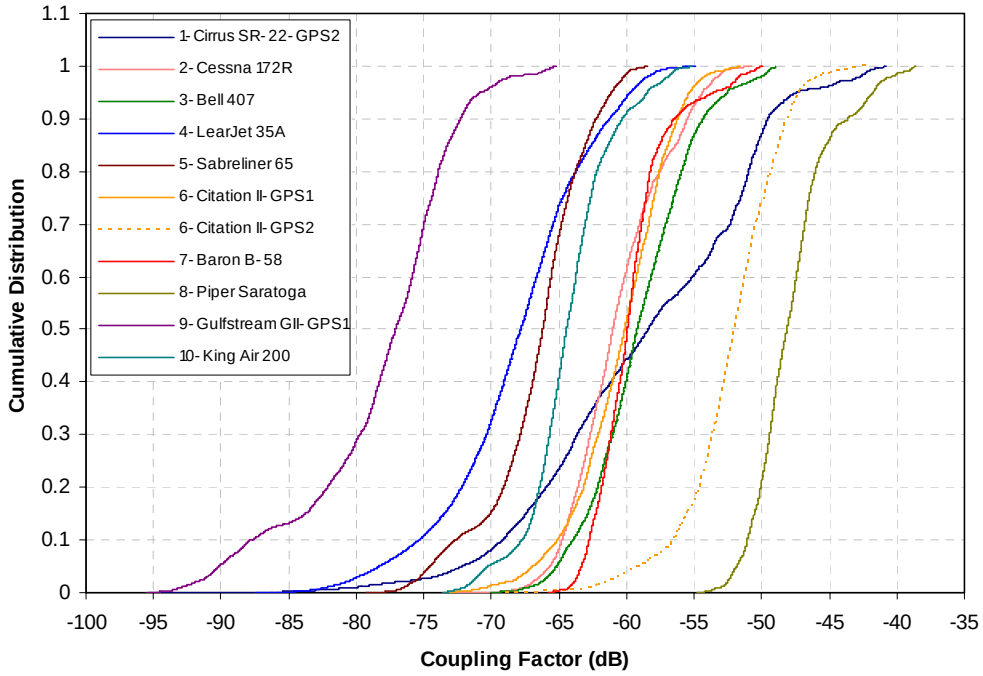

Figure 5-7: GPS IPC cumulative distribution comparison.

Table 5-1a: IPC (in dB) Summary for VOR/LOC, VHF-Com and GS

Aircraft\ Systems	VOR/LOC	VHF-Com		GS
		VHF-Com 1	VHF-Com 2	
Cirrus SR-22	-22.0	-8.7	-27.1	-41.4
Cessna 172R	-26.9	-14.3		-36.3
Bell 407	-17.6	-21.2		
LearJet 35A	-29.8		-35.5	-38.3
Sabreliner 65	-38.1			-46.7
Citation II	-36.1	-35.1	-26.9	-41.0
Baron B-58		-16.6	-28.6	-43.7
Piper Saratoga	-27.9	-15.9	-17.0	-46.3
Gulfstream GII	-42.7	-22.2	-35.1	-52.1
King Air 200	-41.1	-35.6	-30.2	-40.2

Table 5-1b: IPC (in dB) Summary for ATC, DME, TCAS (&TCAD) and GPS

Aircraft\ Systems	DME		ATC	TCAS/ TCAD	GPS	
	DME or DME 1	DME 2			GPS 1	GPS2
Cirrus SR-22			-43.5	-33.4		-40.8
Cessna 172R			-45.1		-50.8	
Bell 407			-43.3		-48.3	
LearJet 35A	-54.0		-52.4		-54.9	
Sabreliner 65					-58.4	
Citation II	-48.5		-55.2	-52.8	-51.6	-42.0
Baron B-58			-50.1	-41.0	-49.9	
Piper Saratoga	-51.6		-51.6		-38.6	
Gulfstream GII	-61.1		-63.5	-58.4	-65.2	
King Air 200	-49.4	-44.7	-52.2		-55.3	

6 Conclusions

Interference path loss measurements were performed on ten general aviation aircraft for multiple radio systems. The results show significant data variations among different aircraft models. Comparison with previously measured larger aircraft class shows that the aircraft considered generally have much higher coupling values. Interference risk is potentially higher as a result. In addition, data cumulative distribution curves appear similar in shape for several different aircraft models. Further analysis is needed to validate and utilize this characteristic.

7 References

[1] T. X. Nguyen, S. V. Koppen, J. J. Ely, R. A. Williams; L. J. Smith, and M. T. Salud, "Portable Wireless LAN Device and Two-Way Radio Threat Assessment for Aircraft Navigation Radios", NASA/TP-2003-212438, July 2003; and NASA/TM-2004-213010.

[2] T. X. Nguyen, S. V. Koppen, L. J. Smith, R. A. Williams and M. T. P. Salud, "Third Generation Wireless Phone Threat Assessment for Aircraft Communication and Navigation Radios", NASA/TP-2005-213537, March 2005.

[3] RTCA/DO-199, "Potential Interference to Aircraft Electronic Equipment from Devices Carried Aboard", September 16, 1988.

[4] RTCA/DO-233, "Portable Electronic Devices Carried On Board Aircraft", Prepared by SC-177, August 20, 1996.

[5] RTCA/DO-294B, "Guidance on Allowing Transmitting Portable Electronic Devices (T-PEDs) on Aircraft", December 13, 2006.

[6] M. Jafri, J. Ely, and L. Vahala, "Graphical and Statistical Analysis of Airplane Passenger Cabin RF Coupling Paths to Avionics" 22nd Digital Avionics Systems Conference, October 12-16, 2003

[7] RTCA/DO-235A, "Assessment of Radio Frequency Interference Relevant to the GNSS", December 5, 2002. Table 2-2 footnote.

Appendix A: Transmit Antenna's Mismatch and Efficiency Correction Factor

This appendix develops the IPL correction factor for the antenna mismatch and the efficiency factor. The goal was to accurately derive the true radiated power from the input power. The correction factors developed in this appendix are only used for comparison against the farfield gain correction factor used in the main report. They were not applied in any data presented earlier. The discussion on the comparison can be found in Section 3.4.1.

As previously noted, the biconical antenna used was a Schwarzbeck UBAA 9114 balun with BBVU 9135 biconical elements. The antenna has unknown efficiency factor. It also has high Voltage Standing Wave Ratio (VSWR) below approximately 300 MHz, and can potentially affect many aircraft radio bands such as LOC, VOR and VHF-Com. This appendix illustrates the steps and calculations involved in characterizing the antenna's balun efficiency, and in developing the correction factor.

Figure A-1 illustrates the main elements of a biconical antenna. The antenna is composed of a long handle, which houses a balun at B. This balun provides impedance matching between the 50-ohm connector at A and the radiating biconical elements at C. The total antenna mismatch at A can be characterized using a vector network analyzer by measuring either the antenna's $|S_{11}|$ or VSWR. $|S_{11}|$ and VSWR can be computed directly from one another using a simple text book formula. $|S_{11}|$, or VSWR, generally includes contributions from multiple mismatch locations, such as the connector, the balun, or the terminal C. As discussed later, laboratory measurements show that the VSWR is dominated by contributions from C for this antenna model.

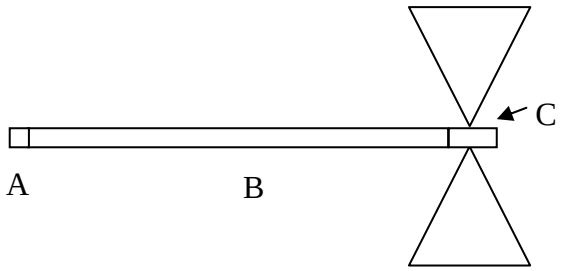

Figure A-1: Biconical antenna illustration for correction factor calculation

Antenna efficiency is typically associated with power loss due to heating. It is also typically more difficult to characterize than $|S_{11}|$. Due to all-metal construction and size (relative to wavelength) of the radiating element, it is reasonable to assume that any efficiency loss in the metal biconical element is minimal, and the antenna efficiency is dominated by loss within the balun. The developed correction factor only accounts for the efficiency loss within the balun.

In developing the correction factor, it was necessary to characterize the antenna mismatch mechanisms and to measure the balun efficiency. The biconical radiating elements were removed from the balun. In its place, thick aluminum foil was used to totally encase the location C, thereby shorting out the terminals and preventing radiation loss. The purpose was to create a "short" condition to reflect all power delivered to location C. A vector network analyzer was then used to characterize the reflection loss in the remaining antenna section from 50 MHz to 1 GHz.

With the terminal at C shorted, time-domain characterizations show that the mismatch at C was the only dominant contribution to the $|S_{11}|$ for the entire frequency range. Other mechanisms were at least 30 dB smaller in magnitude. This finding greatly simplifies the antenna efficiency calculation. Reflection loss in dB, $|S_{11}|_{dB}$, represents the *two-way* path loss between A and C. *One-way* power loss is simply half, or $0.5*|S_{11}|_{dB}$. This is also equal to the balun efficiency in dB, ε_{dB}. In linear units,

$$\varepsilon = 10^{(0.1)(0.5)|S_{11}|_{dB}} \tag{A-1}$$

With the antenna biconical element *re-attached* to the balun, and since location C is the dominant reflection mechanism, the total radiated power P_{rad} is then:

$$P_{rad} = P_{in}\,\varepsilon\,(1 - |\Gamma_c|^2)\,, \tag{A-2}$$

where $|\Gamma_c|^2$ denotes the power reflection coefficient at location C. In addition, power reflection coefficient $|S_{11}|^2$ measured at A (in linear unit) can be shown to be:

$$\begin{aligned} |S_{11}|^2 &= P_{reflected}/P_{in} \\ &= \varepsilon\,|\Gamma_c|^2\,\varepsilon \\ &= \varepsilon^2\,|\Gamma_c|^2 \end{aligned} \tag{A-3}$$

Equation A-3 accounts for the round-trip balun loss (therefore the term ε^2) and the reflection loss at C. It is relevant to point out that $|S_{11}|$ in Eq. A-3 was measured with the antenna in standard configuration, while $|S_{11}|$ in Eq. A-1 was measured with the biconical element removed and the terminal at C shorted. Combining Eq. A-2 and Eq. A-3 and solving for P_{in} / P_{rad},

$$\frac{P_{in}}{P_{rad}} = \frac{1}{\varepsilon - \dfrac{|S_{11}|^2}{\varepsilon}}\ . \tag{A-4}$$

The correction factor CF, in dB, is simply

$$\begin{aligned} CF &= 10\,log(P_{in} / P_{rad})\,, \\ &= -10\,log\left(\varepsilon - \frac{|S_{11}|^2}{\varepsilon}\right). \end{aligned} \tag{A-5}$$

This formulation was based on the finding that $|S_{11}|$ is dominated by the reflection at location C, which simplifies the calculations. It is not applicable for cases with multiple significant mismatch locations. Application of Eq. A-5 to the network measurement data resulted in the CF in Table A-1 for the three affected aircraft bands.

Table A-1: Biconical Antenna Mismatch and Efficiency Effects and Correction Factor

Bands	Band Average VSWR	|S11| (linear)	Measured Balun Effiency, ε	CF (dB) Corrected for Mismatch only	CF (dB) Corrected for Mismatch and Efficiency
VOR/LOC	17.08	0.8893	0.96	+6.80	+8.66
VHF-Com	16.93	0.8884	0.94	+6.76	+9.99
GS	1.268	0.1180	0.86	+0.06	+0.74

Using Eq. A-5, Figure A-2 illustrates the effects on the correction factor due to variations in ε and VSWR. ε values were chosen to match the measured balun efficiency measured in the three aircraft bands VOR/LOC, VHF-Com and GS. For 100% efficient antenna, ε = 1.

Figure A-2 shows CF for different ε values can be significantly higher than for ε=1, depending on the specific VSWR and balun efficiency value. Therefore, antenna efficiency should not be ignored. Correction for both VSWR and ε should be exercised for this antenna type or antenna with similar designs. This formulation can be generalized to be applicable to antennas with one significant mismatch location behind the one lossy element.

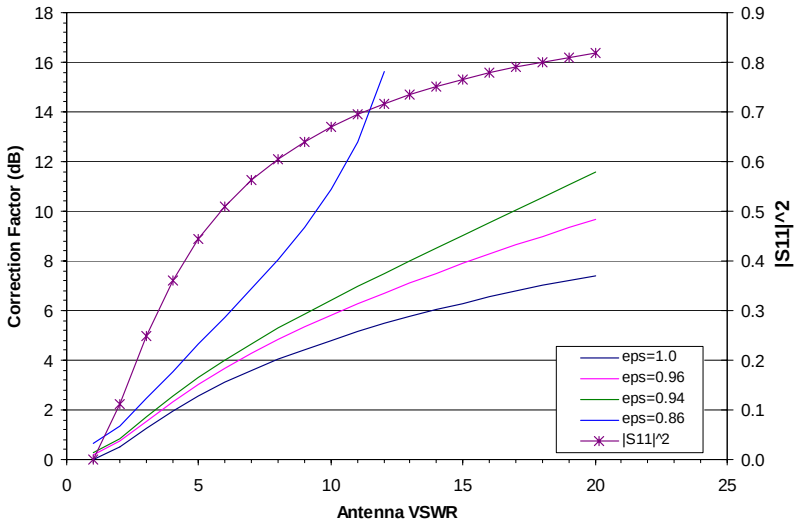

Figure A-2: Biconical antenna's correction factor for antenna efficiency and mismatch.

Appendix B: Comparison of Normalized Interference Path Coupling Factor

This appendix presents the data previously reported in Section 5 but with each data set normalized. The normalization factor was arbitrarily chosen to be average (mean) of the IPC data. The average value for each data trace was computed using each data trace's linear values and then converted to the dB value. As a result of the normalization, each data trace from the plots in Section 5 was shifted according to its average IPL value. In the following charts, the 0 dB coupling factor reflects the average IPC value for each trace.

The purpose of these plots is to demonstrate that most cumulative distribution traces are similar in form, and are shifted in dB values. By normalizing the data, the traces are positioned closer to one another for easier comparison. The charts show that many traces are close to each other in the main groups. However, several of the remaining traces deviate widely from the main group. Tables B-1a and B-1b documents the average IPC values that were used in the normalization.

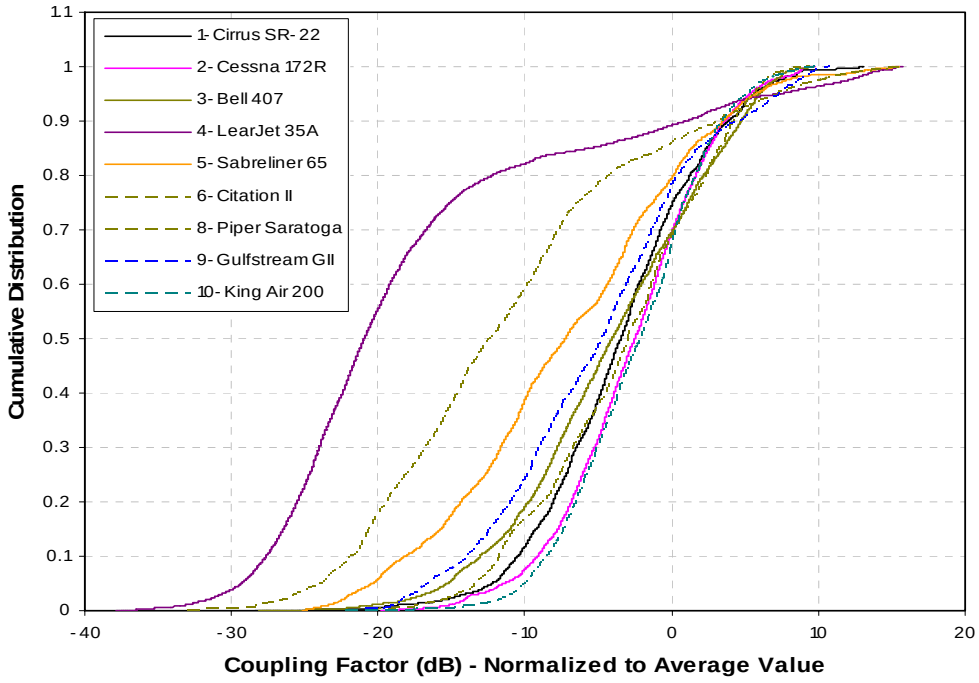

Figure B-1: VOR/LOC normalized IPC cumulative distribution comparison.

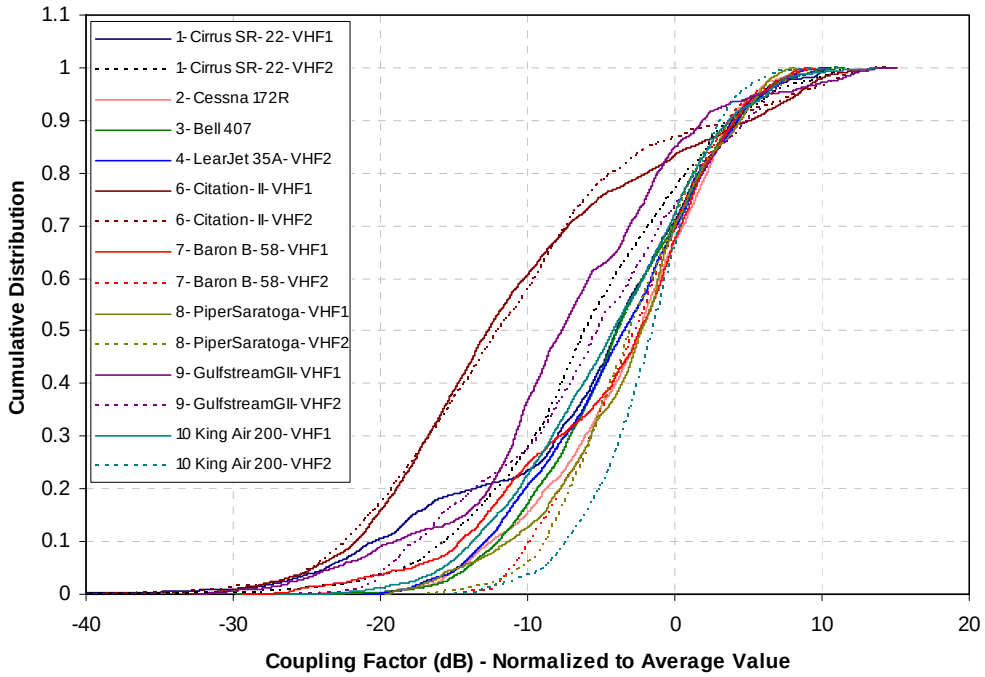

Figure B-2: VHF-Com normalized IPC cumulative distribution comparison.

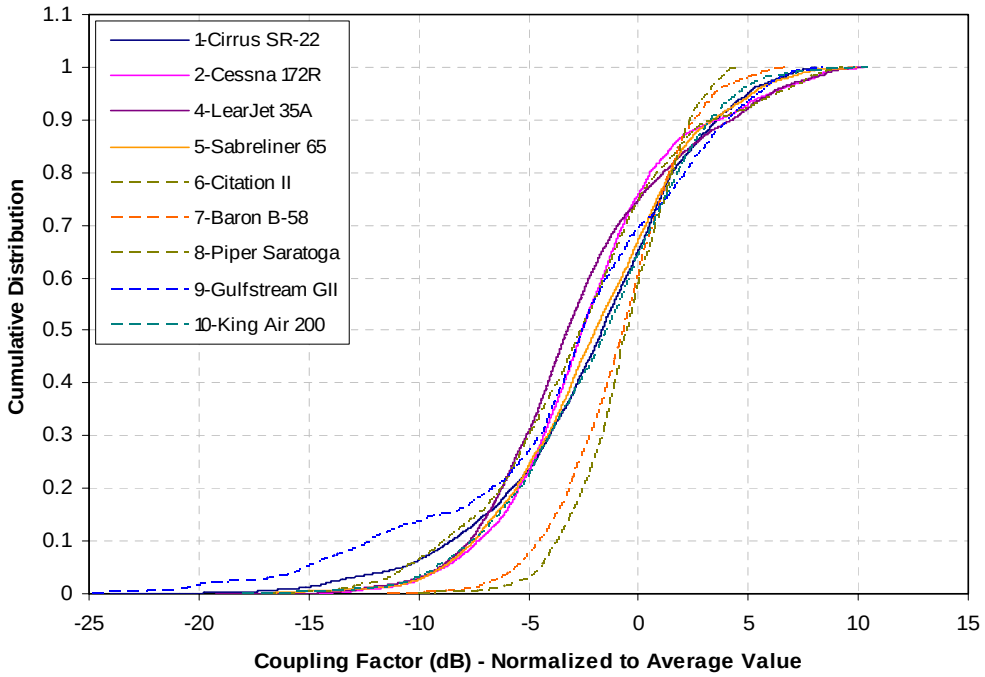

Figure B-3: GS normalized IPC cumulative distribution comparison.

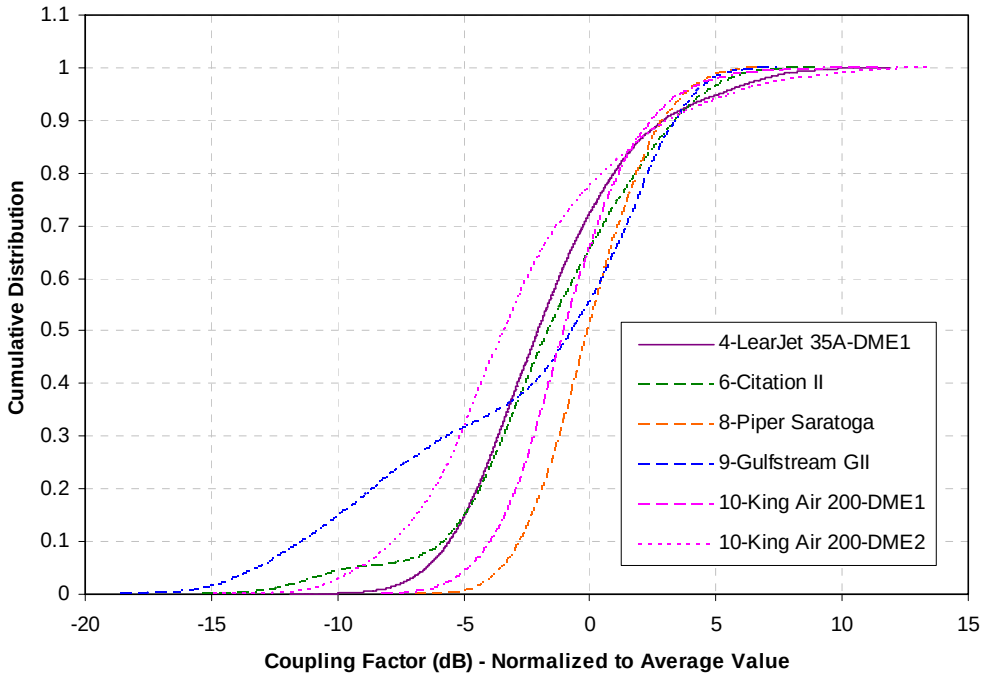

Figure B-4: DME normalized IPC cumulative distribution comparison.

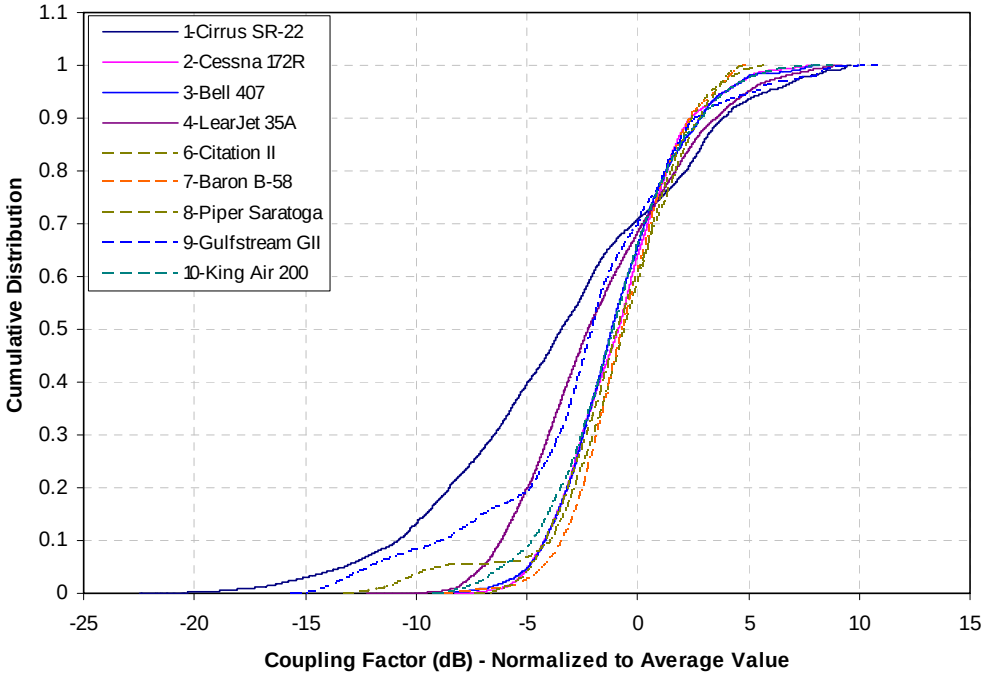

Figure B-5: ATC normalized IPC cumulative distribution comparison.

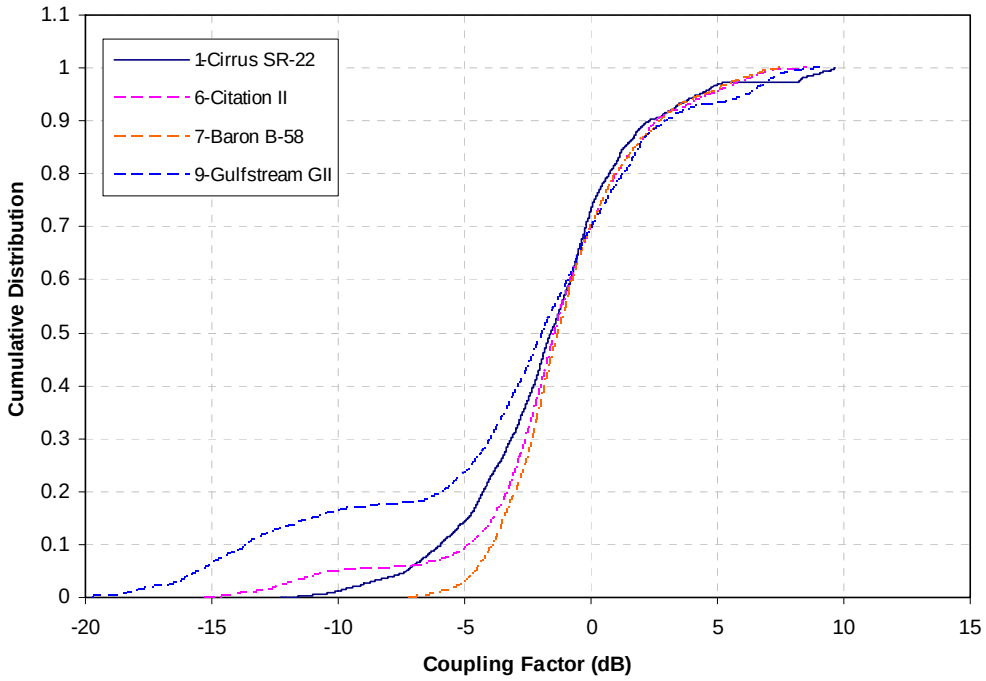

Figure B-6: TCAS (and TCAD) normalized IPC cumulative distribution comparison.

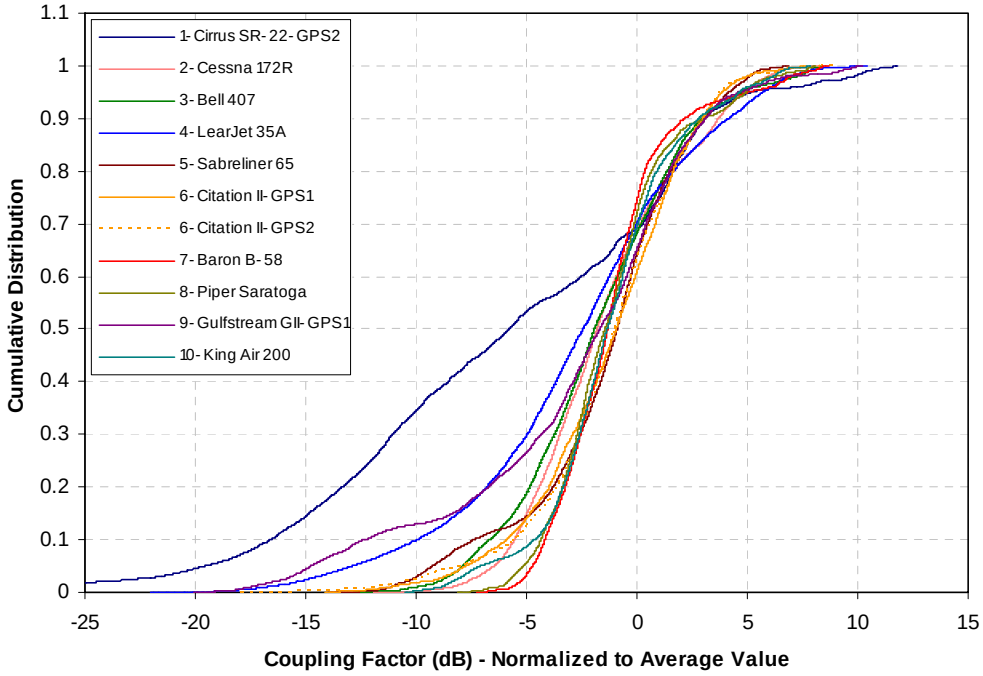

Figure B-7: GPS normalized IPC cumulative distribution comparison.

Table B-1a: Average IPC (in dB) for VOR/LOC, VHF-Com and GS

Aircraft\ Systems	VOR/LOC	VHF-Com		GS
		VHF-Com 1	VHF-Com 2	
Cirrus SR-22	-35.0	-19.3	-39.1	-49.5
Cessna 172R	-36.7	-23.7		-46.6
Bell 407	-27.3	-32.7		
LearJet 35A	-45.6		-46.0	-48.5
Sabreliner 65	-53.6			-56.6
Citation II	-52.0	-50.2	-41.7	-50.4
Baron B-58		-25.8	-38.8	-50.4
Piper Saratoga	-37.3	-24.0	-25.3	-51.0
Gulfstream GII	-53.4	-37.2	-45.2	-60.5
King Air 200	-51.0	-49.3	-41.4	-50.7

Table B-1b: Average IPC (in dB) for ATC, DME, TCAS (&TCAD) and GPS

Aircraft\ Systems	DME		ATC	TCAS/ TCAD	GPS	
	DME or DME 1	DME 2			GPS 1	GPS2
Cirrus SR-22			-53.1	-43.0		-52.6
Cessna 172R			-53.0		-59.2	
Bell 407			-51.5		-57.3	
LearJet 35A	-65.9		-61.6		-65.4	
Sabreliner 65					-65.3	
Citation II	-57.7		-60.9	-61.3	-59.2	-51.0
Baron B-58			-55.2	-48.6	-58.6	
Piper Saratoga	-56.4		-56.4		-46.7	
Gulfstream GII	-68.5		-74.3	-67.4	-75.4	
King Air 200	-60.9	-58.1	-61.0		-63.1	

Appendix C: Large Aircraft Interference Path Coupling Factor

This appendix provides samples of large aircraft peak IPC data for comparison with the small aircraft peak IPC data reported in the Tables 5-1a and 5-1b. These data were measured by different sources at different times, and the methods used were somewhat non-uniform as a result. The measurement differences are not addressed here. Rather, the data are only provided for a first order comparison. Additional information can be found in [1].

Table C-1: Large Aircraft's Peak IPC (in dB) for Various Systems

Aircraft\ Systems	LOC	VOR	VHF-Com	GS	TCAS	GPS
B747	-51.8 -62.7 -55.0 -58.9 -64.8 -55.0	-51.8 -62.7 -55.0 -58.9 -84.7 -76.0	-31.5 -32.3 -35.3 -35.3 -43.2 -40.5, -63.2#, -71.5*	-43.9 -51.0 -49.3 -48.9 -54.6 -53	-63.2 -61.7 -63.3 -64.2	-65.7 -66.3 -64.7 -66.3
DC10	-82.0	-80.0		-77		
L1011	-60.7	-70.3	-56.2, -62.2 *	-64.4		
B757	-51.5 -56.1	-49.9 -46.7	-49.7, -38.0#, -53.0* -36.3 (L), -49.3 (R), -50.3 (C)	-57.5 -58.9	-69.1 -58.6 (T), -57.6 (B)	
B737	-65.0 -56.5 -61.8 -74.2 -62.6 -67.0 -72.7	-65.0 -56.5 -61.8 -74.2 -62.6 -67.0 -76.0	-52.3 -46.8 -50.1 -51.5 -48.6 -52.6 -52.9, -58.4#, -53.2*	-58.9 -60.2 -59.7 -61.7 -61.4 -59.5 -68.8	-53 -52.8 -55.8 -54.3 -56.6 -56.3	-64.9 -64 -71.2 -68.8 -67.4 -67.2
B727	-35, -63 -72	-70, -30, -71 -75	-67, -44, -76	-68 -68		-71
A320	-48.8 -54.0	-65 -59	-51.5, -62.1#, -55.6*	-64.6 -56.0	-54.8 (T), -63.0 (B)	
CV-580		-45		-64		-41
MD-80		-66.2	-57.2, -64.9#, -55.2*	-63.5		
Gulfstream G4						-82.4
Canada RJ	-57.9	-57.9	-36.7 (L), -50.9 (R)	-51.6	-53.1 (T), -54.7 (B)	-43.2
Emb 120	-41.8	-41.8	-28.7 (L), -45.0 (R)	-46.2	-50.7 (T), -48.2 (B)	
ATR72	-63.9	-63.9	-48.4 (L), -43.5 (R)	-57.5		

VHF-Com2 * VHF-Com3 (L): Left Antenna (R): Right (C) Center (T) : Top (B): Bottom

Appendix D: Aircraft Approximate Peak Coupling Locations

This appendix documents general transmitting antenna locations for achieving maximum IPC values. These locations were extracted from the processed data and the measurement log book for the ten aircraft. The table documents general location of the aircraft antenna for each system, and the associated transmit antenna locations for peak coupling. Since each measurement is the peak value of a zone sweep, the locations shown are only approximate. Section 4 shows pictures of the aircraft and aircraft antennas' locations for reference.

Table D-1: Aircraft Peak Coupling Locations

Systems	Approximate Aircraft Antenna Location	Approximate Transmit Antenna Peak Coupling Location
Cirrus SR-22		
VOR/LOC	Top of Tail	Left rear window; right door
VHF-Com1	Top, above rear window	Middle back seat directly under antenna
VHF-Com2	Bottom, behind rear window	Rear windows, seats, cargo
GS	Top of tail	Rear windows
ATC	Bottom, below windshield	Right front and rear passenger
TCAS	Top, above pilot	Left door, rear right passenger, windshield
GPS2	Inside, under glareshield	Near front windshield
Cessna 172R		
VOR/LOC	Top of tail	Windshield; left front and back windows
VHF-Com1	Top, behind pilot	Windshield; cargo
GS	Top of tail	Cargo; left windows
ATC		Right door Left front passenger
GPS2	Top, above pilot	Windshield
Bell 407		
VOR/LOC	Rear of fuselage	Back door sweep; Right back window
VHF-Com1	Bottom, rear of fuselage	Left of windshield Chin window
ATC	Bottom, under chin	Chin window Right front window toward bottom
GPS	Top, center, above 2nd window	Ceiling windows
LearJet 35A		
VOR/LOC	Tail	Windshield
VHF-Com2	Bottom, below 4th window	Windshield, 4th window
GS	Nose	co-pilot seat, windshield,
DME1	Bottom, below bottom of windshield	1st and 3rd left windows, windshield
ATC	Bottom, below nose	Windshield, 1st right window
GPS	Top, above 1st window	Windshield

Sabreliner 65		
VOR/LOC	Nose	Pilot seat, windshield
GS	Nose	Windshield; pilot seat; door
GPS	Top, above door	Windshield
Citation II		
VOR/LOC	Tail	Windshield and pilot seats
VHF-Com1	Top, above body section near engine toward rear of aircraft	Windshield and pilot seats
VHF-Com2	Bottom, between two rear landing gears	Windshield and pilot seats
GS	Nose	Windshield and pilot seats
DME	Left of nose landing gear	Windshield and pilot seats; 1st left window and seats
ATC	Bottom, below door	1st right window; windshield and pilot
TCAS	Bottom and top of cockpit	Windshield and pilot seats
GPS1	Top, above galley front of door	2nd and 3rd right window Windshield
GPS2	Top, above window behind left door, offset to the left	Window behind left door
Baron B-58		
VHF-Com1	Top, above 2nd window	Right door sweep; windshield; cockpit window
VHF-Com2	Bottom, below windshield	Left cockpit window; windshield
GS	Vertical tail	2nd and 3rd left windows
ATC	Bottom, near wings, right hand side	Right door; 2nd right window; 2nd left window
TCAS	Top, above 2nd window	Windshield; 2nd righ and left windows
GPS	Top, above 1st window	Windshield; cockpit left and right windows
Piper Saratoga		
VOR/LOC	Tail	Windshield; 3rd window and door sweep, including cargo door
VHF-Com1	Top, above 2nd and 3rd windows	Windshield 3rd window/left door sweep (including cargo door) Left cockpit window
VHF-Com2	Top, above cargo window	3rd window/left door sweep (including cargo door); 3rd left window; Windshield
GS	Tail	Windshield; cockpit left window and seat
DME	Bottom, below second window	Windshield; 3rd left door; right door
ATC	Bottom, below windshield	Right door; 1st right window and seat
GPS	Top, above cockpit	Windshield
Gulfstream GII		
VOR/LOC	Tail	2nd right window and seat; door
VHF-Com1	Top, above 1st window	Door

VHF-Com2	Bottom, below 1st and 2nd window	1st and 2nd right windows
GS	Nose	1st and 3rd right windows
DME	Bottom, front, below door	1st and 2nd windows
ATC	Bottom, below 3rd window	1st and 5th left windows
TCAS	Top, behind cockpit	Cockpit sweep, door
GPS1	Top, above 1st row seat	1st right window
<u>King Air 200</u>		
VOR/LOC	Tail	3rd and 4th left windows
VHF-Com1	Top, above door (rear)	Cockpit sweep
VHF-Com2	Bottom, behind cockpit	Left door
GS	Nose	Cockpit
DME1	Bottom, below rear door	Cargo
DME2	Bottom, below 1st window	Cockpit sweep; 1st left window
ATC	Bottom, below 5th window	4th and 3rd windows
GPS	Top, behind windshield	Cockpit sweep

REPORT DOCUMENTATION PAGE

Form Approved
OMB No. 0704-0188

1. REPORT DATE *(DD-MM-YYYY)*	2. REPORT TYPE	3. DATES COVERED *(From - To)*
01- 08 - 2007	Technical Publication	

4. TITLE AND SUBTITLE
Small Aircraft RF Interference Path Loss Measurements

5a. CONTRACT NUMBER

5b. GRANT NUMBER

5c. PROGRAM ELEMENT NUMBER

6. AUTHOR(S)
Nguyen, Truong X.; Koppen, Sandra V.; Ely, Jay J.; Szatkowski, George N.; Mielnik, John J.; and Salud, Maria Theresa P.

5d. PROJECT NUMBER

5e. TASK NUMBER

5f. WORK UNIT NUMBER
645846.02.07.07.05

7. PERFORMING ORGANIZATION NAME(S) AND ADDRESS(ES)
NASA Langley Research Center
Hampton, VA 23681-2199

8. PERFORMING ORGANIZATION REPORT NUMBER
L-19370

9. SPONSORING/MONITORING AGENCY NAME(S) AND ADDRESS(ES)
National Aeronautics and Space Administration
Washington, DC 20546-0001

10. SPONSOR/MONITOR'S ACRONYM(S)
NASA

11. SPONSOR/MONITOR'S REPORT NUMBER(S)
NASA/TP-2007-214891

12. DISTRIBUTION/AVAILABILITY STATEMENT
Unclassified - Unlimited
Subject Category 04
Availability: NASA CASI (301) 621-0390

13. SUPPLEMENTARY NOTES
An electronic version can be found at http://ntrs.nasa.gov

14. ABSTRACT

Interference to aircraft radio receivers is an increasing concern as more portable electronic devices are allowed onboard. Interference signals are attenuated as they propagate from inside the cabin to aircraft radio antennas mounted on the outside of the aircraft. The attenuation level is referred to as the interference path loss (IPL) value. Significant published IPL data exists for transport and regional category airplanes. This report fills a void by providing data for small business/corporate and general aviation aircraft. In this effort, IPL measurements are performed on ten small aircraft of different designs and manufacturers. Multiple radio systems are addressed. Along with the typical worst-case coupling values, statistical distributions are also reported that could lead to more meaningful interference risk assessment.

15. SUBJECT TERMS
Interference Path Loss; Aeronautical Communication and Navigation; Interference; Portable Electronic Devices; General Aviation Aircraft

16. SECURITY CLASSIFICATION OF:			17. LIMITATION OF ABSTRACT	18. NUMBER OF PAGES	19a. NAME OF RESPONSIBLE PERSON
a. REPORT	b. ABSTRACT	c. THIS PAGE			STI Help Desk (email: help@sti.nasa.gov)
					19b. TELEPHONE NUMBER *(Include area code)*
U	U	U	UU	121	(301) 621-0390